ADVANCED HEALTHCARE MATERIALS
www.advhealthmat.de

Carbon Nanomaterials in Biological Studies and Biomedicine

*Nagappa L. Teradal and Raz Jelinek**

The "carbon nano-world" has made over the past few decades huge contributions in diverse scientific disciplines and technological advances. While dramatic advances have been widely publicized in using carbon nanomaterials such as fullerenes, carbon nanotubes, and graphene in materials sciences, nano-electronics, and photonics, their contributions to biology and biomedicine have been noteworthy as well. This Review focuses on the use of carbon nanotubes (CNTs), graphene, and carbon quantum dots [encompassing graphene quantum dots (GQDs) and carbon dots (C-dots)] in biologically oriented materials and applications. Examples of these remarkable nanomaterials in bio-sensing, cell- and tissue-imaging, regenerative medicine, and other applications are presented and discussed, emphasizing the significance of their unique properties and their future potential.

1. Introduction

Carbon nanostructures have had a tremendous impact in scientific research and technology progress. The unifying property of zero-dimension fullerenes,[1] one dimensional carbon nanotubes (CNTs),[2] the two-dimensional carbon allotrope graphene[3] and recently synthesized carbon quantum dots[4] is the sp^2-bonded carbon atoms that are generally arranged in hexagonal lattices. These features, combined with the interesting electrical, chemical, and mechanical properties of carbon nanomaterials, have led to numerous applications in diverse fields. The potential of carbon nanomaterials in *biology*–e.g., as conduits for biosensing, bioimaging, and as novel biomimetic materials–has been recognized early on. While carbon nanomaterials have been initially used in biosensing and as potential drug carriers, recent years saw expansion of their applications into regenerative medicine, tissue engineering, bioimaging, and therapeutics. Reviews discussing biological applications of CNTs,[5] graphene,[6] and carbon quantum dots[7,8] have been published.

This Review focuses on biologically oriented applications of the three main families of carbon nanostructures–CNTs, graphene (pristine graphene, graphene oxide, and reduced graphene oxide), and carbon quantum dots. **Figure 1** presents an outline of the contents of this Review article. Our goal is to provide a broad overview of the diverse applications of these nanomaterials, emphasizing the significance of their respective unique properties. Due to the breadth of this field and considerable volume of research papers published we discuss below fraction of the (recent) literature on the subject, and readers are encouraged to expand their knowledge further on specific topics. Overall, we hope that this Review would highlight the significant contributions of carbon nanomaterials to biological research, and their potential for future scientific and technological developments.

Dr. N. L. Teradal, Dr. R. Jelinek
Department of Chemistry and Ilse Katz Institute for Nanotechnology
Ben Gurion University of the Negev
Beer Sheva 84105, Israel
E-mail: razj@bgu.ac.il

DOI: 10.1002/adhm.201700574

2. Carbon Nanotubes and their Derivatives

Carbon nanotubes [abbreviated CNTs; also categorized as single-walled carbon nanotubes (SWCNTs) or multi-walled carbon nanotubes (MWCNTs), **Figure 2**] have been among the early members in the "carbon nanotechnology" universe. The remarkable properties of CNTs, including high tensile strength, mechanical flexibility, and electrical conductivity, have attracted significant scientific and technological interest; Indeed, CNTs are already employed in varied products. Biological applications of CNTs, in particular, have been touted and explored mostly due to the diverse surface chemistry modification pathways enabling attachment of recognition elements and biomolecular cargoes to the nanotubes. These features have opened the way for applications in biosensing, drug delivery, and tissue engineering, discussed below.

A notable aspect of CNTs, which adversely affects their biological applicability is their low *solubility* in aqueous solutions. Specifically, CNTs exhibit high affinity towards agglomeration, mostly due to strong surface interactions. Dispersion of CNTs can be achieved either by covalent or non-covalent modification of their surfaces. Enhanced dispersion of CNTs in aqueous solvents can be accomplished through non-covalent functionalization with biocompatible conjugates such as phospholipid-polyethylene glycol.[9] Attachment of amphiphilic small molecules and polymers has been also reported.[10] Noncovalent functionalization of CNTs is particularly useful as this treatment does not disrupt the carbon lattice, thus generally preserving the physico-chemical properties of CNTs. Ideally, noncovalent functionalization should provide higher water solubility, biocompatibility, stability in various biological solutions and functional groups that are available for further bioconjugation.[9]

2.1. CNT-Based Biosensors

CNTs have been a focus of intensive research as conduits for biosensing applications due to their extensive surface onto

which recognition elements and capture agents can be displayed for detection of biological species. In general, CNT-based biosensors exhibit important advantages, such as high surface area-to-volume ratio, feasibility of immobilizing varied recognition molecules without adversely affecting their biological functions, and fast response times as CNTs can efficiently mediate electron transport processes. Moreover, CNTs exhibit high stability and low surface fouling over time, contributing to practical biosensing applications.[11,12]

2.1.1. Glucose Biosensor

Enzyme-based CNT biosensors have been widely reported. The most common enzyme-based biosensor is the *glucose sensor*, mostly targeted towards monitoring glucose levels in the blood of diabetic patients. **Figure 3** depicts the most ubiquitous glucose sensing mechanism. A glucose-specific enzyme, glucose oxidase (abbreviated as GOx) catalyzes glucose oxidation (i.e., transformation of glucose to gluconolactone). In this process, the enzyme's redox cofactor, flavin adenine mononucleotide (FAD) is converted to its reduced form flavin adenine dinucleotide ($FADH_2$). The process by which the reduced form of the enzyme is converted back to its oxidized state occurs through direct electron transfer from the working electrode, and the obtained electrochemical signal can be related to glucose content (Figure 3).[13]

CNTs in glucose sensing have been mostly used as conduits for electron transport, e.g., as conductive nanowires. Patolsky et al. demonstrated the use of SWCNTs as electrical linkers between the enzyme (FAD) redox centers and the electrodes,[14] in which sensing relied upon the direct electron transfer mechanism (**Figure 4**a). FAD was first covalently attached to the SWCNT terminus, and GOx was subsequently reconstituted upon the immobilized FAD (Figure 4a). In this system, the SWCNTs acted as effective electrical nano-connectors, linking the active site of the enzyme and the electrode surface. In particular, this arrangement enabled electron transport over relatively long distances (>150 nm), while the rate of electron transport was controlled by the length of the SWCNTs. The results of this study revealed the compatibility of SWCNTs with the preparation of novel biomaterial hybrid systems that can be used as biosensing platform for glucose.

Figure 4b outlines another glucose sensor design in which CNTs enhanced electron transfer in a GOx-based sensing platform.[15] The basic assembly comprised of *enzyme precipitate coating electrode (EPC-E)* in which enzyme immobilization enabled the sensitive detection of glucose. The CNTs in that system constituted useful substrates for enzyme coating and also as conduits of electron transport. Notably, significantly enhanced sensitivity (≈7-fold) and charge transfer rate were achieved in a setup that combined EPC-E with CNTs (Figure 4b). The greater sensitivity in the composite EPC-E/CNT was ascribed to the CNTs acting as an "electron transport highway" to increase the efficiency of electron movement from the enzyme active sites to the electrode surface.[15]

Nagappa L. Teradal received his Ph.D. in Chemistry in 2015 from the Karnatak University, Dharwad, India, under the supervision of Prof. J. Seetharamappa. He is currently a postdoctoral research associate with Prof. Raz Jelinek in the Department of Chemistry at Ben-Gurion University of the Negev, Beer Sheva, Israel. His research focuses on the development of advanced nanostructures for various technological applications, especially sensing and catalytic applications.

Raz Jelinek holds the Carole and Barry Kaye Chair in Applied Science at the Department of Chemistry, Ben Gurion University, and is also a founding member of the Ilse Katz Institute for Nanoscale Science and Technology (IKI). Prof. Jelinek's research is broad-based, and he has worked in varied fields including "bottom-up" chemistry, bio- and chemo-sensors, amyloid peptides, membranes, and carbon nanoparticles.

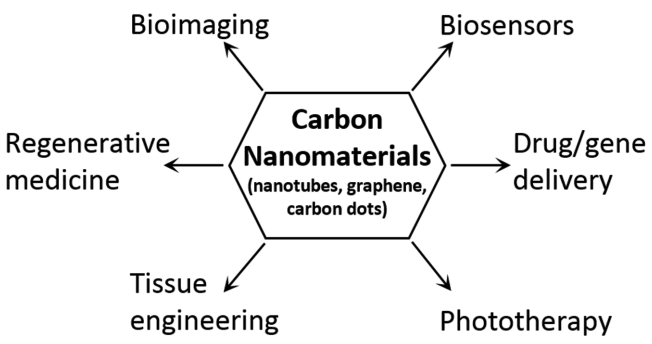

Figure 1. Carbon systems and applications discussed in the Review.

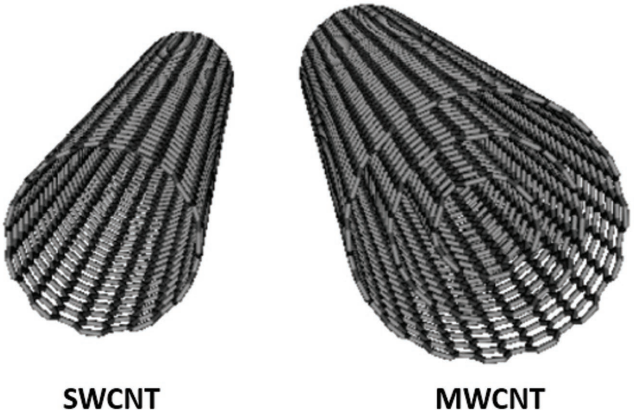

Figure 2. Schemes of a single-walled carbon nanotube (SWCNT) and multi-walled carbon nanotube (MWCNT).

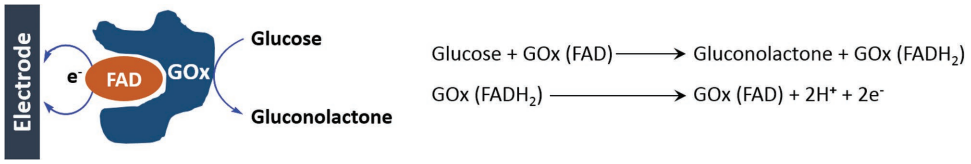

Figure 3. Generic enzyme-mediated glucose sensing. The sensing mechanism is through direct electron transfer. Enzyme containing a prosthetic group of glucose oxidase (GOx) and its cofactor flavin adenine dinucleotide (FAD) are immobilized upon the electrode surface.

Glucose biosensors based on CNT nanocomposites comprising *metal oxide* nanoparticles were also reported. Figure 4c depicts the backbone of a GOx/MnO_2/MWCNT sensor.[16] The presence of the MnO_2 nanoparticles on the surface of the CNTs enhanced the enzymatic activity and reversibility of the GOx-mediated redox processes, in turn enhancing the sensitivity and stability of the electrochemical glucose biosensor. Similar composite sensors comprising MWCNT/ZnO/GOx,[17] MWCNT/Au/GOx,[18] and MWCNTs/gold colloid/poly diallyldimethylammonium chloride) (PDDA)[19] were also reported.

2.1.2. Acetylcholine and Organophosphates Biosensing

CNTs were also employed as core sensor elements for detection of organophosphates (OPs) affecting neurotransmitters such as acetylcholine (ACh). ACh plays an important role in communicating between motor nerves and muscles, especially in the heart, bladder, and stomach.[20] OPs, mostly used as pesticides, are highly toxic to humans as they inhibit the activity of the enzyme acetylcholine esterase (AChE) leading to accumulation of acetylcholine, which may lead muscular paralysis, convulsions, bronchial constriction, and even death by asphyxiation.[21] **Figure 5** depicts CNT-based AChE biosensors facilitating sensitive detection of both OPs and Ach. Specifically, CNTs functioned as an excellent conductive support between the enzyme and electrode surface, enhancing the electrochemical reactivity and stability of the enzyme (AChE). CNT surfaces in particular have been amenable for immobilization of AchE, without adversely affecting its functionality.[20–24]

Different CNT-based supports, Au-MWCNTs/GCE,[22] and MWCNTs/Nanoporous gold electrode (linked through cysteamine)[23] were also used to immobilize the bio-recognition layer comprising AChE for selective sensing of OPs. Notably, the high sensitivity of those sensors for OPs was ascribed to enhanced electrochemical response of the composite electrode affected by the excellent bioactivity of the immobilized enzyme. In other reported schemes, CNTs were interspersed within conductive polymers (CPs) which synergistically enhanced AChE bioactivity and sensor performance.[24] CNT-based sensors were employed for detection of many other biomolecular targets, including galactose,[25] neurotransmitters (dopamine,[26] epinephrine,[27] and norepinephrine[28]), amino acids (i.e., glutamic acid,[29] D- and L-amino acids[30]), immunoglobulins,[31] albumin,[32] and others.

2.1.3. DNA Biosensors

CNTs have been also coupled to deoxyribonucleic acid (DNA) for sensing applications. DNA-based sensors have been widely used in medical diagnostics, forensic science, and other applications.[12] The core sensing elements in DNA biosensors are either single stranded DNA (ssDNA) or double stranded (dsDNA), which constitute the biological recognition layers.

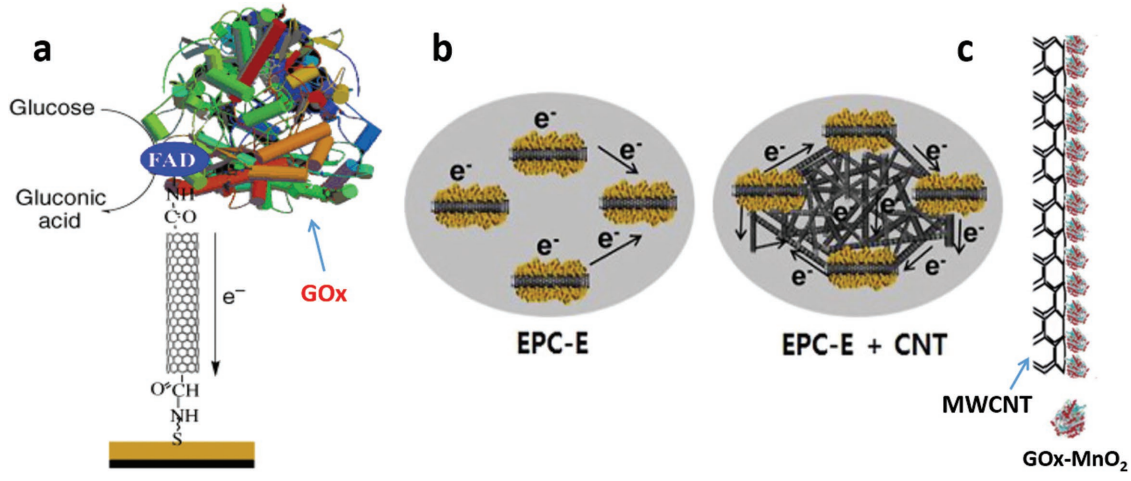

Figure 4. Enzyme-based glucose sensors utilizing SWCNTs. a) The SWCNT serves as a linker between the electrode surface and GOx reconstituted on the FAD units, facilitating electron transport. Reproduced with permission.[14] b) Enhanced sensing properties accomplished by combining enzyme precipitate coated electrode (EPC-E) with free CNTs as electron transfer promoters. Reproduced with permission.[15] Copyright 2015, Elsevier Ltd. c) Electrochemical deposition of MnO_2 on MWCNTs/glassy carbon electrode (GCE), with subsequent immobilization of GOx on the MnO_2/MWCNTs/GCE. Reproduced with permission.[16] Copyright 2016, The Royal Society of Chemistry.

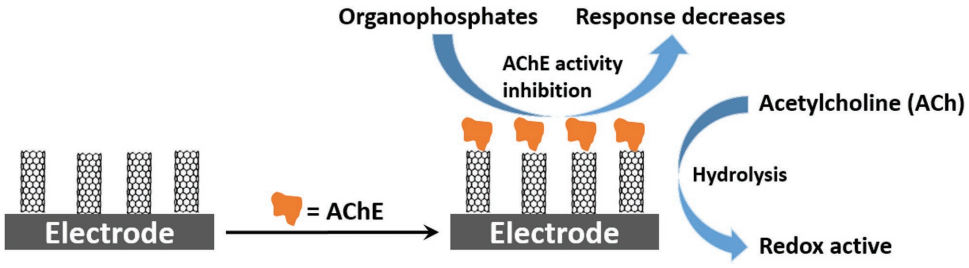

Figure 5. CNT-based acetylcholine esterase (AChE) biosensor for detection of organophosphates and ACh. AChE-decorated CNTs are prepared either by covalent bonding or by conductive polymer wrapping.

Researchers have found that DNA efficiently adsorbs onto CNT surfaces and forms supramolecular complexes which consequently benefit from both the distinctive properties of the nanotubes and the outstanding recognition capabilities of DNA.[33] DNA-coupled CNTs exist as well-defined chemical entities in aqueous solutions due to the strong non-covalent interactions between DNA and the CNTs.[33] As shown in **Figure 6**, DNA can "coil" around CNTs, or binds either onto the basal or the side surface. Functionalization of CNTs with DNA also contributes to greater CNT solubility thus increasing practicality of composite materials as sensors.[34] DNA-CNT hybrids have been used as biosensors for detection of varied analytes, including peroxide,[35] dopamine,[36] proteins[37] and others.

CNT-DNA conjugates have been employed for detection of specific oligonucleotide sequences. In most such systems ssDNA has been used as probe, designed to hybridize complementary target DNA.[32–39] The sensitivity, specificity, and stability of CNT-DNA sensors could be enhanced by further conjugating the hybrid with reduced graphene oxide (rGO)[38] or CuO nanowires.[39] These additives are believed to accelerate electron transport properties of the hybrid materials. Similarly, MWCNTs functionalized with methylene blue (MB) enabled sensitive electrochemical detection of DNA.[40]

In yet another study, Zhao et al. developed a sensing platform based on MWCNT signal amplification and fluorescence polarization (FP) for sensitive and selective detection of DNA methyltransferase (DNA MTase) activity (**Figure 7**).[41] This assay uses a fluorescein amidite (FAM)-labeled DNA probe, which contains a dsDNA part to serve as the specific recognition sequence of both DNA MTase and its corresponding restriction endonuclease, and a ssDNA component for anchoring the DNA to the surface of MWCNTs. In the absence of DNA MTase, this FAM-labeled DNA probe is cleaved by restriction endonuclease, and generates the very short DNA fragments carrying the FAM dye that cannot bind to the MWCNTs. In this situation, the FAM dye exhibits relatively small polarization. However, in the presence of DNA MTase the specific recognition sequence within the FAM-labeled DNA probe is methylated and blocked the cleavage by its corresponding restriction endonuclease. Thus, the FAM-labeled methylated DNA product was adsorbed onto CNTs via strong π–π stacking interactions leading to significant increase in polarization due the slow rotation of the DNA/MWCNT complex.

2.1.4. Cancer Biomarker Detection

Sensors designed to report on specific molecular cancer markers are highly sought for as "early warning" agents in cancer diagnostics. Different classes of CNT biosensors have been developed to detect a wide variety of cancer biomarkers through conjugation with aptamers (oligonucleotide sequences employed for biomolecular recognition,[42] antibodies, peptides, proteins, and enzymes).[43,44] In particular, CNTs have been shown to promote electron transfer reactions involving proteins and enzymes.[45] **Figure 8** outlines a generic experimental scheme for detection of cancer markers by CNT-immobilized antibodies (Abs).[46] The transduction principle in such systems is based upon modulation of the electrical current flowing through the CNTs, induced upon binding of cancer antigens to the Abs immobilized upon the CNTs' surface.[47]

Researchers reported use of antibody-functionalized CNTs for detection of varied cancer biomarkers. A nanostructured CNT "forest" was constructed for ultrasensitive detection of interleukin-6 (IL-6), a multifunctional cytokine characterized as a regulator of immune and inflammatory responses, in serum of disease-free and cancer patients.[48] The immunosensor comprised of an electrically conductive, high surface area substrate featuring densely packed, upright SWCNTs mimicking a "forest" onto which ends specific antibodies (Ab1) were attached. Antigens were bound to the Ab1 molecules, subsequently detected by an enzyme-bound secondary

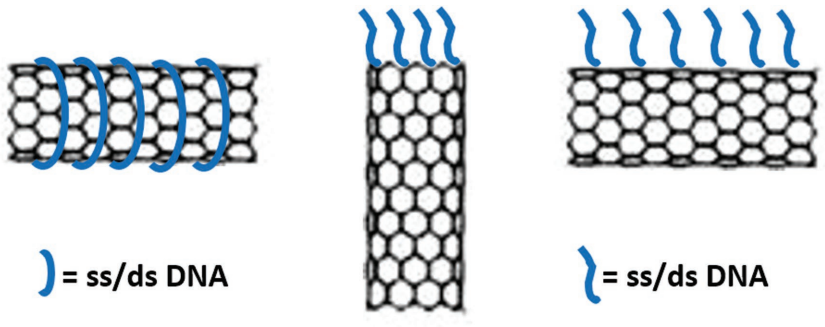

Figure 6. Wrapping of single stranded (ss)/double stranded (ds) DNA on CNT surface. Shown are non-covalent (left) or covalent (middle and right) modification of CNTs with ss/ds DNA.

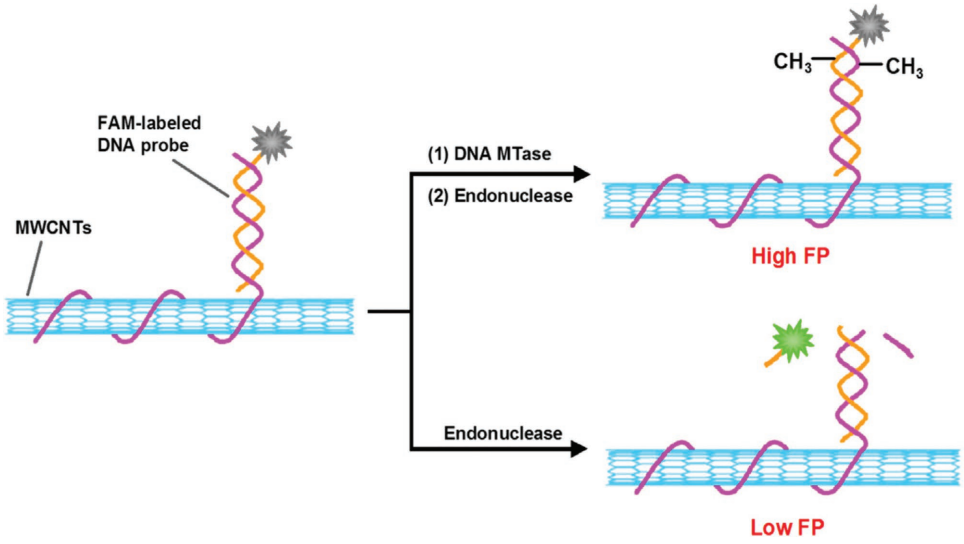

Figure 7. DNA detection by fluorescence polarization using CNTs. The detection strategy uses a fluorescein amidite (FAM)-labeled DNA probe, which contains dsDNA which serves as the recognition sequence of both DNA MTase and its corresponding restriction endonuclease, and single-stranded DNA (ssDNA) residue for anchoring the recognition element to the surface of the MWCNTs via π–π stacking interactions. Reproduced with permission.[41] Copyright 2014, Elsevier Ltd.

antibody. Antibody-loaded MWCNTs facilitated simultaneous detection of the cancer biomarkers prostate specific antigen (PSA) and Interleukin 8 (IL-8).[49]

A different strategy for CNT-based cancer detection was reported in which electrochemical impedimetric immunosensing for cancer biomarkers was accomplished using CNTs modified with Au NPs.[50] In the system, the Au NPs rather than the CNTs functioned as protein-immobilization surfaces. Ultrasensitive chemo-resistive biosensors comprising single MWCNTs embedded in epoxy nanofibers and further displaying monoclonal antibodies (mAbs) for human cardiac biomarkers such as myoglobin, cardiac Troponin I, and creatine kinase were reported.[44]

CNT field-effect transistor (FET) sensors have been recently demonstrated. A case in point is a study depicting detection of the cancer marker osteopontin (OPN).[51] In this method, a genetically engineered OPN-binding protein was covalently bound onto the surface of CNTs, displaying OPN concentration-dependent modulation of source–drain currents. Introduction of "defect sites" upon the CNT sidewalls increased OPN sensitivity through electron scattering. Another strategy achieved sensitive voltammetric detection of cancer cells using vertically aligned MWCNTs which enabled entrapment of cancer cells. Mechanical and electrical interactions between the CNT tips and entrapped cell membranes modulated the system electrical potential.[52,53] The MWCNTs were termed "cellular

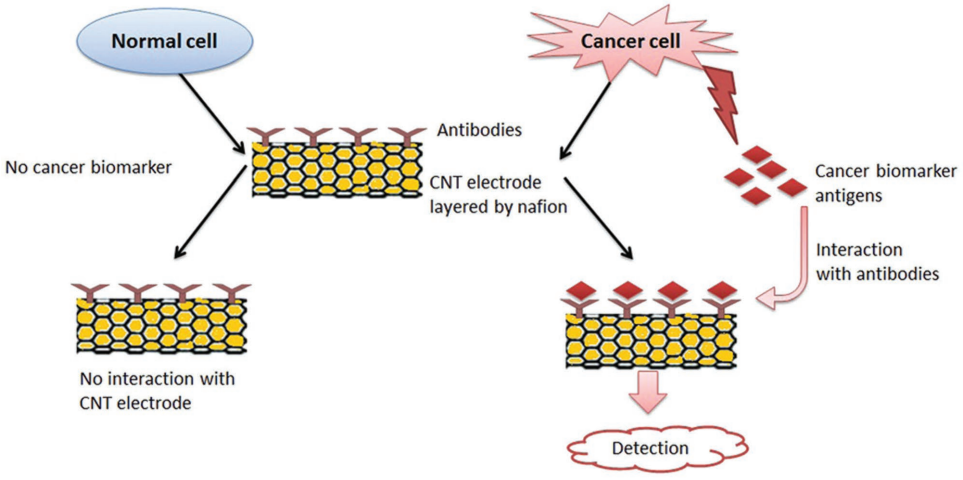

Figure 8. Detection of cancer biomarkers by CNTs. Cancer biomarker antigens dock onto antibodies immobilized upon the CNT surface. Detection of the binding events is accomplished through modulation of electrical current transported in the CNTs. Reproduced with permission.[46] Copyright 2016, The Royal Society of Chemistry.

cancer endoscopes" reporting on the electrical signals produced by single cell membranes.[52]

2.2. CNTs in Drug and Gene Delivery

CNT-based drug delivery systems have been explored for treatment of a variety of diseases, primarily cancer therapy. Two main strategies have been pursued: selective targeting accomplished through functionalization of CNT surfaces with specific tumor recognition elements, and CNT-mediated controlled release of drugs in tumor environments.[54,55] CNTs have been shown to deliver small amounts of drugs to specific tumor sites, thus minimizing systemic toxicity and reducing undesirable side-effects. Chen et al. constructed peptide-modified SWCNTs through a noncovalent approach which were further loaded with the anticancer drug tamoxifen (TAM).[56] This system was tested in vitro and in vivo and showed efficient tumor targeting and high antitumor activity. Functionalized MWCNTs have been used for targeting cancer cell nuclei and releasing the common anticancer drug doxorubicin (DOX).[57] Several studies reported dye-labeling or radioactive-labeling of CNTs to track the release, location, and movement of drugs inside the cell.[58,59]

The release of drug cargo from CNTs at delivery sites is a major challenge in CNT-based drug delivery. pH-induced release of DOX from SWCNTs was reported and evaluated through a two-dye approach (**Figure 9**a).[59] The SWCNTs were first labeled with fluorescein isothiocyanate (FITC) emitting at 520 nm, while DOX was separately labeled with a red dye emitting at 590 nm. Confocal microscopy was then applied to track the location of both SWCNTs and DOX cargo. Notably, release of the drug molecules from the SWCNTs took place in the lysosomes, with subsequent migration into the cytoplasm and finally into the nucleus. The SWCNT carriers, on the other hand, remained in the lysosomes.

Bandyopdhyay et al. reported controlled release of various anti-inflammatory[60] and anti-anginal drugs[61] from nanocomposite membranes comprising CNTs (Figure 9b). Controlled drug release was achieved by tuning the hydrophobic characteristics of a polymer matrix. Essentially, water-induced swelling led to faster release of the encapsulated drug while slower swelling retained the drug for longer duration within in the polymer matrix. Bandyopdhyay and co-workers used varied concentrations of differently functionalized CNTs to tune the hydrophobic characteristics of the polymer nanocomposite and thus the swelling properties.[60,61] Similarly, Pal and co-workers developed carboxymethyl cellulose (CMC) and acid-functionalized MWCNTs which formed biodegradable nanocomposite hydrogel for the sustained release of diclofenac sodium.[62] Notably, ~98% of the diclofenac sodium molecular cargo was not decomposed over time in the release system upon the incorporation of MWCNTs.[62] pH- and temperature-induced controlled release system, polyethyleneglycol (PEG)-functionalized MWCNTs for cancer therapy were reported.[63] That study also showed biocompatibility of the conjugated particles and efficient delivery of the therapeutic compound to tumor cells.

SWCNTs non-covalently coupled to DOX and further functionalized with a tumor-specific ligand (folic acid) shown to exhibit controllable loading/release of DOX as well as selective killing of tumor cells.[55] Following binding to the cell-surface folate receptor, the SWCNTs–ligand complex was cell-internalized through endocytosis. Inside the endosomes, higher acidity induced release of DOX from the SWCNTs, resulting in effective tumor inhibition.[55] In another study, an electroresponsive poly(methylacrylic acid) (PMAA)-based hydrogel matrix containing pristine MWCNTs was assembled for pulsatile drug release.[64] In this system, low electric field was applied for a

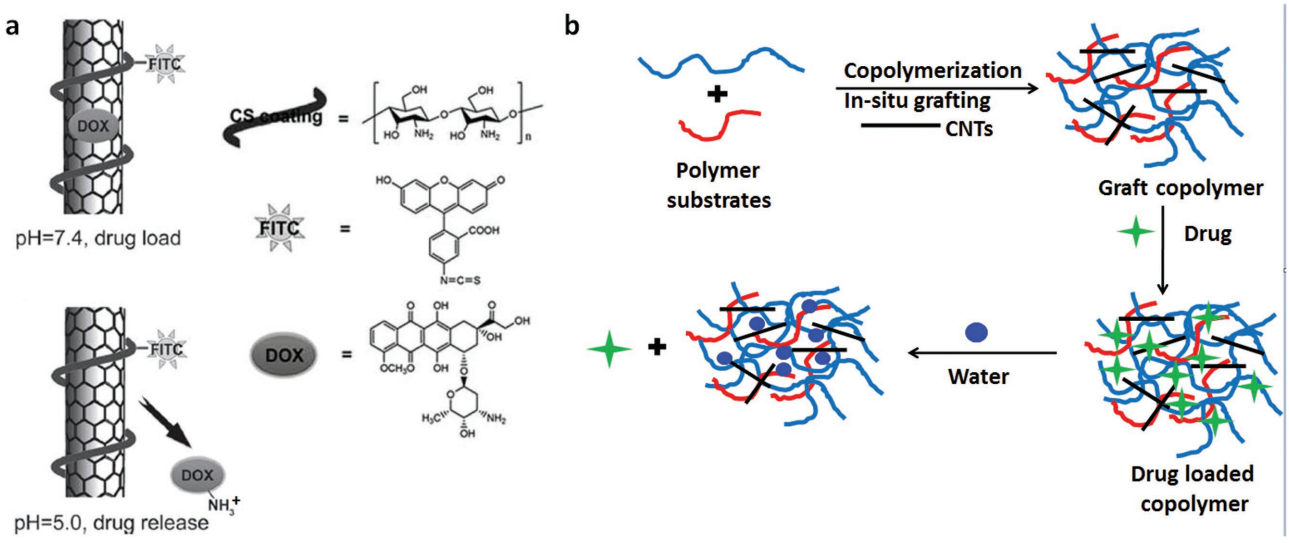

Figure 9. CNT-based drug delivery and release. a) Direct monitoring of DOX release route from carbon nanotubes in living cells, based on a dye labeling method. The dye fluorescein isothiocyanate (FITC) covalently attached to chitosan-coated carbon nanotubes (CS/SWNTs) monitors the nanotube location inside cells. DOX, emitting red fluorescence, was attached to the SWCNTs via π-stacking. pH-induced drug release is shown. Reproduced with permission.[59] b) CNT-based polymer membranes prepared through in situ grafting method for controlled drug release. Controlled release of the embedded drugs was achieved upon swelling of the copolymer matrix with water molecules.

short duration to induce disintegration of the hydrogel and consequent drug release; the incorporated CNTs aided the electrical stimulation and drug release.[64]

CNTs have also contributed to the burgeoning research in *gene therapy*. Therapeutically active oligonucleotides, including plasmid DNA (pDNA), small hairpin RNA (shRNA) small-interfering RNA (siRNA) and micro-RNA (miRNA), have all been used to either overexpress or inhibit expression of target proteins.[65] In particular, functionalization of CNTs with cationic groups has enabled delivery of negatively charged DNA into cells. In contrast to this well-known strategy for DNA delivery, other reported approaches utilized covalent attachment of linear pDNA to carboxylated MWCNTs.[66] The resulting bioconjugate was successfully transported into *Escherichia coli* cells and the transformed cells able to express green fluorescent protein, inspected manually on ampicillin agar plates.

DNA (e.g., gene) delivery is not only the most important but also the most problematic aspect of gene therapy. CNTs were applied for combined gene and drug delivery into human gastric cancer cells (**Figure 10**).[67] Synergistic cancer cell death was achieved by a targeted delivery system comprising B-cell plasmid lymphoma-extra-large (pBcl-xL)-specific shRNA and a very low DOX content, which simultaneously activated an intrinsic apoptotic pathway. Specifically, modified branched polyethylenimine (PEI) was grafted through a polyethylene glycol (PEG) linker to carboxylated SWCNTs. The SWCNT-PEG-PEI conjugate was covalently attached to an aptamer targeting overexpressed nucleolin receptors on tumor cell surface and loaded with the therapeutic drug DOX. Overall, this system revealed that a combination of shRNA-mediated gene-silencing strategy with chemotherapeutic agents constituted a valuable and safe approach for antitumor activity.[67] Similar positively charged functionalized polymeric units on CNTs were employed for docking genes and deliver them to cellular targets.[67,68] SWCNTs were also conjugated to small interfering RNA (siRNA) designed as a vehicle for gene therapy of pancreatic cancer.[69]

Recent studies have shown effective *protein delivery* into cells through coupling with CNTs. Chen et al. conjugated SWCNTs with therapeutic proteins[70]; the SWCNTs in that system served both as nanocarriers for the protein cargo as well as photothermal agents – generating heat following illumination with near infrared (NIR) light, cleaving the protein-nanotube bond, and releasing the protein. This strategy was demonstrated for delivery and NIR-activation of a therapeutic protein, saporin in living cells (**Figure 11**).[70] The activity of

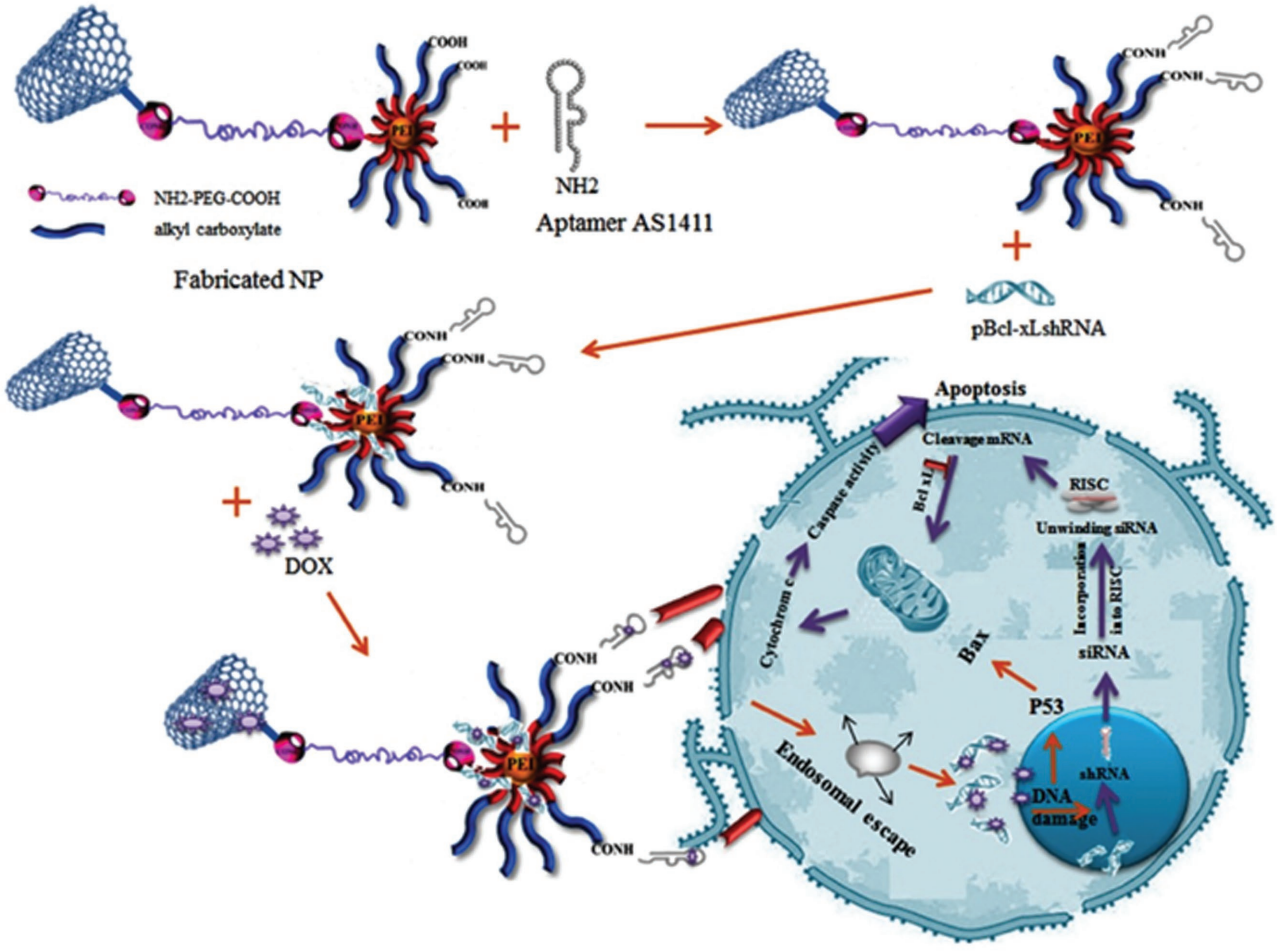

Figure 10. Gene and drug delivery mediated by CNTs. Modified branched SWCNT-PEG-PEI covalently attached to AS1411 aptamer as the nucleolin ligand to target the co-delivery system to the tumor cells. Reproduced with permission.[67] Copyright 2017, Elsevier Ltd.

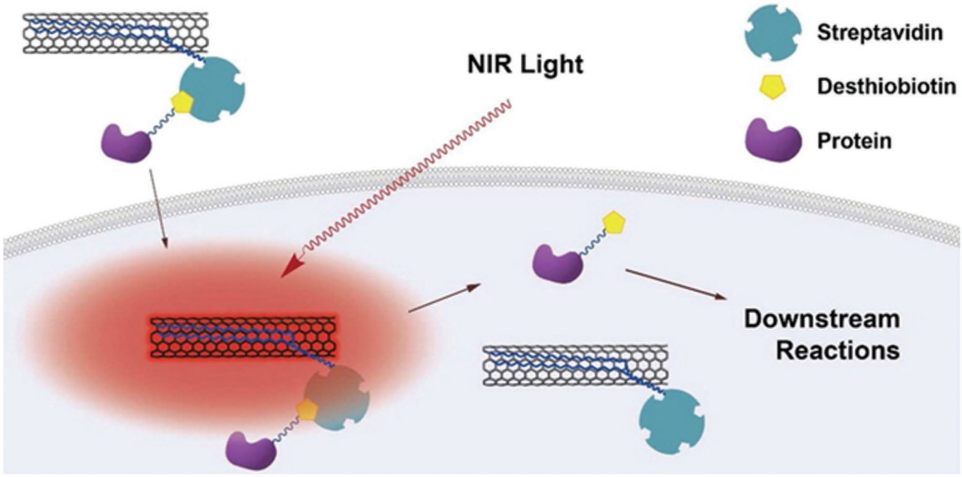

Figure 11. Photothermal activation of SWCNT-delivered proteins. A therapeutic protein is chemically conjugated onto the surface of SWCNTs via a desthiobiotin–streptavidin linkage. Following cell internalization, NIR irradiation generates localized heating and subsequent breaking of the protein-CNT bond. The released protein then carries out its therapeutic action inside the cell. Reproduced with permission.[70] Copyright 2016, American Chemical Society.

the proteins attached onto the SWCNTs was inhibited due to steric hindrance. However, once inside the cells, NIR irradiation cleaved the linkage between the protein cargo and SWCNTs. The released proteins became active and performed their cellular functions.

Ohta and co-workers have developed another multifunctional CNT-based carrier platform for drug and gene delivery.[71] In this particular system, the researchers PEGylated SWCNTs that were further modified with the cationic amphiphilic peptide, H-(-Lys-Trp-Lys-Gly)$_7$-OH [denoted as (KWKG)$_7$]. This treatment improved the solubility and stability of the composite in cell cultured medium.[71] The PEGylated peptide-functionalized SWCNTs displayed an extensive surface that could be employed for immobilizing of gene cargo.[71] Other examples of CNT-assisted protein delivery into cells were reported.[72]

2.3. CNTs in Photoacoustic Imaging and Phototherapy

Photoacoustic imaging is a new tissue imaging technique providing enhanced spatial resolution through generation of acoustic signals from light-absorbing molecules in biological systems.[73] In many instances, photoacoustic agents are additionally used to increase imaging contrast due to their specific photophysical properties (high molar extinction coefficient, peak absorption in the NIR window (620–950 nm), high photostability, and efficient conversion of heat energy to produce acoustic waves).[74]

CNTs might serve as useful photoacoustic contrast agents as they exhibit absorption peaks in the near infrared (NIR) spectral range and possess lower molar extinction coefficients than gold.[74] In particular, the electronic, and thus optical, properties of CNTs can be tuned through changes to the tube structure (for example, diameter and chirality).[74] CNTs functionalized with peptides,[75] dyes,[76] or silica-coated gold nanorods (sGNRs)[77] were used for photoacoustic tumor imaging. Specifically, bare SWCNTs generated transient photoacoustic signals due the rapidly cleared nanotubes, while SWCNTs coupled to the cyclic Arg-Gly Asp peptide (denoted SWCNT-RGD) bound to the tumor vasculature, generating a continuous photoacoustic signal from the tumor.[75]

SWCNTs coupled to an amine-reactive quencher (SWCNT-QSY) or indocyanine green (SWCNT-ICG) exhibited approximately two orders of magnitude greater photoacoustic contrast in vivo compared to bare SWCNTs. This observation was ascribed to the increase in the particles' optical absorption upon conjugation with the dyes[76] Furthermore, the excellent sensitivity was also aided by the affinity of the RGD motif to cancer-specific receptors in tumor-bearing mice. Cui and co-workers enhanced the NIR absorption of MWCNTs through covalent attachment of silica-coated gold nanorods (sGNRs).[77] The sGNR/MWCNT composite was further conjugated with the tumor specific RGD peptide successfully targeting gastric cancer cells in mice achieving strong photoacoustic imaging.[77]

Phototherapy encompasses light-triggered treatment for tumor ablation and growth inhibition via photodynamic therapy (PDT) and photothermal therapy (PTT). PDT utilizies photosensitized chemical agents responsible for cell toxicity, while in PTT, specific compounds absorb NIR irradiation to generate heat for thermal ablation of cancer cells. CNTs have attracted particular interest because of their extraordinary light-to-heat energy conversion efficiency with a high absorption cross-section of NIR light.[78] PTT applications were reported for bare CNTs[79–81] and CNTs coupled to tumor-specific Abs.[82] SWCNTs were applied as PTT agents together with anticancer drugs, DOX[80] and paclitaxel.[79] CNTs functionalized with noble metals[83] enhanced the photothermal efficacy presumably due to strong plasmonic coupling with the noble metal NPs. Synergistic effects for tumor therapy were reported both in case of PTT and PDT [mediated by the photosensitizer tetrahydroxyphenylchlorin (mTHPC)].[84] In this particular system, the mTHPC was quenched by the MWCNTs (probably due to a charge transfer) and inactivated in the extracellular medium, but once in the cytoplasm after endosomal uptake of the MWCNT complexes it was released and became active following 650 nm light irradiation.[84] Importantly, when CNTs

sequestered in the lysosomes were irradiated at 808 nm, local heating was generated, inducing cellular damage and apoptosis.

CNTs were also examined in photoacoustic imaging-guided phototherapy, which generally utilizes materials obtained by complexing photosensitizers with PTT nanomaterials. For example, SWCNTs coupled to indocyanine Green (ICG) and hyaluronic acid nanoparticles (HANP),[85] Chlorin e6 (Ce6)[86] or cyanine 5.5 (Cy5.5)[87] acted as photoacoustic imaging substances for guiding the particles towards the PTT targets. These new biocompatible materials allow complementary imaging modalities and improved tumor accumulation for PDT/PTT treatment compared to the components applied individually. Known magnetic resonance imaging (MRI) contrast agents such as gadolinium (Gd),[88] MnO with polyethylene glycol (PEG)[89] and Mn2+ (chelated with polydopamine–polyethylene glycol (PDA–PEG) polymer)[90] were also tagged with CNTs for tumor cell imaging.

2.4. CNTs in Tissue Engineering and Regenerative Medicine

The unique physico-chemical properties of CNTs make them good candidates for use as multi-functional nanomaterials in tissue engineering and regenerative medicine applications.[91] CNTs have been examined as useful platforms for improving the mechanical and electrical properties of artificial tissue scaffolds,[92–94] bone regeneration,[95] augmentation,[96] and cell stimulation actuators.[97] The addition of CNTs significantly improve the conductivity of gelatin methacrylate (GelMA) hydrogels[91,94] and chitosan-hydrogel,[93] improving the spontaneous beating frequencies and physiological functions of encapsulated cardiomyocytes. CNTs were used to increase the mechanical properties of gelatin nanofibers and scaffolds for myotubes (multinucleated cells, containing at least three nuclei), and upregulated the activation of mechanotransduction-related genes.[92]

Interesting applications of CNTs as components of scaffolds mediating cell stimulation have been described. Shin et al. seeded cardiomyocytes onto crosslinked gelatin methacrylate (GelMA) hydrogels reinforced with COOH-MWCNTs.[91] The researchers noticed a 3-fold enhancement in spontaneous beating frequency of the cardiomyocytes in comparison to GelMA-only hydrogels. Specifically, significantly low external voltage was sufficient to induce cell beating due to increased electrical conductivity of the hybrid hydrogels incorporated within the CNTs. These findings were attributed to the presence of aligned sarcomeric structures with tight intercellular junctions. In yet another study, incorporating of SWCNTs in gelatin/chitosan solutions improved the conductivity of hydrogels even at very low concentrations (<100 ppm), thereby aiding signal transmission, promoting functional maturation and synchronous beating of the cardiomyocytes.[95] Specifically, 3D porous chitosan frameworks with different contents of nanocrystalline hydroxyapatite and SWCNTs were fabricated to support the growth of human osteoblasts (bone-forming cells). Two types of SWCNTs were synthesized through arc discharge, with a magnetic field (B-SWCNT) and without (N-SWCNT), and were utilized for improved bone regeneration.[95] The presence of B-SWCNTs in chitosan nanocomposite had a considerable effect on osteoblast attachment and bone regeneration. This might be due to the small aspect ratios of the magnetically synthesized SWCNTs compared to their conventionally synthesized counterparts.

Bio-hybrid tissue actuators (**Figure 12**) constitute an interesting use of CNTs in tissue engineering.[97] In this work, an

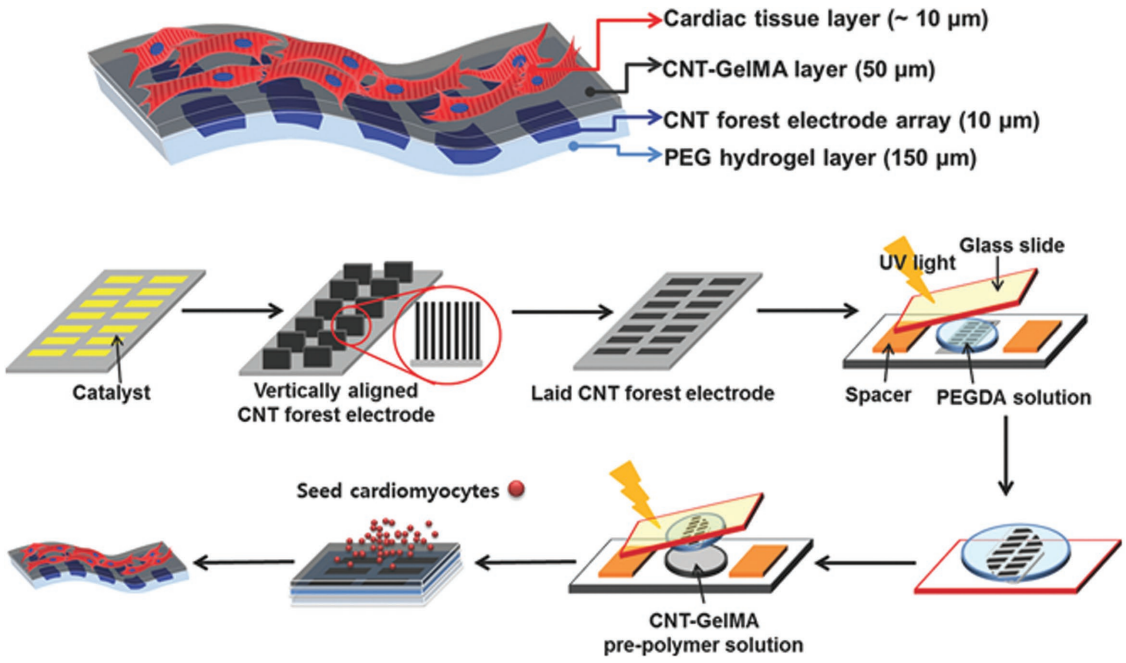

Figure 12. CNT-based tissue actuator. Vertically aligned "CNT forest" microelectrode arrays constructed on a Si substrate utilizing CVD method and used as the catalyst. The CNT forest/PEG hydrogel actuator was released from the Si substrate manually, and then placed over a CNT-methacrylol modified gelatin (GelMA) prepolymer. The final hybrid cell culture scaffold (50 μm thick), prepared upon the irradiation of UV light, which not only polymerized the gel prepolymer but also improved the attachment of CNT-GelMA to the underlying substrate. Reproduced with permission.[97]

aligned CNT "forest" microelectrode arrays were constructed and employed as scaffolds for cell stimulation. The aligned CNTs were embedded within flexible and biocompatible hydrogels exhibiting anisotropic electrical conductivity. Bio-actuators were engineered by culturing cardiomyocytes on the CNT microelectrode-integrated hydrogel constructs. The resulting cardiac tissue featured homogeneous cell organization with improved cell-to-cell coupling and maturation, and displayed outstanding mechanical integrity with incorporated microelectrode arrays and advanced electrophysiological functions exhibiting strong muscle contraction.[96] This centimeter-scale bio-actuator had an excellent mechanical integrity and was capable of spontaneous actuation behavior.[97] Such devices could be used in bio-robotics and drug screening applications.

Hanein and co-workers used CNT electrodes as conduits for retinal prosthetics.[98,99] Specifically, a semiconductor nanorod-CNT (NR-CNT) platform was prepared for wire-free, light induced retina stimulation.[98] CdSe/CdS NRs were covalently attached onto neuro-adhesive, three-dimensional CNT surfaces using polymerized acrylic acid. The interface provided highly efficient photosensitivity and enabled binding between the tissue and the optoelectronic device. The NR-CNT electrodes exhibited good efficiency (i.e., lower threshold for evoking action potentials), durability, flexibility, and demonstrated generation of localized stimulation. In particular, the capacitive charge transfer mechanism and low impedance of CNTs underlined the construction of an effective platform for efficient neuronal light induced stimulation.[98] In another study, the same group used CNT electrodes to stimulate retinal ganglion cells (RGCs) in a mouse model for outer retinal degeneration.[99] In this system, CNTs in the diseased retina enabled gradual remodeling of the inner retina, due to progressive increase of the coupling between RGCs and the CNT electrodes.[99]

Table 1 summarizes the reports discussed above concerning bio-applications of CNTs and their derivatives.

Table 1. CNT-based materials in biological applications.

	Carbon nanotubes	Ref.
1	CNT-based biosensors	
	Glucose biosensor	[13–19]
	Acetylcholine and organophosphates biosensing	[20–24] and [25–32]
	DNA biosensors	[34–41]
	Cancer biomarker detection	[45–52]
2	CNTs in drug and gene delivery	[56–72]
3	CNTs in photoacoustic imaging and phototherapy	[74–90]
4	CNTs in tissue engineering and regenerative medicine	[91–99]

3. Graphene-Based Materials for Biological Applications

Graphene is a single layer two-dimensional carbon nanomaterial exhibiting unique physicochemical properties, including high surface area, excellent thermal and electrical conductivity, mechanical strength, and ease of functionalization.[100] Graphene, graphene oxide (GO), and reduced graphene oxide (rGO) (**Figure 13**) are the most common graphene forms and have been used in wide range of applications. Pristine graphene (Figure 13a) is a single-crystalline lattice of sp^2-bonded carbon atoms adopting honeycomb-like patterns.[101] Polycrystalline graphene is composed of single-crystalline graphene grains of distinct orientations with a mosaic-like organization restricted by specific grain boundaries generating topological defects, generally termed dislocations.[102] Graphene oxide (GO) (Figure 13b) is a honeycomb lattice with sp^2-bonded carbon atoms incorporating sp^3 carbon "defects", displaying oxygen-containing functional groups, such as carboxyl groups exposed on the edges and hydroxyl and epoxy groups on the basal planes.[103] Reduced GO (rGO, Figure 13c) comprises of GO, reduced through chemical or physical methods.[104]

In contrast to pristine graphene, which is hydrophobic and thus not soluble in water, GO and rGO can be manipulated and made water-soluble, which is often crucial in biosensing and biological applications. The lateral size of these graphene derivatives modulates the capacity and kinetics of molecular adsorption.[105] Indeed, water solvation properties and varied surface functionalization routes have made GO and rGO promising platforms for biological applications. Furthermore, heterogeneous electron transfer (HET) kinetics of graphene derivatives are directly related to their oxygen content and the density of defect sites, which directly affect their

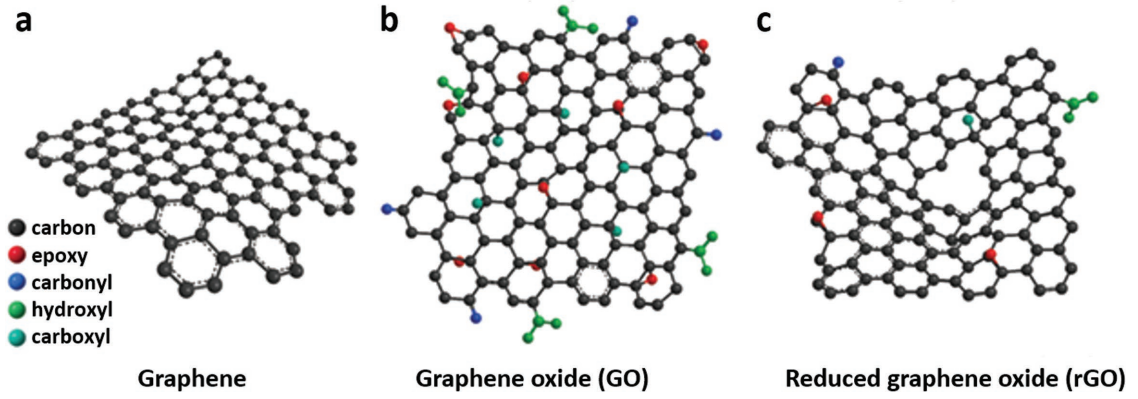

Figure 13. Graphene derivatives. Graphene (a), graphene oxide (b), and reduced graphene oxide (c).

functionalization efficiencies and thus contribute to their biomedical applicability.[106]

Most biological applications of graphene and graphene derivatives have been directed at *sensing*. This is mostly due to the unique physicochemical properties of graphene, particularly high surface area available for binding of target molecules, excellent conductivity providing a sensitive transduction mechanism, relative ease of functionalization, and feasibility of mass production. Below we summarize the main research avenues for graphene utilization.

3.1. Graphene-Based Biosensors

3.1.1. Glucose Biosensing

Graphene has been successfully employed as a component in *glucose* sensors, likely the most important biomedical sensing application. Graphene, in general, facilitates direct electrochemical conversion of glucose-oxidase (GOx), the enzyme at the core of numerous glucose sensors.[107] For example, researchers reported sensitive glucose biosensors based on direct electron transfer between GOx and electrode, GOx was either covalently attached or self-assembled upon the surface of electrochemically reduced graphene oxide (abbreviated as ErGO).[108] In those systems, the electron transfer properties of the rGO scaffold were readily tuned through the electrochemical reduction method thus enhancing the direct electron transfer between surface-immobilized GOx and the conductive substrate (GCE), in turn increasing the sensing performance.[108] Superior glucose sensing properties of nitrogen- and sulfur-doped graphene together with GOx was also reported.[109] The improved performance was ascribed to interactions between the N and S heteroatoms. Similar studies have focused on preparation of nanocomposites comprising graphene and conducting polymers. In particular, incorporation of graphene within polymer matrixes exhibiting hydrophilic groups could improve water solubility, enhance the electrical conductivity of graphene, and overall improve the activity of immobilized GOx.[110]

Researchers utilized Au-graphene nanocomposites as glucose biosensors.[111] Au NPs in such materials provided a suitable microenvironment to immobilize GOx and facilitate efficient electron transfer kinetics at the substrate/enzyme interface. Such nanocomposites were prepared either by covalent modification or by electrodeposition of Au NPs. Graphene composites comprising other types of nanoparticles have been developed, mostly designed to effectively immobilize GOx in glucose sensors, including MnO_2/rGO[112] and ZnO-rGO.[113]

Graphene-based field effect transistors (FETs) could be useful biosensing platforms as such devices transduce the enzyme recognition events to electrical signals with very high sensitivity.[114,115] Protein-encapsulated graphene based-FET enzymatic biosensors were reported for glucose sensing. For example, You et al. developed a CVD-grown graphene-FET enzymatic glucose biosensor that utilized silk protein as both device substrate and enzyme immobilization matrix. Through modulating drain-source current of the graphene-FET while sweeping the gate voltage, glucose levels could be continuously monitored.[114]

Graphene-metal hybrids constituted glucose sensors through surface-enhanced Raman scattering (SERS). SERS can enhance the "fingerprints" of target molecules interacting with metal composites' surfaces through both an *electromagnetic mechanism (EM)* and *chemical mechanism (CM)*. EM enhancement is usually obtained with electromagnetic "hot spots" exhibiting strongly enhanced local fields,[116] while CM is based on charge transfer and the mixing of molecular orbitals between adsorbed molecules and the SERS substrate.[116] Graphene or GO, in particular, has been shown to enhance SERS via CM due to the high affinity of probe molecules to the GO/graphene layer. For example, Gupta et al. constructed GO-Au/Ag-NPs as a SERS-active substrate for detection of glucose in blood samples.[117] The sensor further contained mercaptophenyl boronic acid (MBA) which contributed to sensitivity and selectivity through complexation between the boronic acid moieties and diol groups of glucose.

3.1.2. DNA Biosensors

Graphene has been used as a substrate for oligonucleotide immobilization and signal amplification in varied DNA-based biosensors. The considerable surface area of rGO enables high loading of single stranded DNA (ssDNA) probe at the electrode surface, and the high conductivity of graphene accelerates the electron transfer kinetics at the interface.[118–120] **Figure 14** illustrates the general fabrication process and sensing mechanism of such sensors. Specifically, electrochemically reduced GO (ErGO) coated conductive substrates are used to anchor the ssDNA probes.[119] Hybridization with the target DNA strain

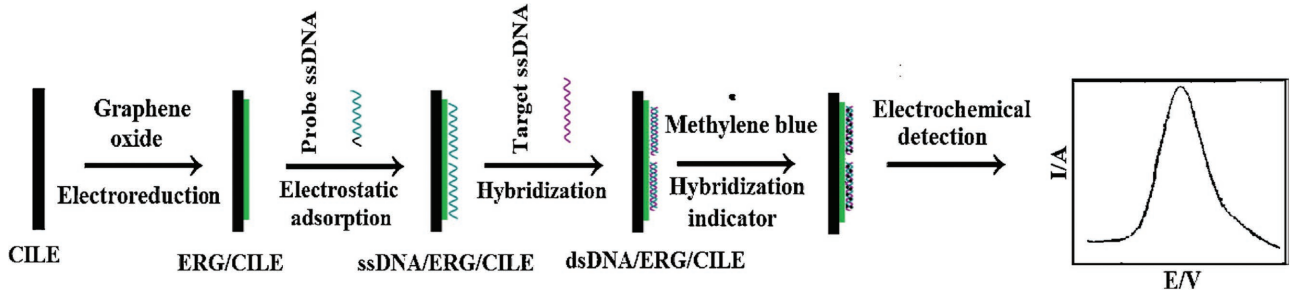

Figure 14. Fabrication of a graphene-based DNA biosensor. Immobilization of probe ssDNA on graphene-modified conductive substrate for the detection of target ssDNA by monitoring the indicator electrochemical response. CILE – carbon ionic liquid electrode, ERG – electrochemically reduced graphene oxide, ssDNA-single standard DNA, dsDNA -double standard DNA. Reproduced with permission.[119] Copyright 2014, Elsevier Ltd.

was monitored by measuring the response of electrochemical indicators, such as potassium ferri/ferro cyanide, methylene blue.

As an example, Sun and co-workers fabricated an electrochemical DNA biosensor for detection of ssDNA sequence related to transgenic maize, employing ErGO-modified carbon ionic liquid electrode (CILE) as the working electrode, and methylene blue (MB) as the hybridization indicator.[119] In this study, the ssDNA sequence was immobilized on the surface of an ErGO/CILE through electrostatic adsorption; indeed, the presence of ErGO increased the amount of probe ssDNA sequence adsorbed, thereby enhancing the sensitivity of biosensor. In yet another study, the probe ssDNA was covalently attached onto the ErGO, making possible sensitive detection of the target ssDNA of HIV-1 gene using $[Fe(CN)_6]^{3-/4-}$ as the hybridization marker.[118] Similarly, Liu et al. coated a GO/graphite fiber hybrid electrode with probe ssDNA through π-stacking interactions between the ssDNA bases and the hexagonal carbon units of GO.[120] In this example, the GO sheets were formed in situ upon the surface of the graphite fibers, in parallel displaying the probe ssDNA.

In some instances, signals emanating from graphene-based DNA biosensors have been amplified through co-addition of Au nanoparticles.[121] Au NPs have been used in such systems to amplify hybridization events of ssDNA through increased loading of probe ssDNA on Au NPs. Chen and co-workers have used N-doped graphene-Au nanocomposite for detection of the human multidrug resistance gene using MB as an electrochemical indicator.[122] Interestingly, N-doped graphene introduced "defect sites" upon the graphene surface to improve the electrocatalytic properties of the indicator at the interface.

An interesting signal amplification strategy was presented using Au nanocluster (NC)/graphene nanohybrids and exonuclease III (Exo III) enzyme-induced cascade.[123] Notably, the graphene-templated Au NC platform was superior to protein-templated AuNCs in electrochemical performance. Niu and co-workers coupled graphene to perylenetetracarboxylic acid diimide (PDI), a p-type organic semiconductor, also incorporating Au NPs.[124] PDI comprises a five-connected benzene ring (core) which bound graphene through π–π interactions, while the two positive side-chains (arms) acted as a bridge to graft AuNPs. The Au–PDI–graphene nano-hybrid exhibited high sensitivity DNA detection and mismatch recognition, and could detect the genetic trace of HIV-1.[124]

A "sandwich-type" DNA detection strategy has been developed, based on a capture probe immobilized on the surface of Au NRs attached onto rGO sheets (**Figure 15**).[125] Specifically, the target DNA strands hybridized with the reporter DNA probe were loaded onto Au NPs, resulting in the formation of capture probe-target DNA-reporter probe "sandwich complex". Voltammetry was used to interrogate the hybridization event by monitoring the peak current of an electrochemical indicator. Au NRs could offer enhanced sensitivity likely due to their capability in loading hundreds of reporter DNA probes. At the same time, the Au NR–rGO conjugates further increased the

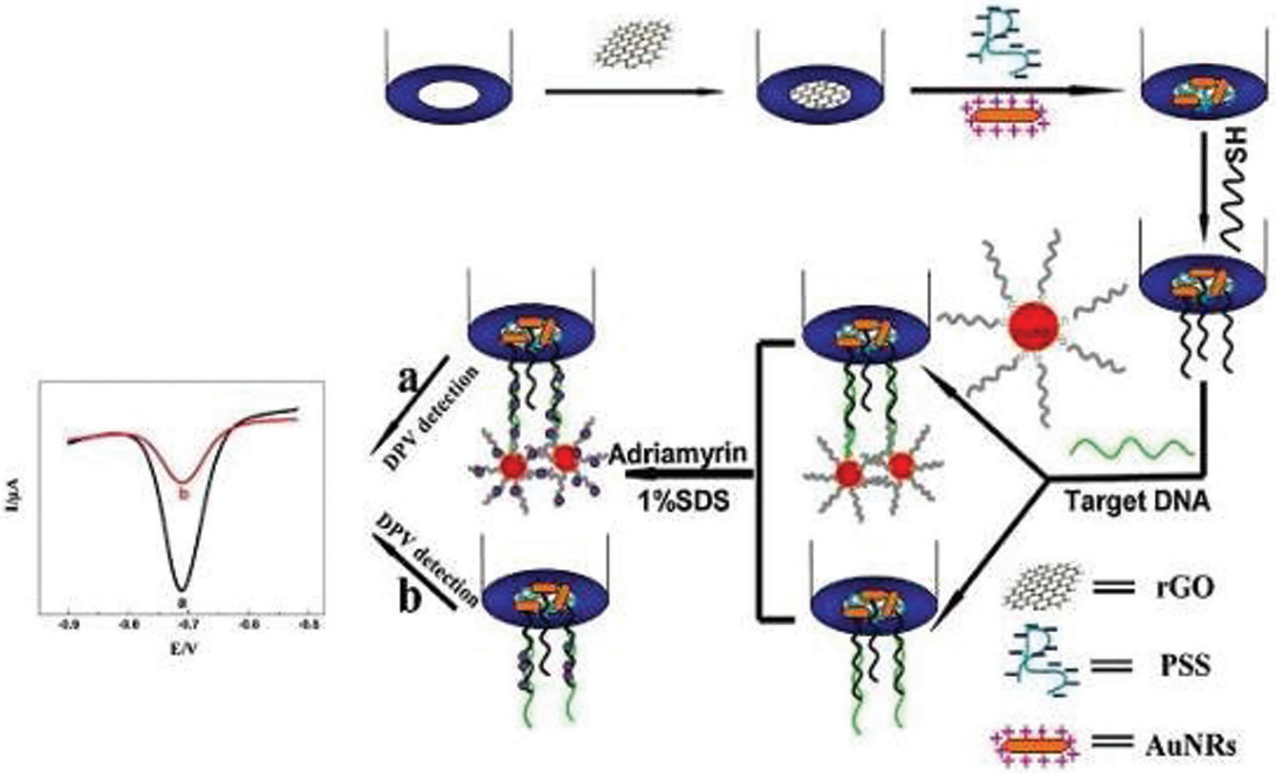

Figure 15. "Sandwich complex" DNA detection using rGO/Au nanorod (NR) composite. The capture probe was anchored onto the Au NRs–rGO through Au-S linkage. Following reaction of the target DNA with the capture and reporter probes a "sandwich complex" i.e., probe-target-reporter probe was formed. Reproduced with permission.[125] Copyright 2014, Elsevier Ltd.

sensor performance. Other self-assembled capture probes on graphene-gold nanocomposites were used in similar sandwich complex gene detection schemes.[126]

A novel biosensor for detection of specific DNA insertion sequences of *Mycobacterium tuberculosis* was developed using rGO–AuNPs as a sensing platform and Au NP–polyaniline (Au–PANI) as a tracer label for signal amplification.[127] In this construct, the rGO-AuNPs matrix was first assembled on a glassy carbon electrode (GCE), providing a large surface area for rapid and efficient electron transfer. The electrochemical signal generated by the Au–PANI nanocomposite following DNA hybridization enabled detection of *M. tuberculosis* with in a low detection limit. A similar PANI-aided rGO-AuNPs nanocomposite sensor for detection of oncogenes was reported.[128]

Zheng et al. fabricated an electrochemical DNA biosensor by exploiting the redox reaction of iron at the core of hemin (an iron-containing porphyrin).[129] The electrochemical transducing interface was formed on AuNPs and a hemin-functionalized rGO-modified GCE. A decrease in the voltammetric response was induced by hybridization between the target DNA and the immobilized probe DNA (pDNA), which consequently blocked the redox reaction of hemin.

Researchers have also used metal oxide NPs in the fabrication of DNA biosensors. Metal oxide NPs in many instances enhanced oligonucleotide hybridization upon the electrode surface. Specifically, NiO/graphene/ssDNA was shown to effectively detect the pathogenic bacterium *Salmonella enteritidis*.[130] Similarly, N-graphene/Fe_3O_4/ssDNA was used for detection of DNA sequences in blood plasma.[131] Similar to other graphene-based sensors discussed above, graphene contributed high conductivity and large surface area, important both for maintaining efficient electron transfer and for providing sites for the deposition of metal oxide nanoparticles. Graphene or rGO-FET biosensors have enabled label-free detection of target ssDNA. In such systems, hybridization induced sensor response through monitoring drain current or drain voltage.[132] Utility and sensitivity of such sensor platforms are related to high carrier mobility and ambipolar fields in graphene, large surface/detection area, and low intrinsic electrical noises.

DNA sensing avenues have been demonstrated via GO-induced fluorescence quenching.[133–135] Graphene-induced quenching has been ascribed to three possible mechanisms: Forster resonance energy transfer (FRET), surface energy transfer (SET), and photo-induced electron transfer. In a recent study, ssDNA *aptamers* served as the recognition elements together with aggregation-induced emission (AIE)-active probes as fluorescent indicators (**Figure 16**).[134] GO served in this system as a fluorescent quencher, overall yielding a label-free "turn-on" DNA sensor with high selectivity and sensitivity. Initially, the ssDNA aptamer (probe ssDNA, P1) and AIE probe formed a complex, resulting in fluorescence enhancement. Subsequent addition of GO significantly quenched the fluorescence of P1-probe complex, due to fluorescence energy transfer between the ssDNA aptamer and GO that exhibit pronounced binding and close proximity. However, in the presence of the complementary ssDNA target (T1), hybridization of T1 with P1 generated a rigid duplex structure (dsDNA, P1-T1), which weakened the binding between DNA and GO thus lowering the fluorescence quenching induced by GO.[134] GO-induced quenching was also employed as a key parameter in development of a sensitive and rapid method for detection of disease-related DNA.[135]

3.1.3. Graphene-Based Sensors for Other Biomolecular Targets

Graphene based materials have been used as *ethanol* sensors.[136–138] In such schemes, both electrochemical and electrochemiluminescence (ECL)-type detection methods have been used. In electrochemical sensing techniques, the electron transfer process of enzymatic reaction (involving alcohol dehydrogenase, denoted as *ADH*) is monitored and is correlated to ethanol concentration.[139] As an example, a graphene–Au nanorod (Au NR) nanocomposite, synthesized by a simple

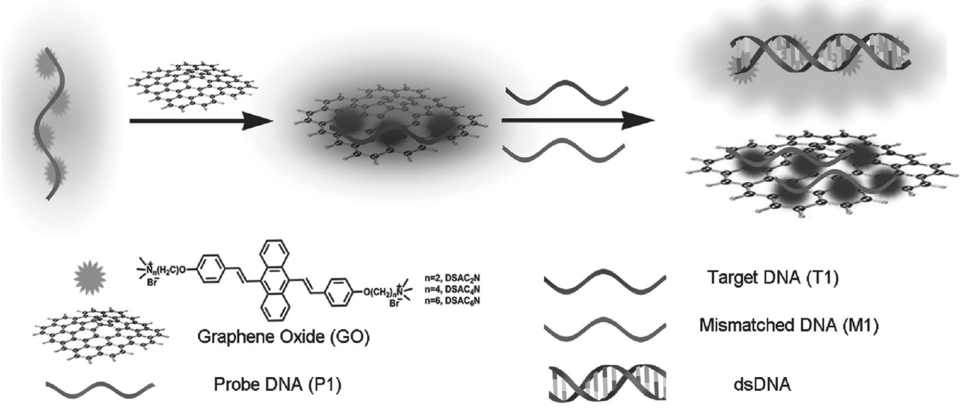

Figure 16. Fluorescence DNA graphene oxide sensing platform. The addition of ssDNA aptamer (probe ssDNA, P1) to an aggregation-induced emission (AIE) probe resulting in the formation aggregated complex of ssDNA aptamer and AIE (P1-probe complex) which enhances the fluorescence. Upon GO addition, the P1-probe fluorescence is quenched due to FRET between the AIE probes and GO. When the target ssDNA (T1) is present, the hybridization of T1 with P1 forms a rigid duplex structure (dsDNA, P1-T1), which weakens binding between the DNA and GO, thereby lowering the fluorescence quenching ability of GO. Reproduced with permission.[134]

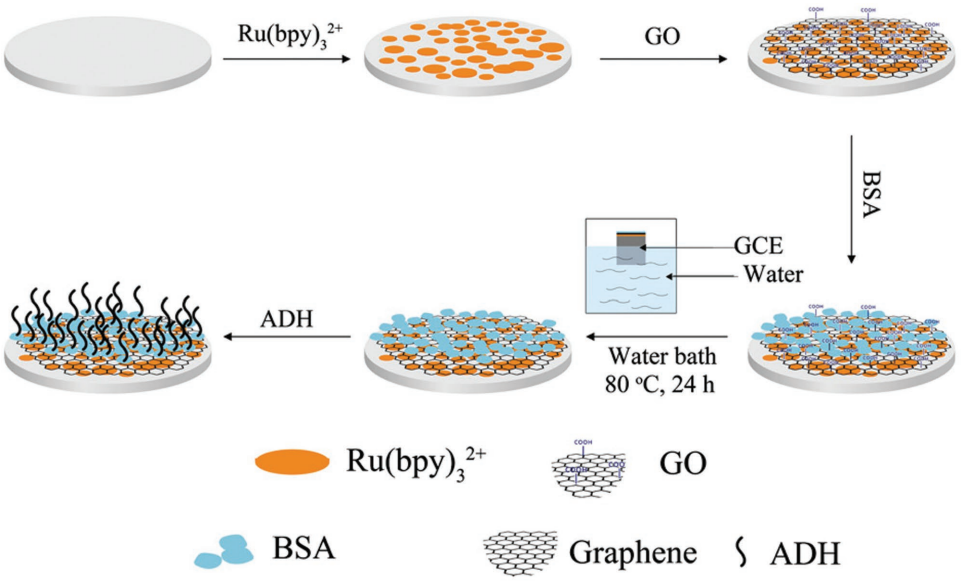

Figure 17. Electrochemiluminescence-based ethanol biosensor. Formation of ECL ethanol biosensor based on $Ru(bpy)_3^{2+}$-graphene/BSA composite film. Ethanol sensing is carried out through the release of $Ru(bpy)_3^{2+}$ from the nanocomposite, $Ru(bpy)_3^{2+}$/enzyme/rGO/bovine serum albumin (BSA). Reproduced with permission.[136] Copyright 2013, Elsevier Ltd.

self-assembly process, provided a suitable environment to retain ADH activity and facilitating the electron transfer process in the enzymatic reaction.[137]

ECL has been also used in conjunction with graphene in ethanol sensing. In its essence, ECL is a process of converting electrochemical energy into radiative energy on the surface of an electrode.[140] ECL has been mostly carried out by organic dyes such as tris(2,2′-bipyridine) ruthenium(II) $[Ru(bpy)_3^{2+}]$.[138] In this context, graphene can provide an effective platform for immobilizing ECL-active molecules.[136] Gao and co-workers fabricated an ECL-based ethanol biosensor based on $Ru(bpy)_3^{2+}$ and enzyme (ADH) immobilized upon a rGO/bovine serum albumin (BSA) composite film. In this case, the $Ru(bpy)_3^{2+}$ was used to increase the ECL signal while the enzyme was employed to attain selectivity towards the ethanol target. **Figure 17** depicts the stages of the ECL sensor construction, in which $Ru(bpy)_3^{2+}$, GO, BSA, and ADH were consecutively deposited upon the electrode.[136] In this example, graphene was prepared hydrothermal reduction of GO (at 80 °C for 24 h).

A similar ECL ethanol biosensor was developed by co-immobilizing the enzyme and $Ru(bpy)_3^{2+}$ on poly (3,4-ethylene dioxythiophene) and polystyrene sulfonate functionalized (PEDOT-PSS) graphene nanocomposite film.[141] In this specific example, positively charged $Ru(bpy)_3^{2+}$ was immobilized on the electrode surface through affinity to the negatively charged PSS. Moreover, the introduction of PEDOT, a conductive polymer, contributed to acceleration of the electron transfer.

Graphene-based materials have been used for detection of *organophosphates (OPs)*.[142–145] Specifically, electrochemical detection of OPs was accomplished by anchoring an enzyme (acetylcholine esterase denoted as AChE) onto Fe_3O_4/graphene[145] or ZnSe quantum dots/graphene-chitosan.[143] These AChE sensors functioned through inhibition of AChE electrochemical activity upon the reaction OPs, making the signal generated inversely proportional to OP concentration. In these systems, Fe_3O_4 or ZnSe quantum dots aided stabilization of the enzyme, while graphene enhanced electron transfer at the sensor interface, thus increasing sensitivity.

Lei and co-workers have reported an *esterase*-coated chitosan/AuNPs/graphene for selective detection of OPs in fruit.[142] Similar to AChE discussed above, inhibition of enzyme activity of plant esterase by OPs has been the sensing principle. Graphene facilitated effective electron transfer and electric conductivity in this sensing platform.[142] ECL and photo-electrochemical (PEC) biosensors were reported for OPs based on enzyme/graphene/quantum dot (QD) composites.[144] Here, rGO was used not only as a substrate to anchor the inorganic QDs and OP-specific enzyme (AChE), but also to significantly amplify the ECL and PEC signals.

3.1.4. Cancer Diagnostics

Carcinoembryonic antigen (CEA), a tumor marker, has been widely used for early recognition of lung cancer, ovarian carcinoma, breast cancers, and cystadenocarcinoma. Electrochemical immunosensors based on graphene derivatives were reported for the detection of CEA via the monitoring of antigen-antibody complexation. For example, Yu et al. have used rGO to immobilize the antibody directed against CEA together with AuNPs and poly(l-Arginine).[146] The combination ofvAuNPs high surface area, excellent electron transfer capabilities of rGO, contributed to high antibody loading upon the electrode surface and pronounced electrochemical responses.

Similar CEA detection schemes, based on anchoring of ultrathin Au-Pt nanowire-decorated thionine/rGO on the glassy carbon electrode (GCE) surface, were reported.[147] Samanman

et al. prepared sensing filaments through a layer by layer assembly, depositing thin films of silver, and then conjugating with a AuNPs-rGO-chitosan nanocomposite functionalized with anti-CEA antibody.[148] Under optimized conditions, the electrochemical response of silver was linearly related to the CEA concentration in the range of 1.0 fg to 1.0 ng·mL^{-1} with a detection limit of 0.1 fg·mL^{-1}. In another work, Au electrodes were initially altered with rGO-SWCNT-chitosan nanocomposite (Chi-rGO-CNTs) followed by electrodeposition of Au and Pt NPs, and then functionalized with anti-CEA antibody.[149] Kumar et al. reported a new graphene paper electrode built on PEDOT:PSS/rGO as a favorable alternative to expensive conventional electrodes (ITO, gold, or GCE).[150] Sandwich-type graphene-based immunosensors for CEA detection have been also reported. High-affinity antibodies and appropriate labels have been usually employed in such systems.[151] In particular, graphene or rGO sheets have been used both for immobilization of primary antibodies (Ab1) and as tracers for labeling the secondary antibodies (Ab2).[152]

A CEA sensor in which the graphene surface was altered with magnetic beads (MBs) that were labeled with CEA antibody (Graphene/MBs-Ab1) was reported.[153] Other sandwich-type architectures of graphene-based electrochemical CEA immunosensors were described.[154] In these systems, graphene could enhance the sensitivity through both conjugating recognition elements and increasing the electron transfer kinetics. The prostate specific antigen (PSA) is another important tumor marker, employed in prostate cancer diagnosis and screening. A methodology based upon highly conductive "wrinkled" rGO/AuNPs, utilized as a sensing element for PSA determination.[155] The 3D immunosensor displayed a linearity in the PSA concentration range of 0.5 to 10 ng·mL^{-1} with detection limit of 0.59 ng·mL^{-1}. Other graphene-based PSA sensors have been recently demonstrated.

A multiplex microfluidic chip combined with a GO-based Forster resonance energy transfer (FRET) approach to produce a screening assay for in situ detection of tumor cells was also described.[156] Particularly, a single fluorophore-labeled aptamer (FAM-Sgc8) was selected as a model of the 'signal-on' molecular probes due to its high affinity for CCRF-CEM cells. In the free state, the FRET probe of GO/FAM-Sgc8 showed a quenched fluorescence because of π–π stacking interactions, whereas in the presence of target cells, the interaction between FAM-Sgc8 and T-cell acute lymphoblastic leukemia cells (CCRF-CEM) cells was strong enough to discharge FAM-Sgc8 from GO consequently recovering the fluorescence.

3.2. Graphene in Drug and Gene Delivery

The biocompatible material, graphene/rGO/GO has been widely used as vehicle for the delivery of drugs/gens to the target site from locate of administration, because of its precise surface area of graphene and ease of polymeric alteration and, conjugation approaches.[157] For example, GO-sodium alginate (SA) conjugate was used as a carrier for the anticancer drug, DOX.[158] In this study, DOX was loaded onto the surface of GO-SA hybrid via pi-pi stacking and hydrogen-bonding interactions. High drug loading onto the carrier matrix and good release profile were achieved. In another study, GO modified with surfactants (hydroxyethyl cellulose-neutral and hydroxyethyl cellulose-anionic surfactant) via noncovalent attachment) was shown to improve the stability and dispersion of a GO-DOX composite under physiological conditions.[159]

DOX delivery has been also achieved by decorating rGO with antibodies or receptors. For example, an anti-human epidermal receptor 2 (anti-HER2) antibody-conjugated poly L-lysine functionalized rGO (anti-HER2-rGO-PLL) nanocarrierfor efficiently delivered DOX to cancer cells over-expressing HER2.[160] The combination of specific antibody and conjugation of PLL, a cell-penetrating peptide, lead to an excellent cell uptake. In a similar approach, folic acid (FA)-rGO (FA-rGO) loaded with DOX showed specific targeting to MDA-MB 231 cancer cells (expressing the FA receptor) and exhibited excellent drug-release efficiency.[161] In other studies, GO functionalized with lactobionic acid (LA), another cancer cell specific ligand, displayed targeting for cancer cells over expressing the ASGPR receptors.[162]

Chen and co-workers prepared a Fe_3O_4–PEG–GO nanocomposite, for both magnetic imaging and drug delivery.[163] The hybrid exhibited good physiological stability and did not adversely affect cell viability. Moreover, high loading of an anti-cancer drug (DOX) was achieved. Notably, the nanocomposite exhibited significantly improved T2-weighted magnetic resonance imaging (MRI) contrast compared to bare Fe_3O_4 NPs, ascribed to formation of Fe_3O_4 NP aggregates upon the GO sheets. In a similar approach, GO grafted with dendrimers capped with amino groups and functionalized with gadolinium diethylene triaminepentaacetate (Gd-DTPA) and an antibody targeted to prostate stem cell antigen (PSCA) was employed for targeting and MR imaging of cancer cells overexpressing PSCA.[164] Yet in another study, pH-responsive supramolecular polymeric shell around a mesoporous silica-coated magnetic GO (Fe_3O_4@GO@mSiO_2) was used for DOX delivery to cancerous tissue in a controlled manner. Fe_3O_4 endowed magnetic field sensitivity of the GO composite, designed to enable delivery DOX to target sites by application of external magnetic fields.[165]

Fluorescent manganese-doped zinc sulfide (ZnS/Mn) nanocrystals were covalently attached to GO-PEG for drug delivery and cell labeling.[166] Specifically, DOX was physically adsorbed onto the GO surface, while PEG enhanced the solubility and biocompatibility of the material. The fluorescent ZnS/Mn nanocrystals used label the HeLa cells.[166] Bare GO and hydroxyl-ethylated GO were used as delivery agents for the anticancer drug methotrexate (MTX).[167–169] MTX was loaded either through covalent bonding (via amide linkage)[167] or by noncovalent bonding,[168] and pH-based release mechanisms were demonstrated. Noncovalent bonding (via π–π stacking and hydrophobic interactions) between the drug cargo and GO was also reported.[169]

Graphene-based materials have been useful conduits for gene delivery.[170] In a representative study, GO-branched polyethylenimine (denoted as BPEI) fabricated through conjugation of low-molecular weight BPEI with GO improved DNA binding and condensation and transfection efficiency. The BPEI–GO hybrid was used as a delivery vehicle for siRNA. In another study, GO nanocarriers were conjugated by covalent linkage

or electrostatic interactions with varied cationic polymers and employed for delivery of plasmid DNA (pDNA).[171]

3.3. Phototherapy Applications of Graphene Derivatives

Graphene materials (GO, rGO, and GO composites) have shown promise as platforms for photothermal therapy (PTT), due to strong interactions with low-frequency photons at infrared frequencies. Graphene derivatives exhibit plasmonic effects upon NIR irradiation generating heat through plasmonic photothermal conversion.[172] GO systems implemented for PTT have included rGO nanomesh (rGONM) functionalized with polyethylene glycol (PEG), arginine–glycine–aspartic acid (RGD) recognition peptide, and cyanine 7 (Cy7).[173] In another study, peptide-conjugated polydopamine-modified rGO (pDA/rGO) was constructed, promoting a "bystander effect" (in which individual damaged cells transfer toxic signals to adjacent cells), and used as a conduit for cancer treatment using NIR-activated PTT.[174]

Lim and co-workers have used a gold nanoshells and nanorods coated with rGO that produce an enhanced PTT effect upon NIR irradiation.[175] Another group reports water soluble Cu_2O nanocrystal–rGO as cancer therapeutic agent.[176] The narrow direct band gap of Cu_2O (2.0–2.2 eV) made this material useful for killing cancerous cells under visible light irradiation. Functionalized rGO, gold nanostars (GNS), and doxorubicin (DOX) (denoted as rGO-GNS@DOX) have been developed for combined photothermal treatment and chemotherapy of metastatic breast cancer.[177] In this example, the NIR absorbance of rGO was enhanced by introduction of in the composite, which will certainly improve the PPT. Many more graphene based reports also available for PTT.

Combined photo acoustic (PA) therapy and PTT were employed by indocyanine green-loaded polydopamine-rGO (ICG-PDA-rGO) for cancer theranostics (e.g., therapy and diagnostics).[178] The nanocomposite induced local hyperthermia thereby killing breast cancer cells under NIR irradiation. In vivo GO-enabled PA imaging in tumor bearing mice was applied demonstrated significantly stronger PA signal than its controls (**Figure 18**). In another study, a theranostic probe Cy5.5-peptide-PEG-GO/Au was prepared through chemical conjugation, in which GO/Au facilitated strong NIR absorbance and higher photoconversion efficiency.[179] This probe possessed high tumor accumulation and significantly enhanced fluorescence and photoacoustic signals for in vivo cell imaging.[179] Recently, size-tunable rGO-coated gold superparticles (e.g., Au nanocrystals forming colloidal assemblies) (rGO-GSPs) were used for both photoacoustic imaging and enhanced photothermal therapy.[180]

3.4. Graphene Biomaterials in Tissue Engineering

Graphene, GO, rGO, and their composites further containing metals or polymers) offer exciting opportunities to stimulate cells in artificial scaffolds, primarily due to their tunable surface properties. In particular, the physicochemical properties of graphene-based materials intimately influence surface interactions of individual cells and cell populations.[181] Several studies explored applications of graphene or GO as substances for *bone*[182–184] and *neural*[185] tissue engineering. In a representative study, graphene constituted a platform for non-covalent display of osteogenic inducers, which accelerate stem cell growth.[182] The oxygen functionalities of GO facilitated differentiation the stem cells through intermolecular

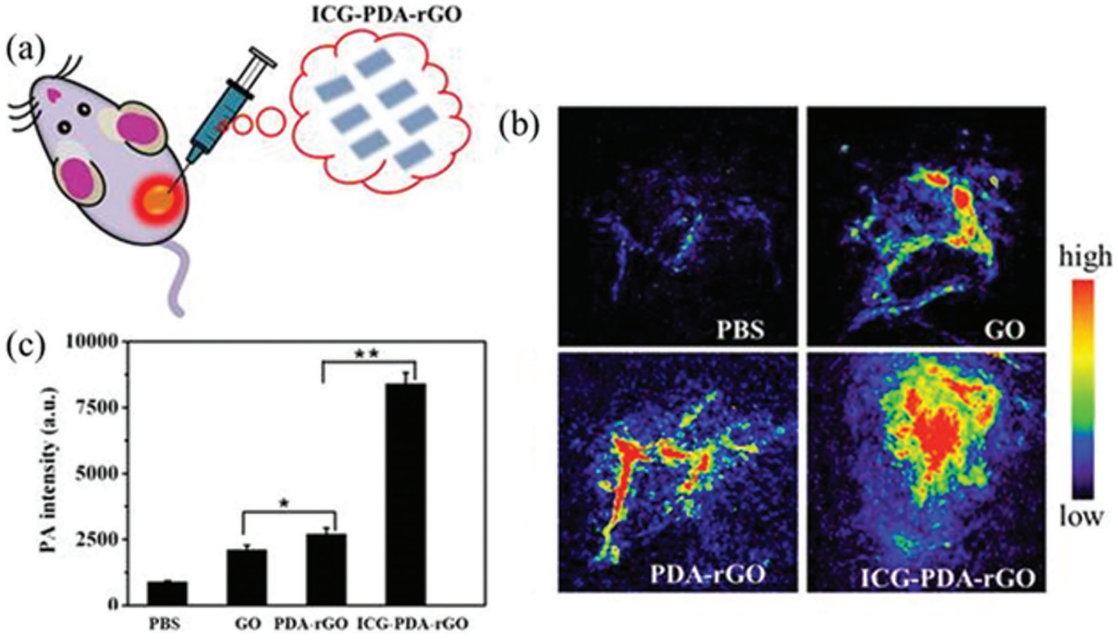

Figure 18. In vivo PA imaging of ICGPDArGO. In vivo PA imaging of tumor treated with PBS, GO, GO composites. Reproduced with permission.[178] Copyright 2016, Ivyspring.

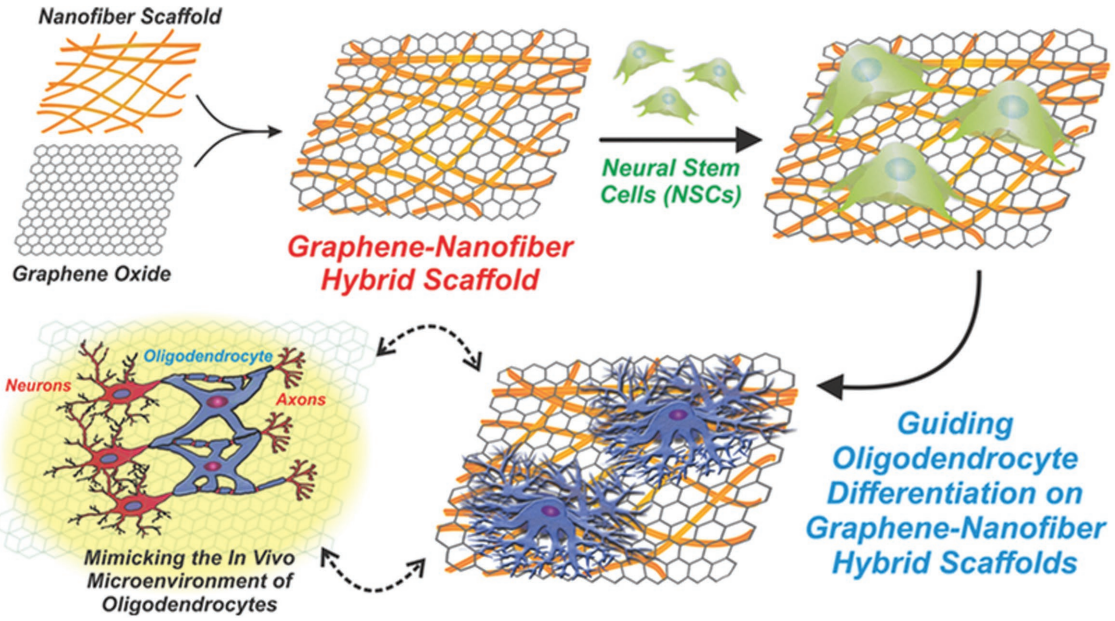

Figure 19. Graphene-nanofiber hybrid scaffolds for stem cell applications. Polymeric nanofibers (prepared by electrospinning) coated with GO and then seeded with neural stem cells (NSCs). NSCs cultured GO-hybrid scaffold enhanced the differentiation of stem cells into oligodendrocyte lineage cells. Reproduced with permission.[186]

interactions (π–π interactions, electrostatic attraction, or hydrogen bonding with cell proteins).[182]

Other interesting graphene nanostructures such as self-supporting graphene hydrogel (SGH) films were employed for rat bone regeneration, primarily due to the corrugated and porous surface of the material which exerted mechanical stimulation on the cytoskeleton.[183] In another study, graphene nanogrids prepared via unzipping of multiwalled carbon nanotubes were used as two dimensional selective templates for differentiation of human mesenchymal stem cells (hMSCs). This was presumed to occur through the induced mechanical stress upon the nanogrids.[184] In other approaches, polymer-functionalized GO could effectively induce stem cell growth, due to the synergetic effect of graphene and the macromolecules.[185] In these studies, biopolymers or synthetic polymers provided surface charge and different chemical moieties such as amine, carboxyl, hydroxyl, and sulfate on the graphene surface, which were important for cell growth and differentiation studies (via effective intermolecular interactions).

In an interesting application, GO-nanofiber hybrid scaffolds selectively guided differentiation of neural stem cells into mature oligodendrocytes, which are the myelinating cells of the central nervous system.[186] **Figure 19** depicts a GO-nanofiber hybrid scaffold composed of polycaprolactone nanofibers coated with GO and seeded with neural stem cells (NSCs). The NSCs cultured on the GO-nanofiber hybrid scaffolds exhibited enhanced stem cell differentiation into oligodendrocyte lineage cells. In this system, the synergetic effect provided by the three dimensional features of the nanofibers and the surface properties of GO were highly beneficial for protein adsorption and cell adhesion.[186] Other examples described growth of functional neural circuits upon graphene matrixes and improved neural performance and electrical signaling in the network through the interactions between graphene and neural stem cells.[187] **Table 2** summarizes the publications discussed above pertaining to biological applications of graphene-based nanostructures.

4. Graphene Quantum Dots and Carbon Dots

Graphene quantum dots (denoted GQDs, **Figure 20**a) and carbon dots (C-dots, Figure 20b) constitute a fairly novel class of zero-dimensional carbon nanostructures.[7,188] These carbon nanoparticles generally exhibit tunable photoluminescence (PL), low photo-bleaching, biocompatibility, and low cytotoxicity, making them viable alternatives to traditional fluorescent dyes, fluorescent proteins, and semiconductor quantum dots.[189] In particular, these features have made GQDs and C-dots useful and promising conduits for biological sensing and bio-imaging applications. In addition, the significant surface area and abundant edge sites contribute to efficient electron transfer

Table 2. Graphene-based nanomaterials for biological and biomedical applications.

	Graphene-based materials	Ref.
1	Graphene-based biosensors	
	Glucose biosensing	[108–117]
	DNA biosensors	[119–135]
	Graphene-based sensors for other biomolecular targets	[136–145]
	Cancer diagnostics	[146–156]
2	Graphene in drug and gene delivery	[158–171]
3	Phototherapy applications of graphene derivatives	[173–180]
4	Graphene biomaterials in tissue engineering	[182–187]

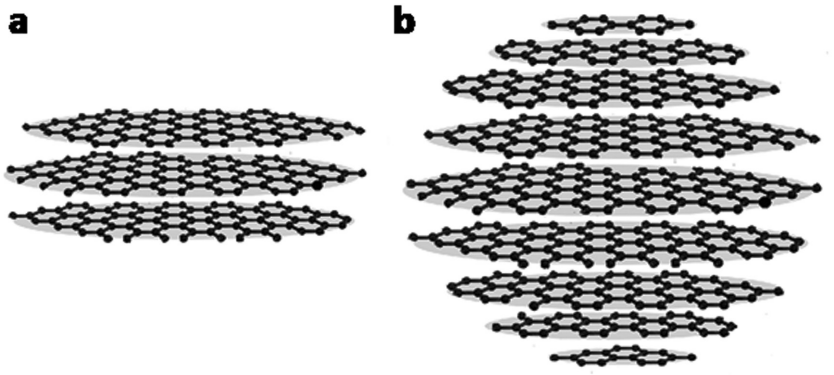

Figure 20. Structural features of graphene quantum dots (a) and carbon dots (b). The graphitic planes are shown.

processes upon GQD and C-dot surfaces, enabling their use in electrochemical sensing and electrocatalytic applications.

4.1. GQD- and C-Dot-Based Biosensors

4.1.1. Glucose Biosensing

Due to the biomedical importance of glucose sensing, many applications have been developed for using GQDs and C-dots as platforms for glucose detection. Qui et al. prepared boron-doped GQDs (BGQDs) through hydrothermal synthesis, and utilized these nanoparticles for selective detection of glucose through an aggregation-induced photoluminescence (PL) increase mechanism.[190] Specifically, rigid BGQDs–glucose aggregates were formed through binding between two cis-diol units in glucose and boronic acid groups upon the BGQDs' surface, restricting the intramolecular rotations and thereby enhancing PL intensity (**Figure 21**). Boronic acid functionalized GQDs, however, often suffers from lack of selectivity among saccharides (e.g., fructose, mannose, galactose, sucrose, lactose and maltose). To address this, Qu et al. prepared GQDs functionalized with phenylboronic acid (3-aminophenylboronic acid functionalized GQDs, e.g., APBA-GQDs.[191] Selective detection of glucose was accomplished through the APBA functional units and surface quenching states (SQS) induced mechanism.

PL quenching was the transduction mechanism in another study depicting C-dots prepared through the carbonization of citric acid and APBA as a passivating agent.[192] In comparison, PL *recovery* of C-dots passivated with 4-cyanophenylboronic acid (CPBA) was used for monitoring blood glucose.[193] Initially, CPBA passivation of the C-dots resulted in PL quenching via charge transfer from C-dots to CPBA; however, addition of glucose gave rise to modulation of electron distribution in the aromatic moiety of CPBA leading to increase of fluorescence emission.

C-dots were also functionalized with boronic acid for detection of glucose in blood serum samples (**Figure 22**).[194] In that study, the C-dots were prepared through hydrothermal carbonization of phenylboronic acid (Figure 22A). PL quenching occurred upon addition of glucose, due to the covalent binding between the cis-diols of glucose and boronic acid of the C-dot surface leading to intercalation among the particles

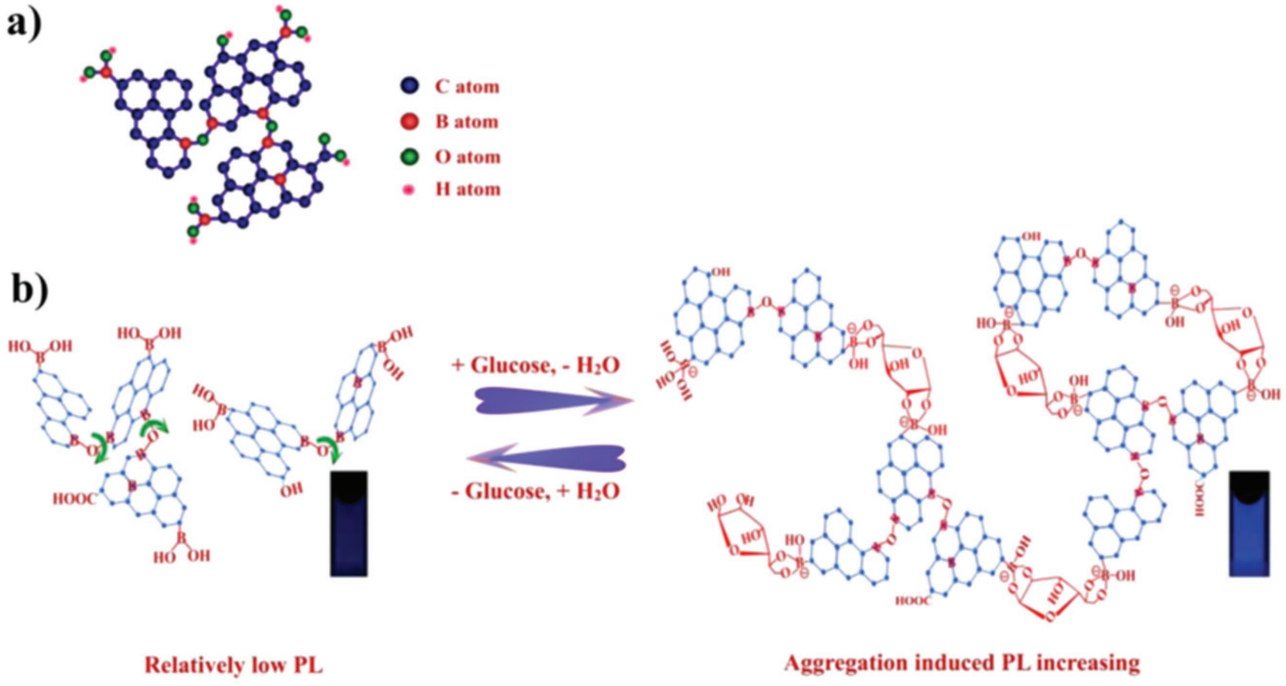

Figure 21. Boron-doped graphene quantum dots (BGQDs) for glucose sensing. a) Schematic structure of BGQDs; b) "Aggregation-Induced PL Increase" Mechanism for glucose sensing by BGQDs. Reproduced with permission.[190] Copyright 2014, American Chemical Society.

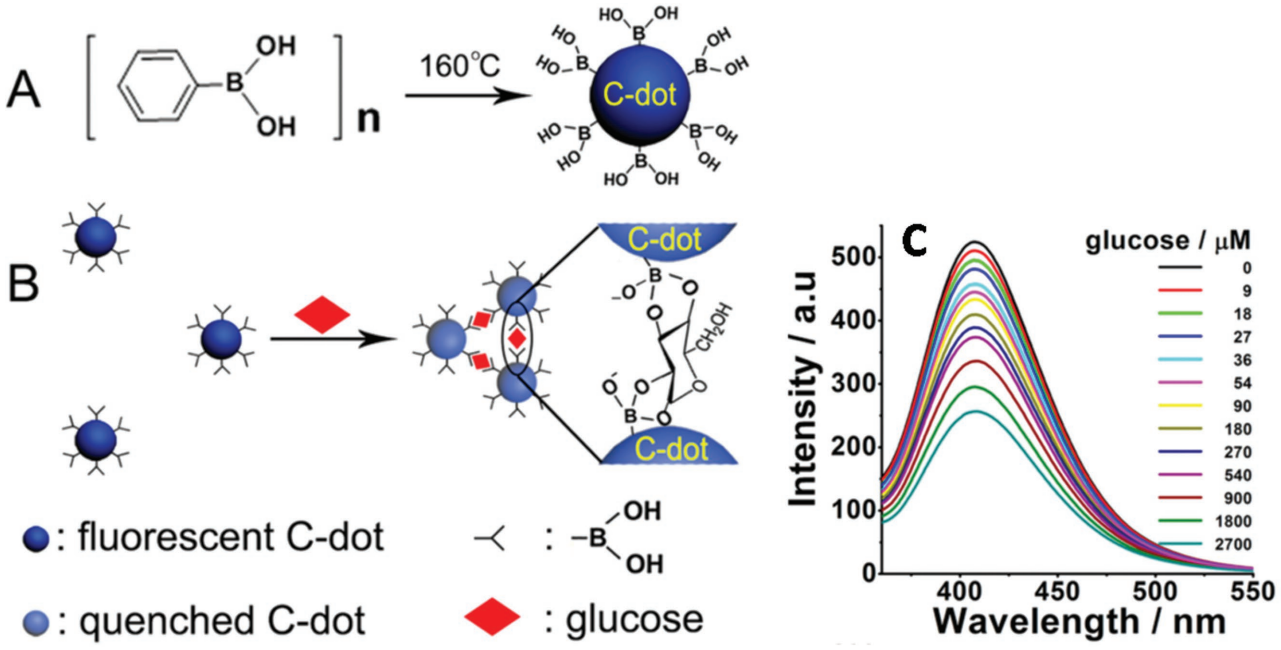

Figure 22. Glucose detection by C-dots prepared from boronic acid. A) Synthesis scheme of the C-Dots; B) Working principle of glucose sensing; intercalation of adjacent boronic acid-functionalized c-dots upon the addition of glucose results in fluorescence quenching; C) Glucose concentration-dependent quenching of C-dot fluorescence emission (excitation at 320 nm). Reproduced with permission.[194] Copyright 2014, American Chemical Society.

(Figure 22B). The covalent network gave rise to quenching of the C-dots' fluorescence as apparent in Figure 22C.

Using similar concepts, hemin-functionalized GQDs[195] and metalloporphyrin-functionalized GQDs[196] coupled to glucose oxidase (GOx) facilitated "on-off" glucose detection in serum samples. In both systems, hydrogen peroxide released following the reaction between GOx and glucose, disrupted the passivated GQDs' surface, resulting in fluorescence quenching (**Figure 23**). Specifically, in the hemin-GQDs catalyzed H_2O_2 reaction, free radicals (hydroxyl and carbon-centered radicals) were generated and induces further oxidation of surface passivated units of GQDs or destroy the passivation of GQDs, leading to significant fluorescence quenching of GQDs (≈86%). In the latter study, the metalloporphyrin induced PL quenching of the GQDs, as its absorbance band overlapped with the emission band of the GQDs; the "on" PL state was re-introduced upon reaction between H_2O_2 and metalloporphyrin to dipyrroles and monopyrroles.[196]

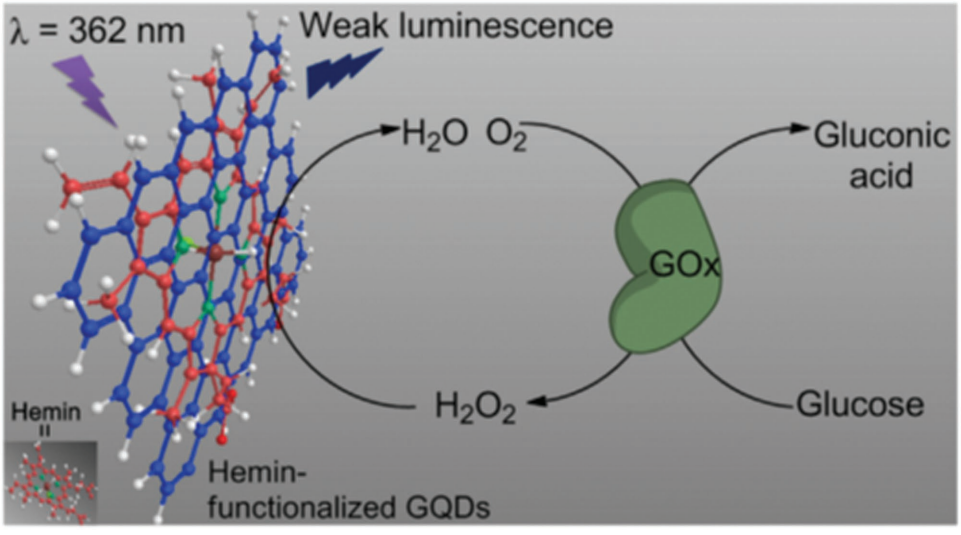

Figure 23. Hemin-functionalized GQDs for glucose detection. Hemin is attached to GQDs through electrostatic and π–π interactions. Hemin in the nanocomposite catalyzes H_2O_2 reaction with the GQDs (generated upon the reaction between glucose and glucose oxidase, GOx) generating free radicals, resulting in fluorescence quenching. Reproduced with permission.[195] Copyright 2014, Elsevier Ltd.

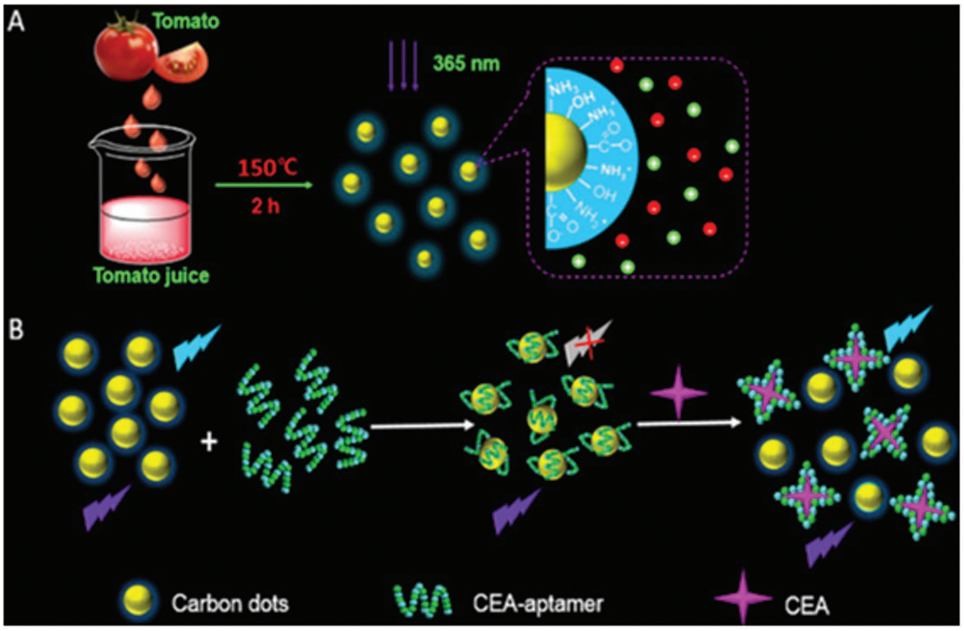

Figure 24. C-dot fluorescence sensor for CEA. A) Synthesis scheme showing the C-dots prepared from tomato juice as the carbon precursor. B) sensing strategy; the fluorescence of the C-dots was quenched upon surface binding of CEA-aptamer; addition of CEA gave rise to fluorescence recovery due to release of the CEA-aptamer from the C-dots through competitive binding. Reproduced with permission.[199] Copyright 2016, Elsevier Ltd.

In an interesting strategy, Zhou and co-workers immobilized C-dots onto glucose-imprinted polymer microgels and demonstrated continuous selective detection of glucose in physiological pH.[197] The glucose-imprinted microgels could reversibly quench the fluorescence signals of the embedded C-dots in response to glucose. In another investigation, GQD nanofibers, prepared through electrospinning of water-soluble GQDs with polyvinyl alcohol (PVA), was utilized for glucose and H_2O_2 detection.[198] The sensing modality was based upon quenching of the GQDs' upon addition of glucose or H_2O_2.

4.1.2. Biomarker Detection

Several types of immunosensors based on C-dots and GQDs have been developed for disease diagnosis. Miao and co-workers prepared COOH-functionalized C-dots through carbonization of tomato juice, and coupled them to aptamers recognizing the carcinoembryonic antigen (CEA), a cancer biomarker (**Figure 24**).[199] In the experiment, the CEA-aptamers were attached onto the C-dots through pi-pi stacking, giving rise to fluorescence quenching. Binding of the CEA to the C-dot-displayed aptamers caused their detachment from the C-dots and concomitant recovery of the C-dots' fluorescence (Figure 24B). This scheme produced continuous, sensitive, and recyclable CEA assay.

A ratiometric nanoprobe was prepared by chelation of Tb^{3+} ions with carboxyl and amine groups upon C-dots' surface, employed for detection of an *anthrax* biomarker, dipicolinic acid (DPA).[200] In this study, prior to DPA addition, the emission spectrum was dominated by the band of C-dots; however

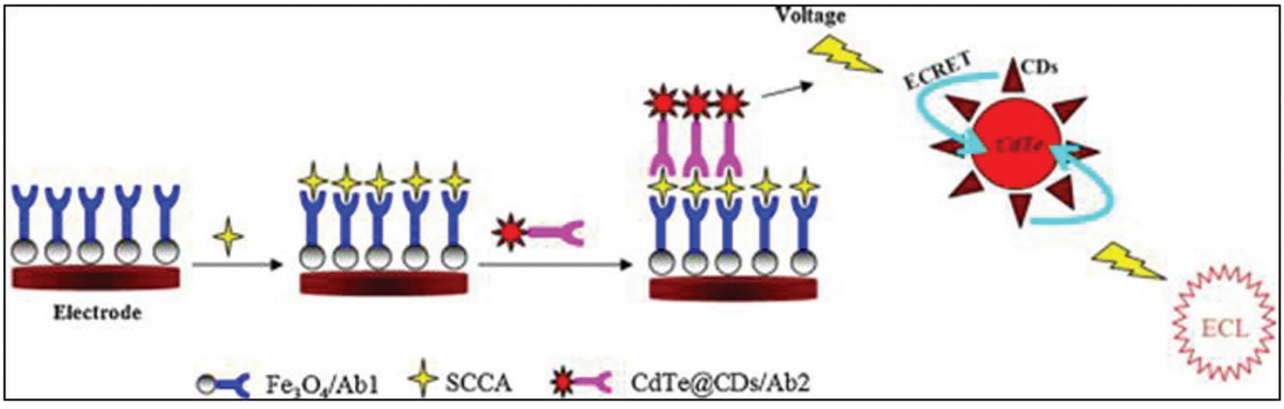

Figure 25. C-dot/nanoparticle ECL for detection of cancer biomarkers. Ab1 was immobilized on a conductive substrate via Fe_2O_3 and Ab2 functionalized with the ECL label CdTe@C-dots. Signal transduction was based upon SCCA sandwich between the two antibodies. Reproduced with permission.[203] Copyright 2014, Elsevier Ltd.

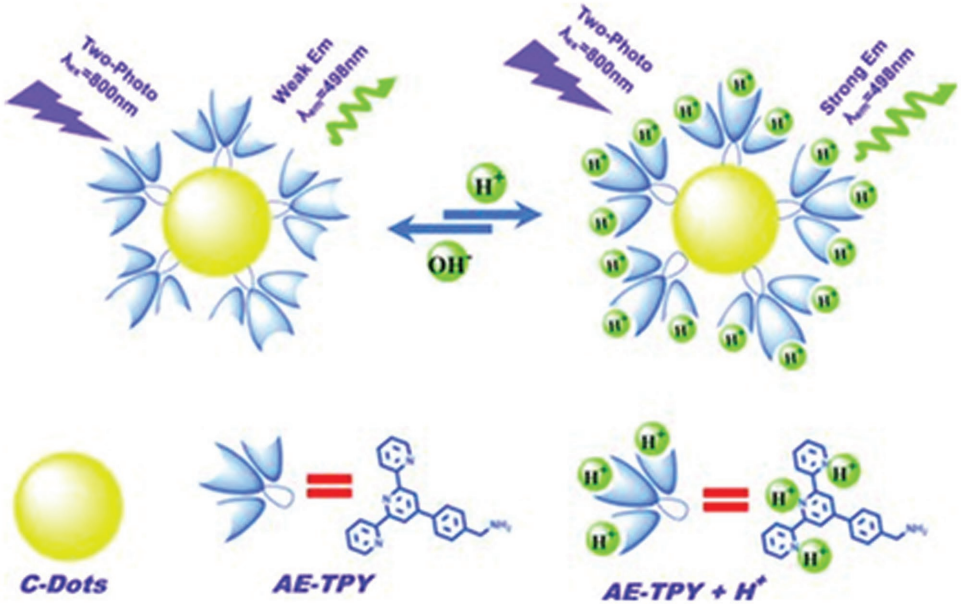

Figure 26. pH sensing by functionalized C-dots. The receptor AE-TPY is bound onto the C-dots through condensation reaction. N atoms upon the C-dots' surface participated in protonation/deprotonation, leading to modulation of C-dots' emission. Reproduced with permission.[208]

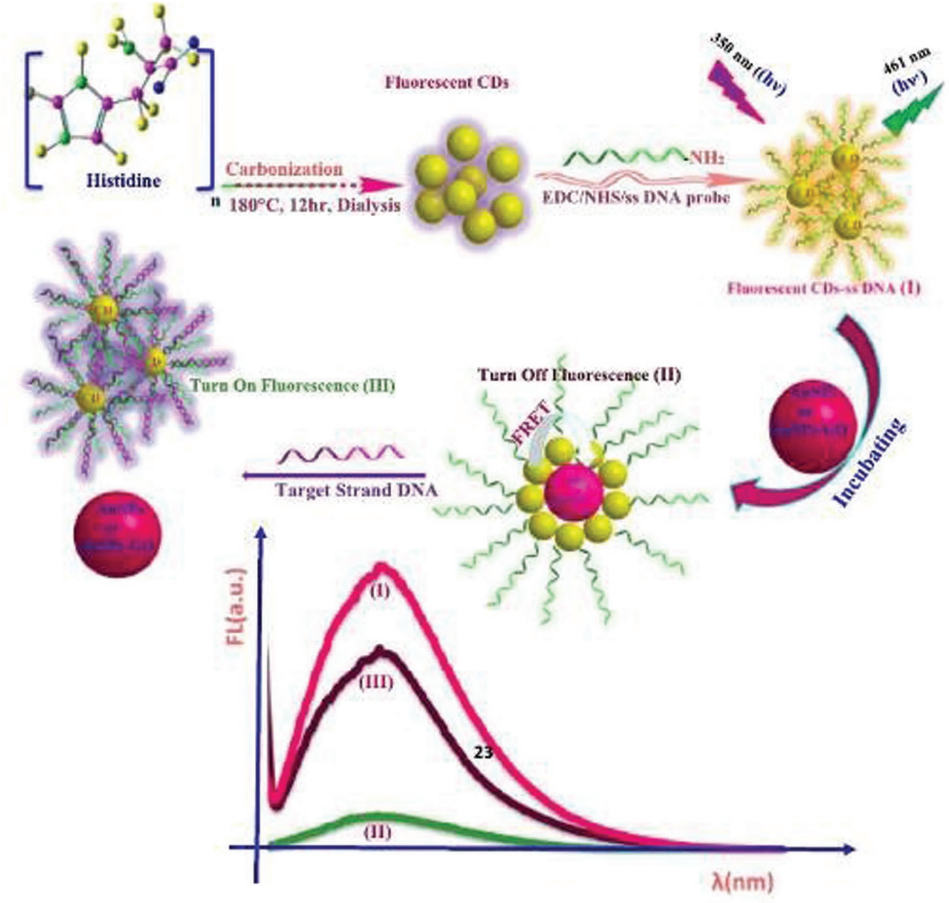

Figure 27. DNA detection by C-dot/AuNPs. The PL of C-dots, prepared upon the carbonization of histidine and further coated with probe ssDNA is quenched upon addition of AuNPs. The C-dots' fluorescence can be recovered in the presence of target ssDNA. Reproduced with permission.[219] Copyright 2017, Elsevier Ltd.

as C-dots and DPA excite with the same wavelength, the emission intensity of the Tb^{3+} ions was enhanced though energy transfer from DPA, in the presence of the marker. The fluorescence peaks of C-dots in aqueous solution were unchanged as a reference, while the Tb^{3+} ions exhibited enhanced fluorescence emission upon binding of DPA, enabling ratiometric DPA detection. A similar detection concept was reported in which Eu^{3+}-functionalized GQDs, prepared through chelation of Eu^{3+} ions onto carboxyl and amine groups upon the GQDs' surface, were used for DPA detection.[201] A rapid and sensitive immunoassay was developed for detection of ovarian cancer biomarkers through chemiluminescence resonance energy transfer (CRET). In the experiment, signal transduction was based upon CRET from a chemiluminescent reagent (luminol) to the GQDs.[202] GQDs offers various advantages, as the energy acceptor avoids the photo-bleaching problem, which is usually associated with organic dyes, and enables efficient energy transfer.

Electrochemiluminescence (ECL) sensors utilizing GQDs or C-dots have been developed for detection of cancer biomarkers. While GQDs and C-dots generally generate weak ECL signals, their coupling to metal or semiconductor NPs enhances their ECL signal through enrichment of C-dots concentration. In a representative example, C-dots/CdTe were synthesized, designed to serve as ECL labels for the sensitive detection of squamous cell carcinoma antigen (SCCA), a cancer biomarker, through electrochemiluminescent resonance energy transfer (ECRET) (**Figure 25**).[203] Specifically, C-dots/CdTes were immobilized on a carrier antibody (C-dots/CdTe@Ab2) for capture of the SCCA antigen in solution. The SCCA was "sandwiched" between Ab2 and another antibody, immobilized on Fe_2O_3-modified electrode (Fe_2O_3 NPs/Ab1). Electrochemically excited species (C-dots/CdTes) emit luminescence upon the recognition SCCA by both the Abs, as shown in Figure 25.[203] In the presented work, two Abs have been used to enable the sensitive detection of biomarkers, one that is Ab2, used to pre-concentrate the antigen and other one that is Ab1, immobilized on the electrode surface for transduction of antigen-Ab2. In addition, both Abs were immobilized on NPs to enhance the sensitivity through enrichment of Abs surface concentration (intern increase the antigen-antibody interaction) and C-dots (which leading to enhance the ECL signal).

In another example, like C-dots, GQDs have been also employed as ECL labels for *cancer* biomarker detection through the above explained mechanism.[204] In the experiment, GQDs assembled PtPd NPs, used as ECL label, to enhance the ECL biosensing performance and Au-Ag NPs, used to modify the electrode substrate to increase the electrochemical reaction.[204] Specifically, the recognition layer constitutes PtPd NPs, employed to enrich the concentration of GQDs to enhance the ECL signal, and Au-Ag NPs which enhanced the electrochemical reaction.

4.1.3. Detection of Metal Ions and pH in Biological Systems

C-dots constitute both efficient electron donors and electron acceptors, enabling detection of metal ions and pH through electrostatic attraction. In particular, functional groups upon C-dots' surface (formed either by carbonizing the carbon precursor containing specified functional groups, or by chemical coupling of desired functional groups after C-dot synthesis) have distinctive affinities to different target metal ions and pH, which results in modulation of the C-dots' fluorescence. Numerous reports of such ion and pH sensors have appeared in the literature. As an example, a fluorescent sensor was demonstrated for intracellular detection Cu^{2+} by C-dots synthesized from citric acid and polyethylenimine (PEI) as carbon precursors via a one-step microwave method at low temperature.[205] In the experiment, the amine groups on the C-dots' surface retained their Cu^{2+} recognition capabilities, quenching the C-dots' fluorescence following addition of small amounts of Cu^{2+} ions. Such quenching can be ascribed to electrostatic interactions between Cu^{2+} and negatively charged residues upon the C-dots' surface, leading to chelation and aggregation of the dots. Cu^{2+}-mediated aggregation and quenching of C-dots' fluorescence was used as a vehicle for copper ion sensing in rat brain's striatum.[206]

C-dots derived from various starting materials were used to detect different ions in physiological solutions and cells, including Hg2+, Ag2+, Cr3+, Fe3+, K+, Cl-, and H+.[205,207] The ion detection mechanisms are similar, involving quenching of the C-dots' PL via electron or energy transfer mechanisms. C-dots have been also employed as pH sensors in living cells and tissues. Tian and co-workers synthesized aminomethylphenylterpyridine (AE-TPY) C-dots to probe pH changes in physiological conditions.[208] The sensing mechanism relies upon PL quenching through the interaction of protons with the surface groups of C-dots (**Figure 26**). In particular, pH sensing in that system exploited two-photon fluorescence (TPF) induced by near infrared (NIR) excitation. Importantly, this C-dot sensor was successfully applied in living cells and tumor tissues.

A multicolor-emitting block copolymer-integrated graphene quantum dots (bcp-GQDs), prepared through

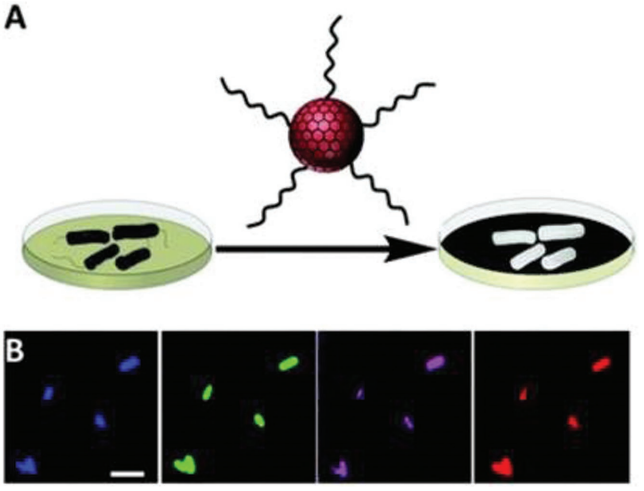

Figure 28. Amphiphilic C-dots for labelling of bacterial cells. A) The bacterial detection scheme. Bacteria were grown in a medium containing amphiphilic C-dots which were inserted into the cell membrane, enabling visualization of the bacteria through fluorescence microscopy. B) Multicolor fluorescence confocal microscopy images of *E. coli* bacterial cells recorded at different excitations (blue-365 nm, green-470 nm, magenta-510 nm and red-540 nm). Scale bar corresponds to 5 µm. Reproduced with permission.[221] Copyright 2015, The Royal Society of Chemistry.

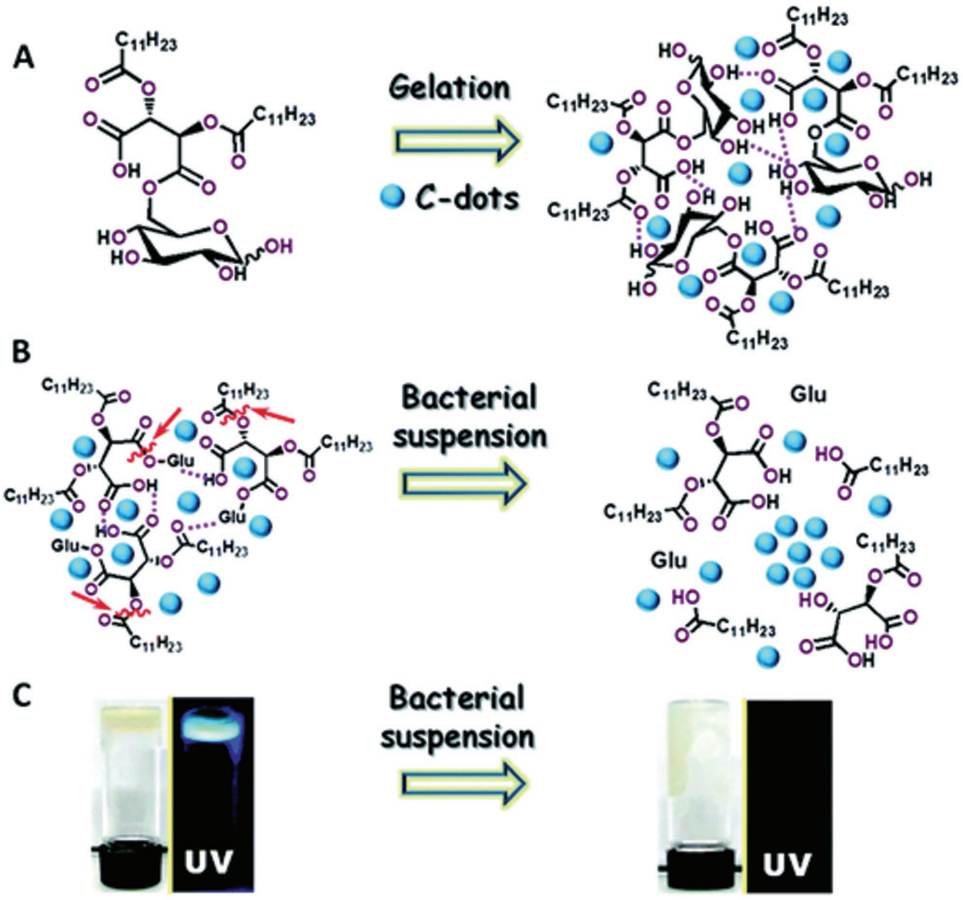

Figure 29. C-dot–hydrogel for bacterial detection. A) The hydrogel was prepared through gelation of an amphiphilic glucose precursor together with C-dots; (B) The fluorescence of the embedded C-dots was quenched upon addition of bacteria due to enzymatic cleavage of ester bonds and consequent aggregation of the embedded C-dots; (C) Digital photographs depicting the hydrogel before and after the addition of bacterial cells, showing fluidization of the gel and concomitant fluorescence quenching. Reproduced with permission.[222] Copyright 2017, The Royal Society of Chemistry.

grafting of blue-emitting thermally responsive block copolymer onto green-emitting GQDs, was employed for simultaneous sensing of temperature, pH, and metal ions.[209] In the experiment, sensing was accomplished through monitoring Förster resonance energy transfer (FRET) between the bcp (emitting in blue) and GQDs (exhibiting green emission), which was dependent upon the different types of stimuli.

Numerous C-dots-based sensors have been reported for detection of diverse biomolecular targets. A C-dot-based ratiometric sensor has been developed for detection of riboflavin.[210] other studies reported the fluorescence turn-on or turn-off C-dots based sensor for the detection of cysteine,[211] dopamine,[212] ascorbic acid,[213] bisphenol,[214] glutathione,[215] guanine,[216] hydroquinone,[217] and chelostral.[218]

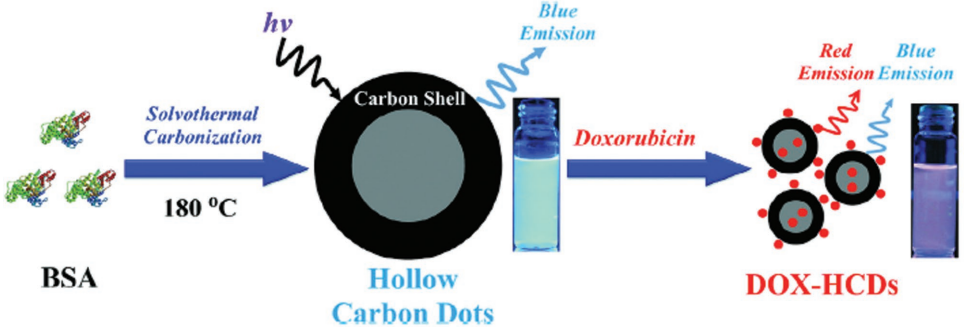

Figure 30. Drug delivery employing hollow C-dots. Hollow C-dots, synthesized through solvothermal carbonization of bovine serum albumin (BSA), used for uploading a drug cargo [doxorubicin (DOX)]. The DOX/C-dot composite particles emitted both in blue (C-dots' fluorescence) and red (DOX fluorescence). Reproduced with permission.[224] Copyright 2013, Elsevier Ltd.

4.1.4. Biosensing of Oligonucleotides

Interactions of specifically designed C-dots with oligonucleotides which result in fluorescence modulation made possible use of C-dots as conduits for DNA sensing. Ultrasensitive detection of DNA sequences related to HIV was accomplished through FRET between C-dots and AuNPs (serving as quenchers) (**Figure 27**).[219] In the experiment, the PL of C-dots functionalized with a probe ssDNA was quenched upon addition of AuNPs through FRET. Recovery of the PL was achieved upon exposure of C-dots-probe ssDNA/AuNps to target ssDNA, affected by dissociation of C-dots-duplex DNA and AuNPs, due to the strong electrostatic repulsion between the negatively charged duplex DNA and AuNPs.

C-dots, prepared though microwave treatment of banana peels, were used as reducing agents and stabilizers of a Pd/Au/C-dot nanocomposite. This material was used for electrochemical detection of *colitoxin* DNA in human serum.[220] Specifically, the probe-DNA was immobilized on the Pd-Au@C-dots through covalent bonding between COOH groups upon the C-dots and the probe DNA which was NH_3^+-terminated. Methylene blue (MB) was used as an electrochemical indicator for monitoring the hybridization between the probe DNA and target DNA.

4.1.5. Bacterial detection

Bacterial cells have been shown to modulate the fluorescence properties of C-dots, opening the way for innovative bacterial sensing strategies. Nandi et al. synthesized amphiphilic C-dots functionalized with hydrocarbon chains for the detection of bacterial cells such as *E. coli*; *S. typhimurium*; *P. aeruginosa*; and *B. cereus*.[221] In the experiment, both the intensity and shift of the C-dots' fluorescence emission were significantly modulated upon insertion of the C-dots into the bacterial cells' membranes, making possible bacterial detection through fluorescence spectroscopy or microscopy (**Figure 28**). Distinct binding profiles of the amphiphilic C-dots have been observed with each bacterial strain, accounting for the different cell surface properties (i.e., different lipid compositions, molecular organization, and macroscopic structures).

In another study, bacterial detection was achieved by employing a hydrogel embedding C-dots (**Figure 29**).[222] Initially, the C-dots were distributed within the hydrogel, stabilized through a network of hyfrogen bonds. In this environment, the fluorescence of the C-dot was high since no aggregation occurred. However, in the presence of bacteria, bacterially secreted esterases induced cleavage of ester bonds within the hydrogel scaffold, resulting in fluidization of the hydrogel. This, in turn, gave rise to aggregation of the embedded C-dots and consequent quenching of their fluorescence.

In another approach, magnetic carbon dots (Mag-C-dots), prepared through combining magnetic Fe_3O_4 NPs and amine-functionalized C-dots, were used for sensing the pathogenic bacteria *Staphylococcus aureus* and *Escherichia coli* in urine samples.[223] The fluorescence intensity of the Mag-C-dots increased, presumably through more pronounced binding of the bacterial cells to the nanoparticles.

4.2. Carbon Dots in Drug Delivery

C-dots offer useful pathways for both drug- and gene-delivery. **Figure 30** depicts *hollow* C-dots, prepared via a carbonization

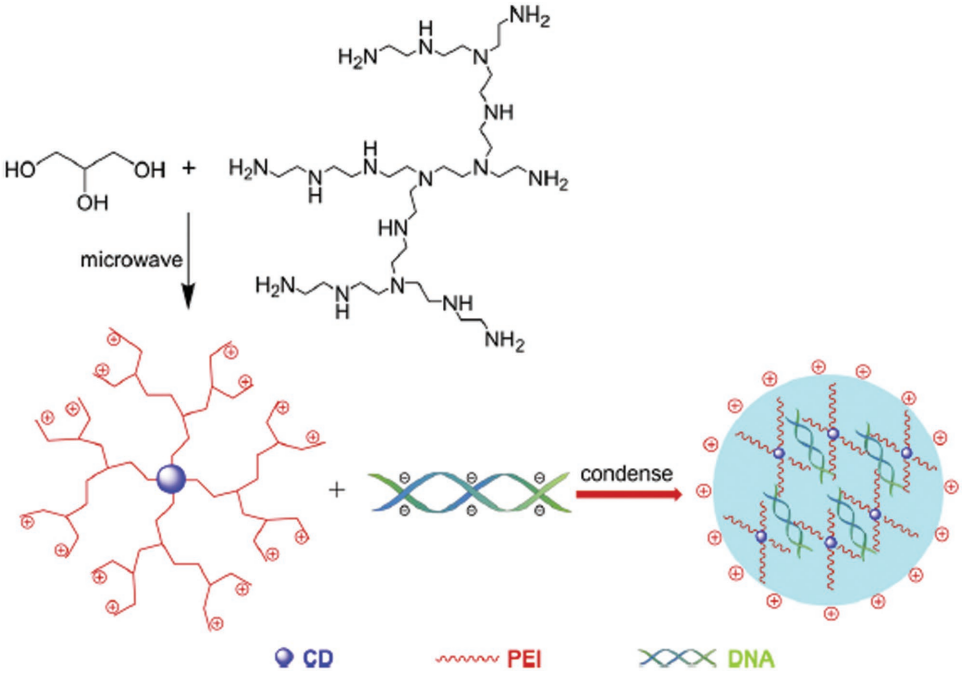

Figure 31. Carbon dots as vehicles for gene transfection. Gene delivery platform comprising polyethylenimine (PEI)-passivated C-dots (synthesized upon the carbonization of glycerol and PEI), employed as a nano-vessel for gene delivery and bioimaging. Reproduced with permission.[225] Copyright 2012, Elsevier Ltd.

process with bovine serum albumin as the carbon source, serving as hosts for drug cargo.[224] Of particular importance is that the C-dots retained their luminescence after loading of drug/gene, thus serving both as a vehicle for drug delivery, as well as for tracking the particles via fluorescence microscopy.[224]

C-dots have been investigated as conduits for delivery of genes by surface passivating with positively charged polymeric materials, thereby delivering genetic material through electrostatic attraction. As an example, Liu et al. successfully prepared a C-dot gene-delivery platform through carbonization of polyethylenimine (PEI), a positively charged polymer. (**Figure 31**).[225] The outer cationic moieties mediated plasmid DNA transfection, and the entrapped C-dots' fluorescence also serves as a vehicle for bio-imaging.

C-dots constituted scaffolds for intracellular delivery of small interfering RNA (siRNA, or "silencing RNA", which is capable of deactivating expression of target genes).[226] The siRNA transport system was prepared through functionalization of the C-dots with PEI, which had a dual role in the system–a carrier for docking the siRNA, and enabling transport of the C-dot complexes across the plasma membrane and cell uptake. In another study, *direct synthesis* of C-dots using oligonucleotides as the carbon source was explored, using the particles as a vehicle for cell imaging (using the C-dots' fluorescence) and drug delivery.[227] The C-dots, which were derived from genomic DNA (isolated from *Escherichia coli*), displayed varied surface groups, thus facilitating drug transport through electrostatic interactions and were readily internalized by different types of cells. In addition, similar to the example above, the C-dots' fluorescence enabled cell imaging.

In an interesting multifunctional system, C-dots served as both target delivery platform, anticancer agents, and imaging constituents.[228] Specifically, the C-dots were functionalized with a *mitochondria-recognition* moiety (triphenylphosphonium, TPP), and a photo-responsive nitric oxide (NO) releasing moiety. NO works as a potent cytotoxic agent due to its inhibition of mitochondrial respiration. The C-dots thus bound and damaged intracellular mitochondria via light induced NO release, initiating apoptosis of the cancer cells (**Figure 32**). In addition, the C-dots' fluorescence allowed assessment of the extent of C-dot buildup and localization within the mitochondria.

In a recent study, amphiphilic C-dots were employed for multicolor cell imaging.[229] In the experiment, C-dots which were surface-functionalized with long hydrocarbon chains, were incorporated within lipid vesicles that were subsequently cell-internalized through endocytic pathways. **Figure 33** depicts confocal fluorescence microscopy images which confirmed successful internalization of the C-dots into the cells, and their homogeneous distribution within cellular environments such as the cytosol and nucleoli.

In another study, C-dots were prepared from three phenylenediamine precursors and employed for imaging epithelial cells (**Figure 34**).[230] The distinct colors of the C-dots were related to the three phenylenediamine isomers (*ortho*, *meta*, and *para*), resulting in difference in their particle size and nitrogen content. Cell labeling was accomplished through incubation of MCF-7 cells with each C-dot species; the live cells were imaged with a confocal microscope under a single 405 nm laser excitation.

FRET was exploited for monitoring drug delivery into cells (**Figure 35**).[231] In that study, surface functional groups of the C-dots served as energy *donor* while the loaded drug compound doxorubicin (DOX) acted as energy *acceptor*. These C-dots were

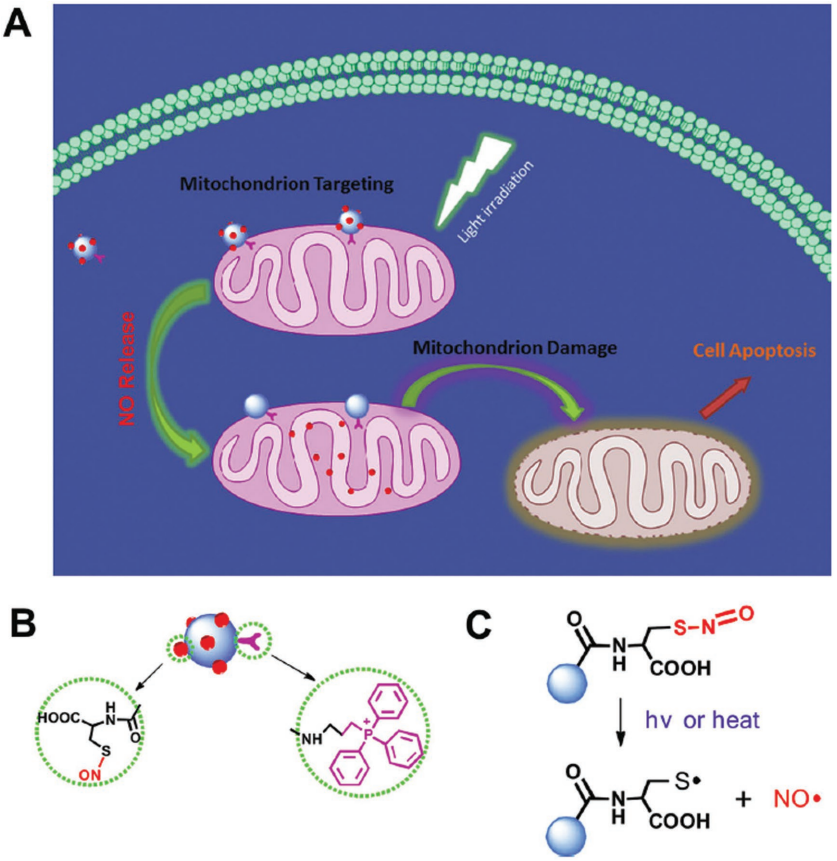

Figure 32. Multifunctional mitochondria-targeting C-dots. A) Outline of the C-dot's activity. C-dots exhibiting a mitochondria-recognition element (triphenylphosphonium, TPP) and photo-responsive NO-release moiety were prepared for targeting and damaging the mitochondria, leading to apoptosis of the cancer cells. B) Representation and surface moiety structures of the C-dots (S-nitrosthiol on the left, and TPP on the right). C) photo responsive release mechanism of NO from the surface passivated moiety. Reproduced with permission.[228] Copyright 2014, The Royal Society of Chemistry.

4.3. Bio-Imaging Applications of C-Dots

The fluorescence properties of C-dots, particularly their excitation-dependent emissions, make these nanoparticle potentially useful for biological imaging applications.

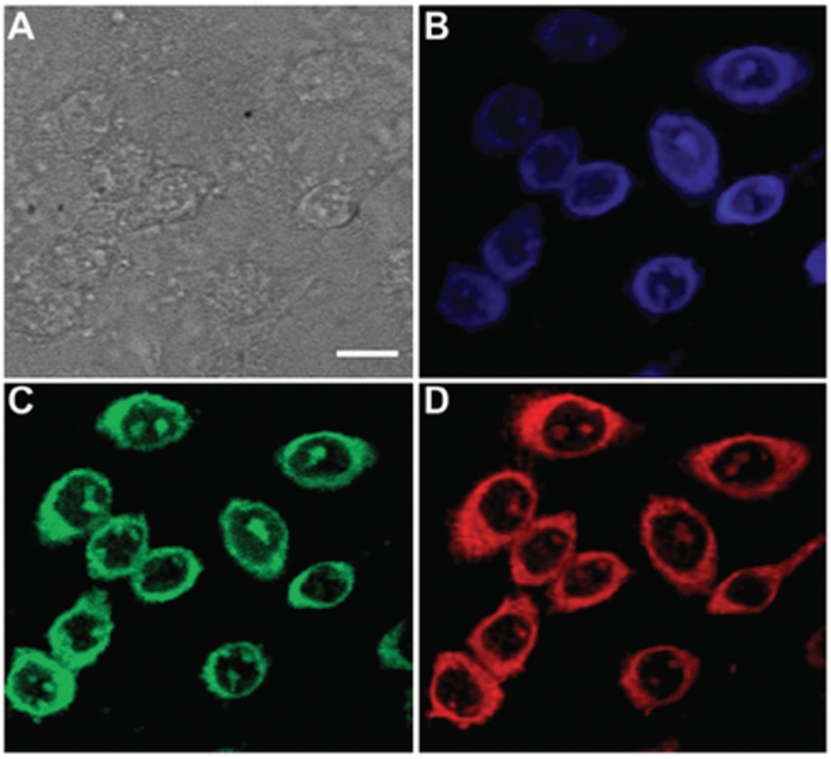

Figure 33. Amphiphilic C-dots employed in cell imaging. Bright-field image (A) and confocal fluorescence microscopy images of epithelial Chinese hamster ovary (CHO) cells incubated with amphiphilic C-dots. The images were recorded at excitation of 405 nm (B); 488 nm (C) and 561 nm (D). Scale bar is 10 µm. Reproduced with permission.[229] Copyright 2014, The Royal Society of Chemistry.

employed for both fluorescence imaging of the cellular targets, and drug distribution through FRET. Specifically, imaging was carried out by uv excitation of the C-dots, energy transfer via FRET to the DOX molecules which consequently exhibited fluorescence emission at 498 nm, allowing for visualization of drug distribution. Importantly, time-dependent imaging studies revealed the decay of the DOX fluorescence as a consequence of their release within the cells.[231]

Cell targeting and imaging through the attachment of recognition elements to C-dots was also carried out. A recent study demonstrated cancer cell imaging by displaying *folic acid* on C-dots' surface (**Figure 36**).[232] Folic acid is a convenient target agent for cancer cells in which the surface folate receptors are over-expressed. In that study, folic acid units were covalently bonded to the C-dots, which were then utilized for the selective tagging of cancer cells, e.g., HeLa cells. In yet another study, C-dots were hydrothermally synthesized from folic acid as carbon precursor, consequently enabling selective imaging of cancer cells.[233]

C-dots have been also used for in vivo imaging. Tumor imaging was demonstrated by using C-dots that were prepared through the carbonization of a mixture containing D-glucose and L-aspartic acid (**Figure 37**).[234] Particularly, these C-dots displayed more pronounced uptake in cancerous *glioma* cells and tumors, likely due to the specific binding of the aspartic acid/glucose elements of the C-dots and *integrins* (cell adhesion proteins) which are overexpressed in glioma cells (Figure 37 Top). In the in vivo experiment, the C-dots preferentially collected in the brains of mice with glioma tumors, demonstrating that the carbon nanoparticles were not only specific but could also be effectively transported across the physiologically important blood-brain barrier (BBB) (Figure 37 bottom).

Other reports presented imaging systems consisting of C-dots conjugated with other reporting modalities. C-dots/*gadolinium ion* conjugates (C-dot-Gd nanoparticles), prepared through the pyrolysis of a positively charged ligand and subsequently coupled to a negatively charged Gd^{3+}-containing complex, can be employed for both fluorescence

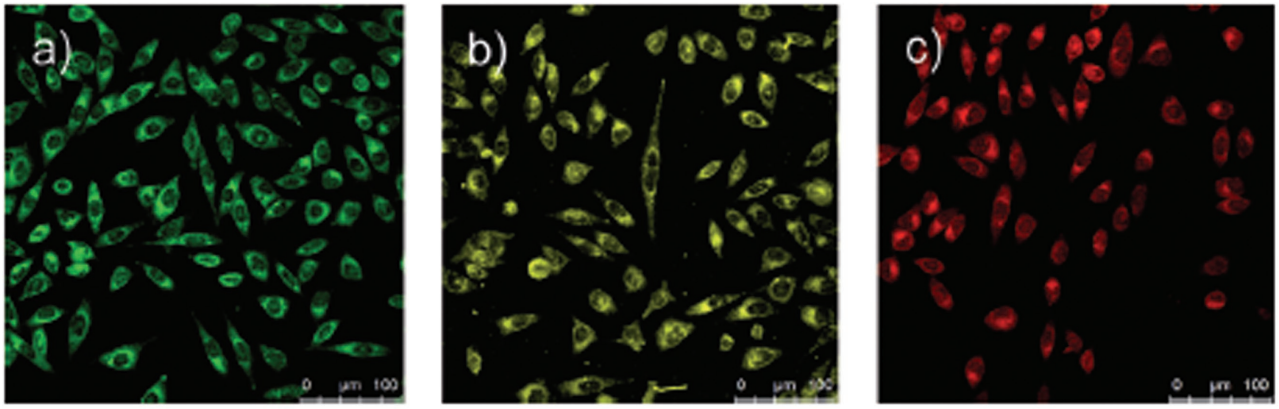

Figure 34. Multicolor cell labeling with C-dots derived from phenylenediamine isomers. Confocal microscopic images (λ_{ex} = 405 nm) of MCF-7 cells treated with C-dots synthesized from *meta*- (a), *ortho*- (b), and *para*- (c) phenylenediamine. Each carbon source produces a corresponding C-dot with a distinct fluorescence emission peak (e.g., different color). Reproduced with permission.[230]

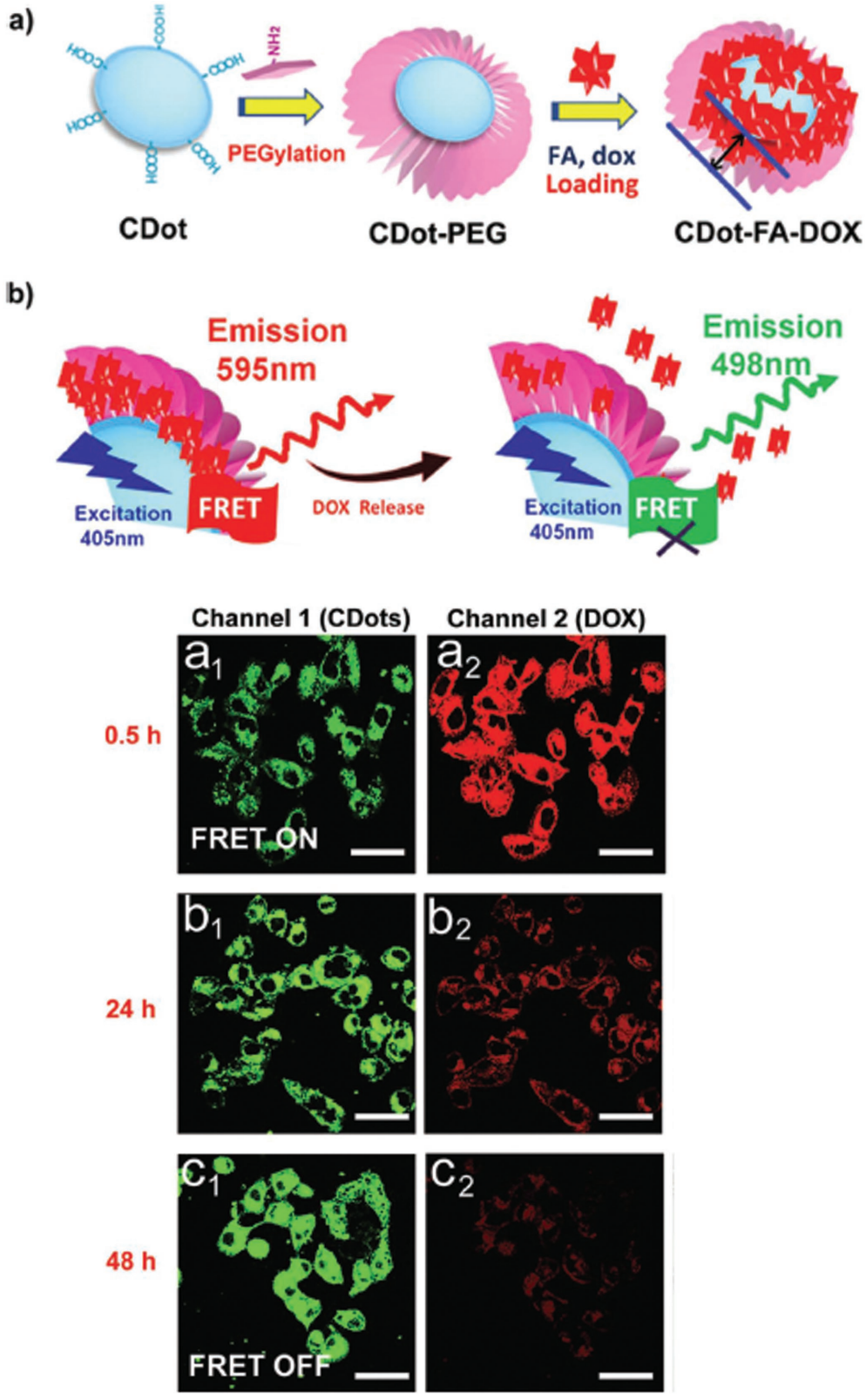

Figure 35. C-dots for screening drug delivery. a) Polyethyleneglycol (PEG) and folic acid (FA) passivated C-dots improving the biocompatibility and cellular targeting. DOX was the drug cargo. b) Before DOX release, the luminescence was produced from DOX (at 595 nm) via FRET between the C-dot and DOX molecules. C-dots emission at 498 nm observed after DOX release. c) Confocal microscopic images of HeLa cells incubated with C-dots-DOX. Lowering of DOX fluorescence and instantaneous enhancement of C-dot fluorescence are recorded. Reproduced with permission.[231]

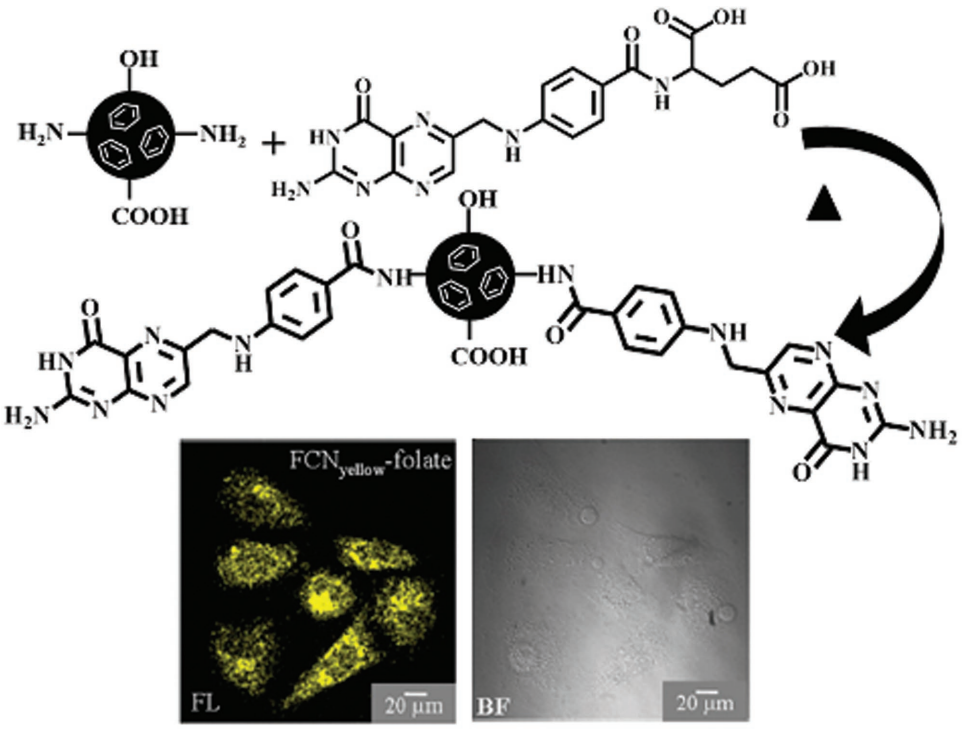

Figure 36. Cancer cell imaging with folic acid-functionalized C-dots. Top) Strategy to prepare folic acid passivated C-dots. Folic acid is covalently linked with C-dots. Bottom) HeLa cells visualized via confocal fluorescence microscopy, treated with yellow C-dots (right image) functionalized with folic acid. Reproduced with permission.[232] Copyright 2013, Nature Publishing Group.

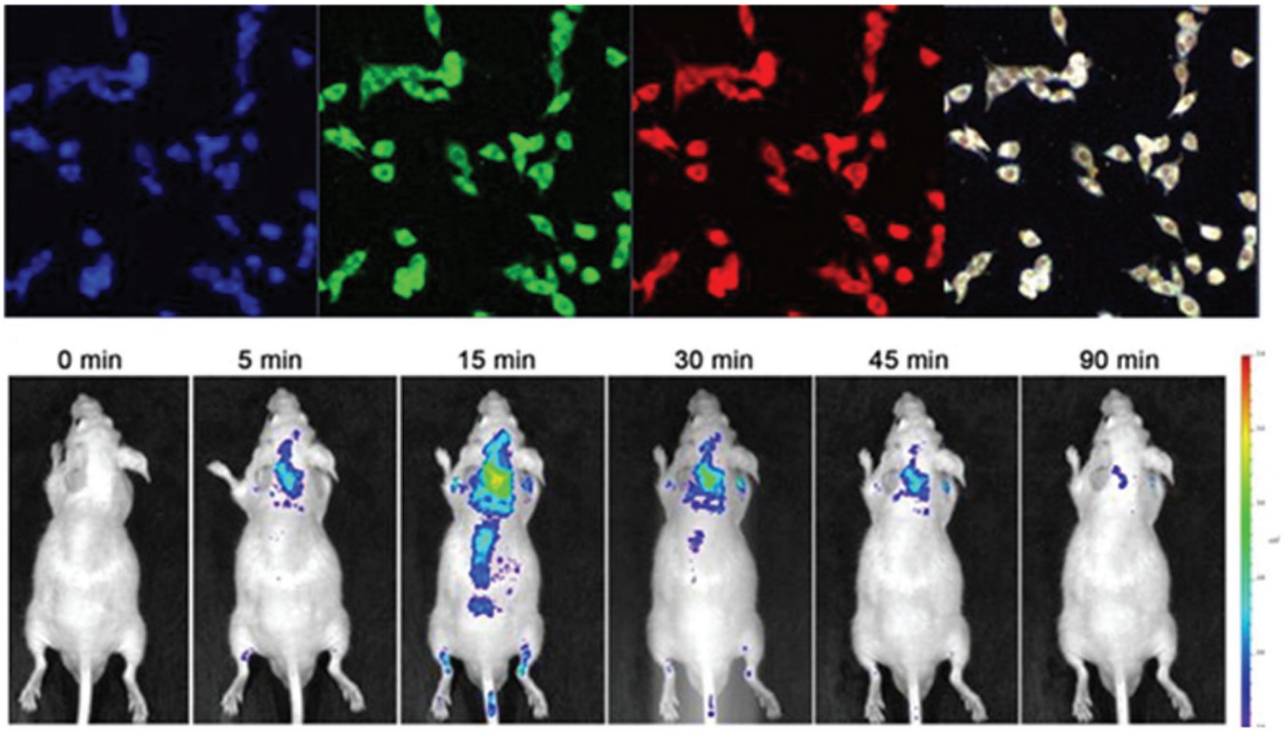

Figure 37. In vitro and in vivo targeting of C-dots prepared from specific ligands as carbon sources. The C-dots, synthesized from amino acid ligands, targeting *glioma cancer cells*, presumably through binding to over-expressed *integrins*. Top row) Cell imaging experiments [exc. 405 nm (A,E), 488 nm (B,F), 555 nm (C,G)], and flow cytometry profiles (D,H) reflecting more significant labeling in case of cancerous C6 cells as compared to non-cancerous L929 cells. Bottom row) In vivo fluorescence images of glioma-bearing mice reveal the amassing of C-dots in the brain and the ensuing systemic clearance. Reproduced with permission.[234] Copyright 2015, American Chemical Society.

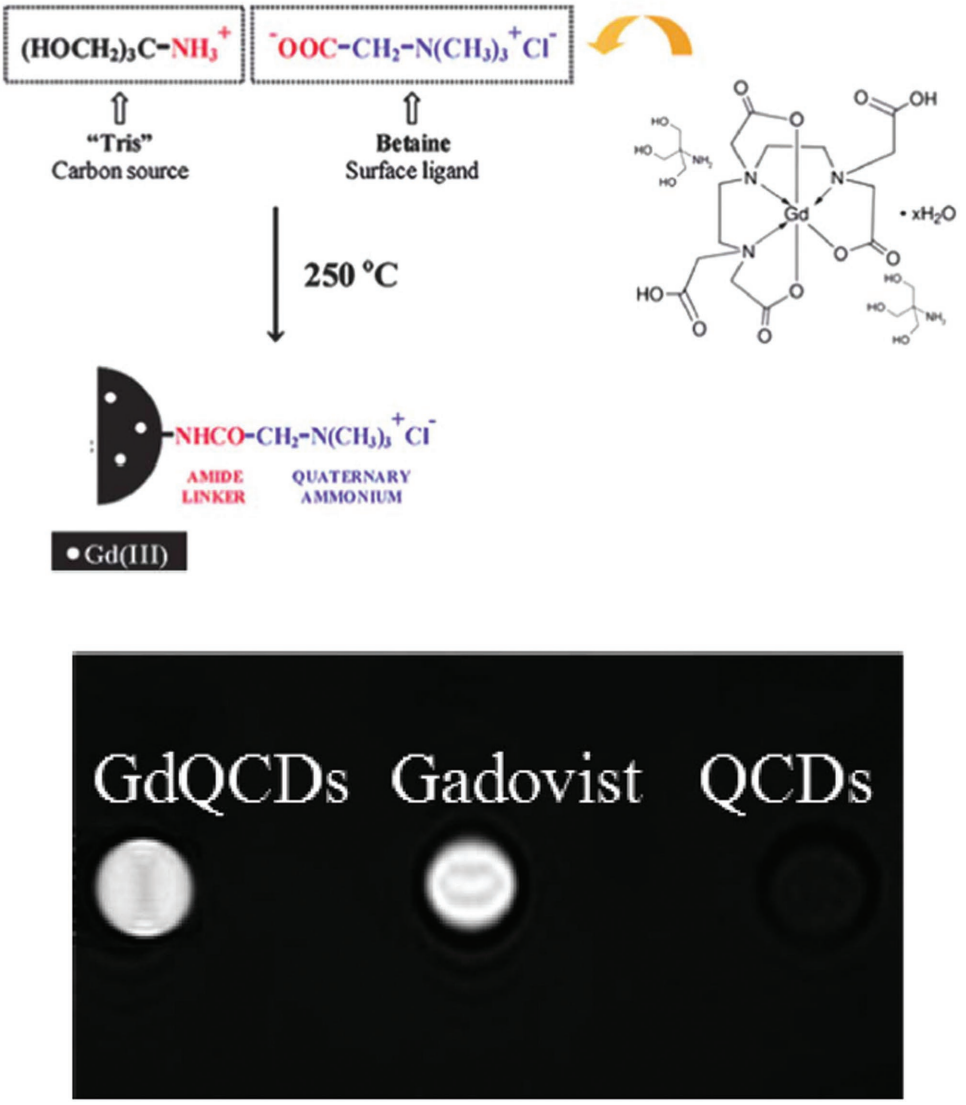

Figure 38. Orthogonal imaging modes using C-dot composites. C-dots incorporating gadolinium ions used for both fluorescence imaging and magnetic resonance imaging. A) The Gd^{3+} ions are incorporated into the C-dot matrix through pyrolysis of a mixture comprised of the carbon source, positive ligand, and Gd^{3+} complex. B) T1-weighted magnetic resonance images (MRI) exhibiting substantial brightness of the gadolinium-C-dot composites (GdQC-dots), analogous to a commercially available MRI contrast agent (Gadovist). No MRI contrast was seen in the case of those C-dots which did not contain Gd^{3+}. Reproduced with permission.[235] Copyright 2012, The Royal Society of Chemistry.

and magnetic resonance imaging (**Figure 38**).[235] Gadolinium is a common contrast agent in magnetic resonance imaging (MRI), reducing the T1 relaxation of water protons and consequently enhancing their magnetic resonance signal.

4.4. C-Dots in Photodynamic Therapy

C-dots have been utilized in photodynamic therapy (PDT). In PDT, tumor cells are destroyed upon exposure to oxygen radicals, released upon light irradiation of a "photosensitizer" (PS). For example, Chen et al. reported a PDT strategy based upon *two-photon* absorbance by C-dots (**Figure 39**).[236] The PDT system consisted of C-dots covalently bound to a porphyrin derivative (TMPyP), employed as the PS. A fundamental restriction of the use of standalone TMPyP as a PS therapeutic compound is that it absorbs light only in the visible spectrum. The designed C-dots platform were able to absorb light in the NIR (700 nm) region which, crucially, penetrates through tissues. Upon irradiation by NIR light, the C-dots emitted light which wavelength coincided with the excitation of TMPyP; the resultant energy transfer activated the TMPyP release of triplet oxygen radicals and subsequent cell killing.

In another study, GQDs could serve as PDT agents generating singlet oxygen radicals (reactive oxygen species, ROS) likely due to the transfer of the excitation energy of the C-dots

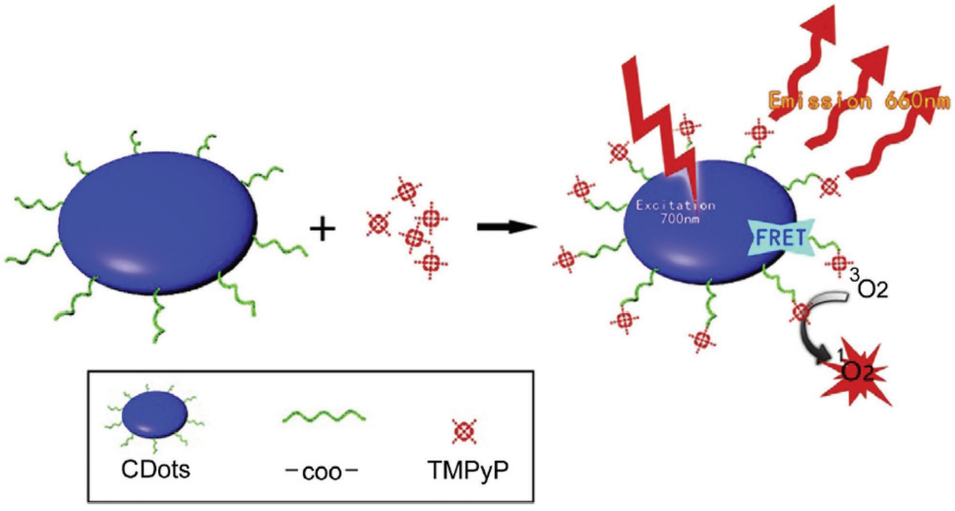

Figure 39. C-dots in photodynamic therapy (PDT). The C-dots are covalently attached to TMPyM (the photosensitizer). C-dots are irradiated with near infrared (NIR) light, transferring energy to the TMPyP. In the photodynamic process triplet oxygen is generated, leading to cell killing. Reproduced with permission.[236] Copyright 2014 Elsevier Ltd.

to an "excited triplet state" (**Figure 40**).[237] As described in Figure 40, energy required for generating reactive oxygen species (singlet or triplet oxygen) could be produced through two transitions – the excited singlet state to the triplet state, and the triplet state to the ground state of the GQDs. This *multi-state sensitization* mechanism differs significantly from the *single transition* photosensitization mechanism in conventional PDT agents and may enable more efficient PDT activity through the production of high concentrations of reactive oxygen species by the GQDs. **Table 3** outlines publications discussed above focusing on biological and biomedical applications of carbon dots.

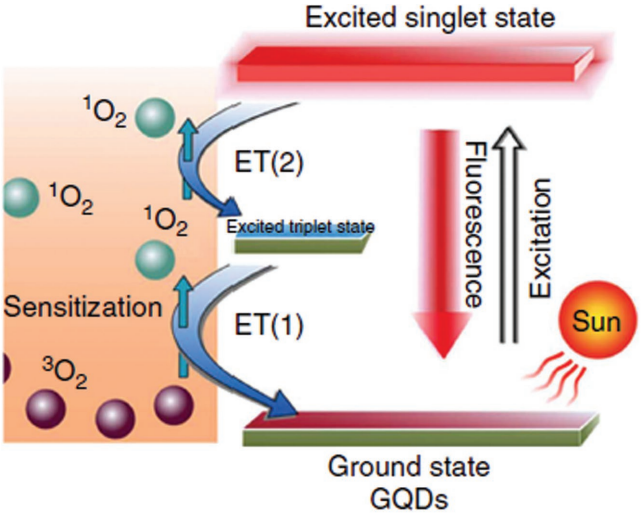

Figure 40. Multi-state sensitization model for photodynamic therapy in GQDs. Mechanisms for generation of reactive oxygen species by GQDs, demonstrating greater effectiveness in comparison with conventional photosensitizers which rely on single energy transitions. Reproduced with permission.[237] Copyright 2014, Nature Publishing Group.

5. Clinical and Practical Aspects

Although carbon nanomaterials represent an important niche in the field of innovative materials for next-generation nanomedicines, no carbon nanomaterial-based therapeutic products have won regulatory approval yet. Clinical trials of CNTs as components of external medical devices for cancer diagnostics were initiated in 2011[238] and as breath nanosensors for gastric cancer.[239] The apparent disparity between the significant activity and progress in carbon nanomaterial research and scant advances in the realm of practical biomedical applications might certainly be a detrimental issue for further advances in the field.

A prominent issue that is naturally pivotal for potential future therapeutic applications of carbon is *toxicity*. Potential adverse effects of CNTs, graphene, graphene oxide, and their derivatives have been discussed in several reviews.[240] Specifically, there is a need to identify safe morphologies and delivery routes of therapeutic carbon nanomaterials. Non-specific adsorption of carbon nanomaterials to biological molecules in vivo is

Table 3. Biological applications of GQDs and C-dots.

	Graphene quantum dots and carbon dots	Ref.
1	GQD- and C-dot-based biosensors	
	Glucose biosensing	[190–198]
	Biomarker detection	[199–204]
	Detection of metal ions and pH in biological systems	[205–218]
	Biosensing of oligonucleotides	[219,220]
	Bacterial detection	[221–223]
2	Carbon dots in drug delivery	[224–228]
3	Bio-imaging applications of C-dots	[229–235]
4	Photodynamic therapy	[236,237]

considered another important factor affecting their toxicity profile. Graphene, for example, nonspecifically binds to proteins in vivo by π-stacking interactions and electrostatic interactions.[241] GO displaying reactive COOH and OH groups can be conjugated with various functional proteins, leading to irreversible denaturation (or activation) of proteins and potential long-term toxicity.[242] Graphene was also shown to nonspecifically bind to various proteins, even when it is functionalized with targeting residues such as aptamers.[133] In addition, nonspecific binding of chemotherapeutic agents delivered by carbon nanomaterials leads to undesired side effects on normal tissues and insufficient dosages for killing target cancer cells.[243]

Other safety issues need to be researched before wider acceptance of carbon nanomaterials for therapeutic applications. Among the central questions are aspects pertaining to circulation and long-term fate (clearance rate) in blood, interactions of graphene with human blood cells and proteins. Other physiological issues include the effects of carbon nanomaterials on ion channels and cell signaling pathways. Further, investigating interactions of carbon nanoparticles with pulmonary surfactant proteins and their overall pulmonary responses are critical due to inhalation of these materials. In addition, the effects of carbon nanomaterials on the immune system, reproductive systems, and neural networks have yet to be thoroughly investigated.[244]

Technologies for minimizing potentially adverse environmental effects of carbon nanomaterials have been pursued. Biodegradation technologies may be able to meet this need. For example, recent studies have reported that peroxidase enzyme-based processes could lead to oxidative degradation of carbon nanoparticles in biological systems.[245] On a cellular level, a degradation process has been demonstrated for carbon nanotubes[246] and graphene.[247] Very few studies are currently available on the capacity of phagocytic cells or specific tissues to induce carbon nanomaterial degradation following in vivo administration in animal models.[248]

Bacteria and other microorganisms have been proposed as conduits for degradation of carbon nanomaterials in the environment either through oxidation or through reduction reactions. As an example, Liu et al. successfully isolated a naphthalene degrading bacterium from the contaminated soil in a graphite mine, that could degrade graphitic materials including GO, graphite, and reduced GO (rGO).[249] Interestingly, the bacterium had different degrading effects on different carbon materials. Specific enzymes have been also employed for carbon nanoparticle removal. *Myeloperoxidase* has been shown to oxidize SWCNTs.[250] It has been also shown that binding of SWCNTs to human serum albumin through electrostatic interactions between the SWCNTs' carboxyl groups and arginine residues of the protein, and π–π stacking interactions of SWCNTs with the tyrosine residues significantly enhanced SWCNT biodegradation.[251]

6. Conclusions

Carbon nanomaterials, specifically carbon nanotubes (CNTs), graphene, and carbon quantum dots, have been used as powerful platforms for diverse biological and biomedical applications. These nanomaterials have been employed as biosensors, drug and gene delivery vehicles, bio-imaging agents, therapeutic materials, and tissue engineering scaffolds. The contributions of these carbon nanomaterials to such diverse applications have been aided by the unique physico-chemical properties of these nanostructures, their biocompatibility, and the varied routes of surface derivatization. While technical and conceptual challenges still need to be addressed, carbon nanomaterials will likely continue to be used in numerous and expanding biological applications.

Acknowledgements

We are grateful for the Ministry of Science and Technology, China-Israel Grant Program for financial support.

Conflict of Interest

The authors declare no conflict of interest.

Keywords

biomedical applications, carbon nanotubes, carbon quantum dots, graphene

Received: May 4, 2017
Revised: June 12, 2017
Published online: August 4, 2017

[1] H. W. Kroto, J. R. Heath, S. C. O'Brien, R. F. Curl, R. E. Smalley, *Nature* **1985**, *318*, 162.
[2] S. Iijima, *Nature* **1991**, *354*, 56.
[3] K. S. Novoselov, A. K. Geim, S. V. Morozov, D. Jiang, Y. Zhang, S. V. Dubonos, I. V. Grigorieva, A. A. Firsov, *Science* **2004**, *306*, 666.
[4] a) D. Pan, J. Zhang, Z. Li, M. Wu, *Adv. Mater.* **2010**, *22*, 734; b) Y.-P. Sun, B. Zhou, Y. Lin, W. Wang, K. S. Fernando, P. Pathak, M. J. Meziani, B. A. Harruff, X. Wang, H. Wang, *J. Am. Chem. Soc.* **2006**, *128*, 7756.
[5] a) G. Hong, S. Diao, A. L. Antaris, H. Dai, *Chem. Rev.* **2015**, *115*, 10816; b) R. Alshehri, A. M. Ilyas, A. Hasan, A. Arnaout, F. Ahmed, A. Memic, *J. Med. Chem.* **2016**, *59*, 8149; c) F. Lu, L. Gu, M. J. Meziani, X. Wang, P. G. Luo, L. M. Veca, L. Cao, Y. P. Sun, *Adv. Mater.* **2009**, *21*, 139.
[6] a) V. Georgakilas, J. N. Tiwari, K. C. Kemp, J. A. Perrnan, A. B. Bourlinos, K. S. Kim, R. Zboril, *Chem. Rev.*, **2016**, *116*, 5464; b) S. Pattnaik, K. Swain, Z. Lin, *J. Mater. Chem. B* **2016**, *4*, 7813; c) J. Lee, J. Kim, S. Kim, D.-H. Min, *Adv. Drug Deliv. Revs.* **2016**, *105*, 275.
[7] X. T. Zheng, A. Ananthanarayanan, K. Q. Luo, P. Chen, *Small* **2015**, *11*, 1620.
[8] a) S. N. Baker, G. A. Baker, *Angew. Chem. Int. Ed.* **2010**, *49*, 6726; b) L. Li, G. Wu, G. Yang, J. Peng, J. Zhao, J.-J. Zhu, *Nanoscale* **2013**, *5*, 4015.
[9] Z. Liu, S. M. Tabakman, Z. Chen, H. Dai, *Nat. Protocols* **2009**, *4*, 1372.
[10] a) H.-C. Wu, X. Chang, L. Liu, F. Zhao, Y. Zhao, *J. Mater. Chem.* **2010**, *20*, 1036; b) V. C. Moore, M. S. Strano, E. H. Haroz, R. H. Hauge, R. E. Smalley, J. Schmidt, Y. Talmon, *Nano Lett.*

2003, *3*, 1379; c) A. B. Bourlinos, D. Gournis, D. Petridis, T. Szabó, A. Szeri, I. Dékány, *Langmuir* **2003**, *19*, 6050; d) L. Q. Xu, W. J. Yang, K.-G. Neoh, E.-T. Kang, G. D. Fu, *Macromolecules* **2010**, *43*, 8336; e) T. A. Pham, N. A. Kumar, Y. T. Jeong, *Synth. Met.* **2010**, *160*, 2028.

[11] C. B. Jacobs, M. J. Peairs, B. J. Venton, *Anal. Chim. Acta* **2010**, *662*, 105.

[12] N. Yang, X. Chen, T. Ren, P. Zhang, D. Yang, *Sens. Actuat. B: Chemical* **2015**, *207*, 690.

[13] a) S. Vaddiraju, I. Tomazos, D. J. Burgess, F. C. Jain, F. Papadimitrakopoulos, *Biosens. Bioelectron.* **2010**, *25*, 1553; b) J. Wang, *Electroanalysis* **2001**, *13*, 983.

[14] F. Patolsky, Y. Weizmann, I. Willner, *Angew. Chem. Int. Ed.* **2004**, *43*, 2113.

[15] J. H. Kim, S.-A. Jun, Y. Kwon, S. Ha, B.-I. Sang, J. Kim, *Bioelectrochem.* **2015**, *101*, 114.

[16] M. Vesali-Naseh, A. A. Khodadadi, Y. Mortazavi, A. A. Moosavi-Movahedi, K. Ostrikov, *RSC Adv.* **2016**, *6*, 31807.

[17] a) P. N. Manikandan, H. Imran, V. Dharuman, *Anal. Methods* **2016**, *8*, 2691; b) S. Palanisamy, S. Cheemalapati, S.-M. Chen, *Int. J. Electrochem. Sci.* **2012**, *7*, 8394.

[18] B.-Y. Wu, S.-H. Hou, F. Yin, Z.-X. Zhao, Y.-Y. Wang, X.-S. Wang, Q. Chen, *Biosens. Bioelectron.* **2007**, *22*, 2854.

[19] Y. L. Yao, K. K. Shiu, *Electroanalysis* **2008**, *20*, 1542.

[20] H. Heli, M. Hajjizadeh, A. Jabbari, A. Moosavi-Movahedi, *Biosens. Bioelectron.* **2009**, *24*, 2328.

[21] A. H. Crisp, M. G. Gelder, S. Rix, H. I. Meltzer, O. J. Rowlands, *Brit. J. Psychiatry* **2000**, *177*, 4.

[22] a) D. Du, M. Wang, J. Cai, Y. Qin, A. Zhang, *Sens. Actuat. B: Chemical* **2010**, *143*, 524; b) N. Jha, S. Ramaprabhu, *Nanoscale* **2010**, *2*, 806.

[23] J. Ding, H. Zhang, F. Jia, W. Qin, D. Du, *Sens. Actuat. B: Chemical* **2014**, *199*, 284.

[24] M. Kesik, F. E. Kanik, J. Turan, M. Kolb, S. Timur, M. Bahadir, L. Toppare, *Sens. Actuat. B: Chemical* **2014**, *205*, 39.

[25] B. Dalkıran, P. E. Erden, E. Kılıç, *Anal. Bioanal. Chem.* **2016**, *408*, 4329.

[26] a) A. Azadbakht, M. Roushani, A. R. Abbasi, S. Menati, Z. Derikvand, *Mater. Sci. Eng.: C* **2016**, *68*, 585; b) S. F. Rahman, K. Min, S.-H. Park, J.-H. Park, J. C. Yoo, D.-H. Park, *Korean J. Chem. Eng.* **2016**, *33*, 3442.

[27] Ş. Alpat, K. Özdemir, S. Kılınç Alpat, *J. Sens.* **2016**, *2016*, 5653975.

[28] S. Mukdasai, V. Langsi, M. Pravda, S. Srijaranai, J. D. Glennon, *Sens. Actuat. B: Chemical* **2016**, *236*, 126.

[29] B. Batra, C. Pundir, *Biosens. Bioelectron.* **2013**, *47*, 496.

[30] a) S. Lata, B. Batra, P. Kumar, C. Pundir, *Anal. Biochem.* **2013**, *437*, 1; b) S. Lata, B. Batra, N. Singala, C. Pundir, *Sens. Actuat. B: Chemical* **2013**, *188*, 1080; c) Q. Wang, X. Lin, J. Xu, C. Xuan, S. Zhu, Y. Fu, *J. Electrochem. Soc.* **2016**, *163*, B373; d) Q. Xia, Y. Huang, X. Lin, S. Zhu, Y. Fu, *Biochem. Eng. J.* **2016**, *113*, 1.

[31] a) Y. Liu, Y. Liu, H. Feng, Y. Wu, L. Joshi, X. Zeng, J. Li, *Biosens. Bioelectron.* **2012**, *35*, 63; b) H. Zarei, H. Ghourchian, K. Eskandari, M. Zeinali, *Anal. Biochem.* **2012**, *421*, 446.

[32] Y.-T. Chang, J.-H. Huang, M.-C. Tu, P. Chang, T.-R. Yew, *Biosens. Bioelectron.* **2013**, *41*, 898.

[33] a) M. Zheng, A. Jagota, E. D. Semke, B. A. Diner, R. S. Mclean, S. R. Lustig, R. E. Richardson, N. G. Tassi, *Nat. Mater.* **2003**, *2*, 338; b) M. Zheng, E. D. Semke, *J. Am. Chem. Soc.* **2007**, *129*, 6084.

[34] V. Karachevtsev, A. Y. Glamazda, V. Leontiev, O. Lytvyn, U. Dettlaff-Weglikowska, *Chem. Phys. Lett.* **2007**, *435*, 104.

[35] Z. Liang, R. Lao, J. Wang, Y. Liu, L. Wang, Q. Huang, S. Song, G. Li, C. Fan, *Int. J. Mol. Sci.* **2007**, *8*, 705.

[36] C. Hu, Y. Zhang, G. Bao, Y. Zhang, M. Liu, Z. L. Wang, *J. Phys. Chem. B* **2005**, *109*, 20072.

[37] Z. Wu, Z. Zhen, J.-H. Jiang, G.-L. Shen, R.-Q. Yu, *J. Am. Chem. Soc.* **2009**, *131*, 12325.

[38] A. Benvidi, M. D. Tezerjani, S. Jahanbani, M. M. Ardakani, S. M. Moshtaghioun, *Talanta* **2016**, *147*, 621.

[39] M. Chen, C. Hou, D. Huo, M. Yang, H. Fa, *Appl. Surf. Sci.* **2016**, *364*, 703.

[40] J. Li, E.-C. Lee, *Sens. Actuat. B: Chemical* **2017**, *239*, 652.

[41] Y. Huang, M. Shi, L. Zhao, S. Zhao, K. Hu, Z.-F. Chen, J. Chen, H. Liang, *Biosens. Bioelectron.* **2014**, *54*, 285.

[42] a) Y.-E. Choi, J.-W. Kwak, J. W. Park, *Sensors* **2010**, *10*, 428; b) M. Ferrari, *Nat. Revs. Cancer* **2005**, *5*, 161; c) N. G. Portney, M. Ozkan, *Anal. Bioanal. Chem.* **2006**, *384*, 620.

[43] a) M. R. Kierny, T. D. Cunningham, B. K. Kay, *Nano Revs.* **2012**, *3*, 17240; b) M. Ramanathan, M. Patil, R. Epur, Y. Yun, V. Shanov, M. Schulz, W. R. Heineman, M. K. Datta, P. N. Kumta, *Biosens. Bioelectron.* **2016**, *77*, 580.

[44] D. P. Matta, S. Tripathy, S. R. K. Vanjari, C. S. Sharma, S. G. Singh, *Biomed. Microdevices* **2016**, *18*, 111.

[45] F. Yuan, Y. Deng, W. Zhou, M. Zhang, Z. Li, *Nano Res.* **2016**, *9*, 1701.

[46] S. Kumar, R. Rani, N. Dilbaghi, K. Tankeshwar, K.-H. Kim, *Chem. Soc. Rev.* **2017**, *46*, 158.

[47] Z. Wang, Z. Dai, *Nanoscale* **2015**, *7*, 6420.

[48] R. Malhotra, V. Patel, J. P. Vaqué, J. S. Gutkind, J. F. Rusling, *Anal. Chem.* **2010**, *82*, 3118.

[49] Y. Wan, W. Deng, Y. Su, X. Zhu, C. Peng, H. Hu, H. Peng, S. Song, C. Fan, *Biosens. Bioelectron.* **2011**, *30*, 93.

[50] E. Arkan, R. Saber, Z. Karimi, M. Shamsipur, *Anal. Chim. Acta* **2015**, *874*, 66.

[51] M. B. Lerner, J. D'souza, T. Pazina, J. Dailey, B. R. Goldsmith, M. K. Robinson, A. C. Johnson, *ACS Nano* **2012**, *6*, 5143.

[52] M. Abdolahad, M. Janmaleki, M. Taghinejad, H. Taghnejad, F. Salehi, S. Mohajerzadeh, *Nanoscale* **2013**, *5*, 3421.

[53] M. Abdolahad, M. Taghinejad, H. Taghinejad, M. Janmaleki, S. Mohajerzadeh, *Lab Chip* **2012**, *12*, 1183.

[54] a) C. Chen, X.-X. Xie, Q. Zhou, F.-Y. Zhang, Q.-L. Wang, Y.-Q. Liu, Y. Zou, Q. Tao, X.-M. Ji, S.-Q. Yu, *Nanotechnol.* **2012**, *23*, 045104; b) H. Huang, Q. Yuan, J. Shah, R. Misra, *Adv. Drug Deliv. Revs.* **2011**, *63*, 1332.

[55] Z. Ji, G. Lin, Q. Lu, L. Meng, X. Shen, L. Dong, C. Fu, X. Zhang, *J. Colloid Interface Sci.* **2012**, *365*, 143.

[56] C. Chen, L. Hou, H. Zhang, L. Zhu, H. Zhang, C. Zhang, J. Shi, L. Wang, X. Jia, Z. Zhang, *J. Drug Target* **2013**, *21*, 809.

[57] M. Das, R. P. Singh, S. R. Datir, S. Jain, *Mol. Pharm.* **2013**, *10*, 3404.

[58] a) G. Cirillo, S. Hampel, U. G. Spizzirri, O. I. Parisi, N. Picci, F. Iemma, *BioMed Res. Int.* **2014**, *2014*; b) M. Mohseni, K. Gilani, Z. Bahrami, N. Bolourchian, S. A. Mortazavi, *Iranian J. Pharm. Res.: IJPR* **2015**, *14*, 359; c) A. Servant, C. Bussy, K. Al-Jamal, K. Kostarelos, *J. Mater. Chem. B* **2013**, *1*, 4593.

[59] B. Kang, J. Li, S. Chang, M. Dai, C. Ren, Y. Dai, D. Chen, *Small* **2012**, *8*, 777.

[60] a) A. Giri, T. Bhunia, L. Goswami, A. B. Panda, A. Bandyopadhyay, *RSC Adv.* **2015**, *5*, 41736; b) A. Giri, T. Bhunia, S. R. Mishra, L. Goswami, A. B. Panda, A. Bandyopadhyay, *RSC Adv.* **2014**, *4*, 13546; c) A. Giri, T. Bhunia, A. Pal, L. Goswami, A. Bandyopadhyay, *Eur. Polym. J.* **2016**, *74*, 13.

[61] T. Bhunia, A. Giri, T. Nasim, D. Chattopadhyay, A. Bandyopadhyay, *Carbon* **2013**, *52*, 305.

[62] B. Mandal, D. Das, A. P. Rameshbabu, S. Dhara, S. Pal, *RSC Adv.* **2016**, *6*, 19605.

[63] A. Pistone, D. Iannazzo, S. Ansari, C. Milone, M. Salamò, S. Galvagno, S. Cirmi, M. Navarra, *Int. J. Pharm.* **2016**, *515*, 30.
[64] A. Servant, L. Methven, R. P. Williams, K. Kostarelos, *Adv. Healthcare Mater.* **2013**, *2*, 806.
[65] J. Wang, Z. Lu, M. G. Wientjes, J. L.-S. Au, *AAPS J.* **2010**, *12*, 492.
[66] C. Geyik, S. Evran, S. Timur, A. Telefoncu, *Biotechnol. Progr.* **2014**, *30*, 224.
[67] S. Taghavi, A. H. Nia, K. Abnous, M. Ramezani, *Int. J. Pharm.* **2017**, *516*, 301.
[68] a) Y.-P. Huang, I.-J. Lin, C.-C. Chen, Y.-C. Hsu, C.-C. Chang, M.-J. Lee, *Nanoscale Res. Lett.* **2013**, *8*, 267; b) C. Spinato, D. Giust, I. A. Vacchi, C. Ménard-Moyon, K. Kostarelos, A. Bianco, *J. Mater. Chem. B* **2016**, *4*, 431.
[69] T. Anderson, R. Hu, C. Yang, H. S. Yoon, K.-T. Yong, *Biomaterials Sci.* **2014**, *2*, 1244.
[70] H. Li, X. Fan, X. Chen, *ACS Appl. Mater. Interfaces* **2016**, *8*, 4500.
[71] T. Ohta, Y. Hashida, F. Yamashita, M. Hashida, *J. Pharm. Sci.* **2016**, *105*, 2815.
[72] a) J. Chen, S. Chen, X. Zhao, L. V. Kuznetsova, S. S. Wong, I. Ojima, *J. Am. Chem. Soc.* **2008**, *130*, 16778; b) Y. Hashida, T. Umeyama, J. Mihara, H. Imahori, M. Tsujimoto, S. Isoda, M. Takano, M. Hashida, *J. Pharm. Sci.* **2012**, *101*, 3398; c) S. Zhou, Y. Hashida, S. Kawakami, J. Mihara, T. Umeyama, H. Imahori, T. Murakami, F. Yamashita, M. Hashida, *Int. J. Pharm.* **2014**, *471*, 214.
[73] A. G. Bell, *Am. J. Sci.* **1880**, 305.
[74] J. Weber, P. C. Beard, S. E. Bohndiek, *Nat. Methods* **2016**, *13*, 639.
[75] A. De La Zerda, C. Zavaleta, S. Keren, S. Vaithilingam, S. Bodapati, Z. Liu, J. Levi, B. R. Smith, T.-J. Ma, O. Oralkan, *Nat. Nanotechnol.* **2008**, *3*, 557.
[76] A. de Zerda, S. Bodapati, R. Teed, S. Y. May, S. M. Tabakman, Z. Liu, B. T. Khuri-Yakub, X. Chen, H. Dai, S. S. Gambhir, *ACS Nano* **2012**, *6*, 4694.
[77] C. Wang, C. Bao, S. Liang, H. Fu, K. Wang, M. Deng, Q. Liao, D. Cui, *Nanoscale Res. Lett.* **2014**, *9*, 1.
[78] a) M. J. O'connell, S. M. Bachilo, C. B. Huffman, V. C. Moore, M. S. Strano, E. H. Haroz, K. L. Rialon, P. J. Boul, W. H. Noon, C. Kittrell, *Science* **2002**, *297*, 593; b) J. Zhang, Z. Qiao, P. Yang, J. Pan, L. Wang, H. Wang, *Chin. J. Chem.* **2015**, *33*, 35.
[79] P. Jeyamohan, T. Hasumura, Y. Nagaoka, Y. Yoshida, T. Maekawa, D. S. Kumar, *Int. J. Nanomedicine* **2013**, *8*, 2653.
[80] H. K. Moon, S. H. Lee, H. C. Choi, *ACS Nano* **2009**, *3*, 3707.
[81] L. Zhang, P. Rong, M. Chen, S. Gao, L. Zhu, *Nanoscale* **2015**, *7*, 16204.
[82] a) H.-T. Chou, T.-P. Wang, C.-Y. Lee, N.-H. Tai, H.-Y. Chang, *Mater. Sci. Eng.: C* **2013**, *33*, 989; b) S. Han, T. Kwon, J. E. Um, S. Haam, W. J. Kim, *Adv. Healthcare Mater.* **2016**, *5*, 1147; c) L. Wang, J. Shi, H. Zhang, H. Li, Y. Gao, Z. Wang, H. Wang, L. Li, C. Zhang, C. Chen, *Biomaterials* **2013**, *34*, 262.
[83] a) J. Song, F. Wang, X. Yang, B. Ning, M. G. Harp, S. H. Culp, S. Hu, P. Huang, L. Nie, J. Chen, *J. Am. Chem. Soc.* **2016**, *138*, 7005; b) D. Wang, C. Hou, L. Meng, J. Long, J. Jing, D. Dang, Z. Fei, P. J. Dyson, *J. Mater. Chem. B* **2017**; c) X. Wang, C. Wang, L. Cheng, S.-T. Lee, Z. Liu, *J. Am. Chem. Soc.* **2012**, *134*, 7414.
[84] I. Marangon, C. Ménard-Moyon, A. K. Silva, A. Bianco, N. Luciani, F. Gazeau, *Carbon* **2016**, *97*, 110.
[85] G. Wang, F. Zhang, R. Tian, L. Zhang, G. Fu, L. Yang, L. Zhu, *ACS Appl. Mater. Interfaces* **2016**, *8*, 5608.
[86] L. Xie, G. Wang, H. Zhou, F. Zhang, Z. Guo, C. Liu, X. Zhang, L. Zhu, *Biomaterials* **2016**, *103*, 219.
[87] X. Liang, W. Shang, C. Chi, C. Zeng, K. Wang, C. Fang, Q. Chen, H. Liu, Y. Fan, J. Tian, *Cancer Lett.* **2016**, *383*, 243.
[88] a) L. Hou, X. Yang, J. Ren, Y. Wang, H. Zhang, Q. Feng, Y. Shi, X. Shan, Y. Yuan, Z. Zhang, *Int. J. Nanomed.* **2016**, *11*, 607; b) S. Wang, Q. Lin, J. Chen, H. Gao, D. Fu, S. Shen, *Carbon* **2017**, *112*, 53.
[89] S. Wang, Q. Zhang, P. Yang, X. Yu, L.-Y. Huang, S. Shen, S. Cai, *ACS Appl. Mater. Interfaces* **2015**, *8*, 3736.
[90] H. Zhao, Y. Chao, J. Liu, J. Huang, J. Pan, W. Guo, J. Wu, M. Sheng, K. Yang, J. Wang, *Theranostics* **2016**, *6*, 1833.
[91] S. R. Shin, S. M. Jung, M. Zalabany, K. Kim, P. Zorlutuna, S. bok Kim, M. Nikkhah, M. Khabiry, M. Azize, J. Kong, *ACS Nano* **2013**, *7*, 2369.
[92] S. Ostrovidov, X. Shi, L. Zhang, X. Liang, S. B. Kim, T. Fujie, M. Ramalingam, M. Chen, K. Nakajima, F. Al-Hazmi, *Biomaterials* **2014**, *35*, 6268.
[93] S. Pok, F. Vitale, S. L. Eichmann, O. M. Benavides, M. Pasquali, J. G. Jacot, *ACS Nano* **2014**, *8*, 9822.
[94] S. R. Shin, H. Bae, J. M. Cha, J. Y. Mun, Y.-C. Chen, H. Tekin, H. Shin, S. Farshchi, M. R. Dokmeci, S. Tang, *ACS Nano* **2012**, *6*, 362.
[95] O. Im, J. Li, M. Wang, L. G. Zhang, M. Keidar, *Int. J. Nanomed.* **2012**, *7*, 2087.
[96] E. Hirata, C. Ménard-Moyon, E. Venturelli, H. Takita, F. Watari, A. Bianco, A. Yokoyama, *Nanotechnol.* **2013**, *24*, 435101.
[97] S. R. Shin, C. Shin, A. Memic, S. Shadmehr, M. Miscuglio, H. Y. Jung, S. M. Jung, H. Bae, A. Khademhosseini, X. S. Tang, *Adv. Funct. Mater.* **2015**, *25*, 4486.
[98] L. Bareket, N. Waiskopf, D. Rand, G. Lubin, M. David-Pur, J. Ben-Dov, S. Roy, C. Eleftheriou, E. Sernagor, O. Cheshnovsky, *Nano Lett.* **2014**, *14*, 6685.
[99] C. G. Eleftheriou, J. B. Zimmermann, H. D. Kjeldsen, M. David-Pur, Y. Hanein, E. Sernagor, *Biomaterials* **2017**, *112*, 108.
[100] a) P. Avouris, C. Dimitrakopoulos, *Mater. Today* **2012**, *15*, 86; b) B. H. Nguyen, V. H. Nguyen, *Adv. Natural Sci.: Nanosci. Nanotechnol.* **2016**, *7*, 023002; c) Y. Yang, A. M. Asiri, Z. Tang, D. Du, Y. Lin, *Mater. Today* **2013**, *16*, 365.
[101] L. Rodríguez-Pérez, M. Á. Herranz, N. Martín, *Chem. Commun.* **2013**, *49*, 3721.
[102] O. V. Yazyev, Y. P. Chen, *Nat. Nanotechnol.* **2014**, *9*, 755.
[103] D. R. Dreyer, S. Park, C. W. Bielawski, R. S. Ruoff, *Chem. Soc. Rev.* **2010**, *39*, 228.
[104] B. J. Hong, Z. An, O. C. Compton, S. T. Nguyen, *Small* **2012**, *8*, 2469.
[105] J. Lee, Y. Yim, S. Kim, M.-H. Choi, B.-S. Choi, Y. Lee, D.-H. Min, *Carbon* **2016**, *97*, 92.
[106] a) M. F. El-Kady, R. B. Kaner, *Nat. Commun.* **2013**, *4*, 1475; b) E. Morales-Narváez, L. Baptista-Pires, A. Zamora-Gálvez, A. Merkoçi, *Adv. Mater.* **2017**, *29*, 1604905.
[107] a) Y. Shao, J. Wang, H. Wu, J. Liu, I. A. Aksay, Y. Lin, *Electroanalysis* **2010**, *22*, 1027; b) M. Zhou, Y. Zhai, S. Dong, *Anal. Chem.* **2009**, *81*, 5603.
[108] a) B. Liang, L. Fang, G. Yang, Y. Hu, X. Guo, X. Ye, *Biosens. Bioelectron.* **2013**, *43*, 131; b) B. Unnikrishnan, S. Palanisamy, S.-M. Chen, *Biosens. Bioelectron.* **2013**, *39*, 70; c) K. Vijayaraj, S. W. Hong, S.-H. Jin, S.-C. Chang, D.-S. Park, *Anal. Methods* **2016**, *8*, 6974.
[109] G. Chen, Y. Liu, Y. Liu, Y. Tian, X. Zhang, *J. Electroanal. Chem.* **2015**, *738*, 100.
[110] a) M. M. Barsan, M. David, M. Florescu, L. Tugulea, C. M. Brett, *Bioelectrochemistry* **2014**, *99*, 46; b) M. David, M. M. Barsan, M. Florescu, C. Brett, *Electroanalysis* **2015**, *27*, 2139; c) S. Li, J.-X. Xiong, C.-X. Chen, F.-Q. Chu, Y. Kong, L.-H. Deng, *Mater. Technology* **2017**, *32*, 1; d) C. Ruan, W. Shi, H. Jiang, Y. Sun, X. Liu, X. Zhang, Z. Sun, L. Dai, D. Ge, *Sens. Actuat. B: Chemical* **2013**, *177*, 826.
[111] a) S.-J. Li, T.-W. Chen, N. Xia, Y.-L. Hou, J.-J. Du, L. Liu, *J. Solid State Electrochem.* **2013**, *17*, 2487; b) P. Rafighi, M. Tavahodi, B. Haghighi, *Sens. Actuat. B: Chemical* **2016**, *232*, 454.

[112] a) Y. Liu, X. Zhang, D. He, F. Ma, Q. Fu, Y. Hu, *RSC Adv.* **2016**, *6*, 18654; b) A. E. Vilian, V. Mani, S.-M. Chen, B. Dinesh, S.-T. Huang, *Indust. Eng. Chem. Res.* **2014**, *53*, 15582.
[113] Y. Zhao, W. Li, L. Pan, D. Zhai, Y. Wang, L. Li, W. Cheng, W. Yin, X. Wang, J.-B. Xu, *Sci. Rep.* **2016**, 6.
[114] X. You, J. J. Pak, *Sens. Actuat. B: Chemical* **2014**, *202*, 1357.
[115] J. W. Park, C. Lee, J. Jang, *Sens. Actuat. B: Chemical* **2015**, *208*, 532.
[116] X. Li, W. C. Choy, X. Ren, D. Zhang, H. Lu, *Adv. Funct. Mater.* **2014**, *24*, 3114.
[117] V. K. Gupta, N. Atar, M. L. Yola, M. Eryılmaz, H. Torul, U. Tamer, İ. H. Boyacı, Z. Üstündağ, *J. Colloid Interface Sci.* **2013**, *406*, 231.
[118] Q. Gong, H. Yang, Y. Dong, W. Zhang, *Anal. Methods* **2015**, *7*, 2554.
[119] W. Sun, Y. Lu, Y. Wu, Y. Zhang, P. Wang, Y. Chen, G. Li, *Sens. Actuat. B: Chemical* **2014**, *202*, 160.
[120] J. Zhang, A. Li, X. Yu, W. Guo, Z. Zhao, J. Qiu, X. Mou, J. P. Claverie, H. Liu, *Adv. Mater. Interfaces* **2015**, *2*.
[121] a) S. Hajihosseini, N. Nasirizadeh, M. S. Hejazi, P. Yaghmaei, *Mater. Sci. Eng.: C* **2016**, *61*, 506; b) S. M. Khoshfetrat, M. A. Mehrgardi, *RSC Adv.* **2015**, *5*, 29285; c) H.-z. Pan, H.-w. Yu, N. Wang, Z. Zhang, G.-c. Wan, H. Liu, X. Guan, D. Chang, *J. Biotechnol.* **2015**, *214*, 133.
[122] M. Chen, C. Hou, D. Huo, J. Bao, H. Fa, C. Shen, *Biosens. Bioelectron.* **2016**, *85*, 684.
[123] W. Wang, T. Bao, X. Zeng, H. Xiong, W. Wen, X. Zhang, S. Wang, *Biosens. Bioelectron.* **2017**, *91*, 183.
[124] W. Zhang, F. Li, Y. Hu, S. Gan, D. Han, Q. Zhang, L. Niu, *J. Mater. Chem. B* **2014**, *2*, 3142.
[125] A. Shi, J. Wang, X. Han, X. Fang, Y. Zhang, *Sens. Actuat. B: Chemical* **2014**, *200*, 206.
[126] A.-L. Liu, G.-X. Zhong, J.-Y. Chen, S.-H. Weng, H.-N. Huang, W. Chen, L.-Q. Lin, Y. Lei, F.-H. Fu, Z.-l. Sun, *Anal. Chim. Acta* **2013**, *767*, 50.
[127] C. Liu, D. Jiang, G. Xiang, L. Liu, F. Liu, X. Pu, *Analyst* **2014**, *139*, 5460.
[128] L. Wang, E. Hua, M. Liang, C. Ma, Z. Liu, S. Sheng, M. Liu, G. Xie, W. Feng, *Biosens. Bioelectron.* **2014**, *51*, 201.
[129] Y. Ye, J. Gao, H. Zhuang, H. Zheng, H. Sun, Y. Ye, X. Xu, X. Cao, *Microchimica Acta* **2017**, *184*, 245.
[130] W. Sun, X. Wang, Y. Lu, S. Gong, X. Qi, B. Lei, Z. Sun, G. Li, *Mater. Sci. Eng.: C* **2015**, *49*, 34.
[131] M. Chen, C. Hou, D. Huo, H. Fa, Y. Zhao, C. Shen, *Sens. Actuat. B: Chemical* **2017**, *239*, 421.
[132] a) B. Cai, S. Wang, L. Huang, Y. Ning, Z. Zhang, G.-J. Zhang, *ACS Nano* **2014**, *8*, 2632; b) J. Ping, R. Vishnubhotla, A. Vrudhula, A. C. Johnson, *ACS Nano* **2016**, *10*, 8700; c) X. Zhang, Y. Zhang, Q. Liao, Y. Song, S. Ma, *Small* **2013**, *9*, 4045; d) C. Zheng, L. Huang, H. Zhang, Z. Sun, Z. Zhang, G.-J. Zhang, *ACS Appl. Mater. Interfaces* **2015**, *7*, 16953.
[133] C. H. Lu, H. H. Yang, C. L. Zhu, X. Chen, G. N. Chen, *Angew. Chem.* **2009**, *121*, 4879.
[134] H. Wang, K. Ma, B. Xu, W. Tian, *Small* **2016**, *12*, 6613.
[135] J. Zhang, M. Tao, Y. Jin, *Analyst* **2014**, *139*, 3455.
[136] W. Gao, Y. Chen, J. Xi, S. Lin, Y. Chen, Y. Lin, Z. Chen, *Biosens. Bioelectron.* **2013**, *41*, 776.
[137] L. Li, H. Lu, L. Deng, *Talanta* **2013**, *113*, 1.
[138] W. Miao, *Chem. Rev.* **2008**, *108*, 2506.
[139] Y. Kitagawa, K. Kitabatake, I. Kubo, E. Tamiya, I. Karube, *Anal. Chim. Acta* **1989**, *218*, 61.
[140] S. Swanson, S. Jacobs, D. Mytych, C. Shah, S. Indelicato, R. Bordens, *Dev. Biol. Standard.* **1998**, *97*, 135.
[141] Y. Gao, J. Li, X. Yang, Q. Xiang, K. Wang, *Electroanalysis* **2014**, *26*, 382.
[142] J. Bao, C. Hou, M. Chen, J. Li, D. Huo, M. Yang, X. Luo, Y. Lei, *J. Agric. Food. Chem.* **2015**, *63*, 10319.
[143] J. Dong, H. Zhao, F. Qiao, P. Liu, X. Wang, S. Ai, *Anal. Methods* **2013**, *5*, 2866.
[144] a) H. Liang, D. Song, J. Gong, *Biosens. Bioelectron.* **2014**, *53*, 363; b) Q. Liu, J. Cai, J. Huan, X. Dong, C. Wang, B. Qiu, K. Wang, *Analyst* **2014**, *139*, 1121.
[145] H. Wang, G. Zhao, D. Chen, Z. Wang, G. Liu, *Int. J. Electrochem. Sci.* **2016**, *11*, 10906.
[146] S. Yu, X. Cao, M. Yu, *Microchem. J.* **2012**, *103*, 125.
[147] a) J. Han, J. Ma, Z. Ma, *Biosens. Bioelectron.* **2013**, *47*, 243; b) W. Lu, J. Ge, L. Tao, X. Cao, J. Dong, W. Qian, *Electrochim. Acta* **2014**, *130*, 335.
[148] S. Samanman, A. Numnuam, W. Limbut, P. Kanatharana, P. Thavarungkul, *Anal. Chim. Acta* **2015**, *853*, 521.
[149] X. Jiang, Y. Chai, R. Yuan, Y. Cao, Y. Chen, H. Wang, X. Gan, *Anal. Chim. Acta* **2013**, *783*, 49.
[150] S. Kumar, S. Kumar, S. Srivastava, B. K. Yadav, S. H. Lee, J. G. Sharma, D. C. Doval, B. D. Malhotra, *Biosens. Bioelectron.* **2015**, *73*, 114.
[151] X. Pei, B. Zhang, J. Tang, B. Liu, W. Lai, D. Tang, *Anal. Chim. Acta* **2013**, *758*, 1.
[152] a) Y. Cheng, R. Yuan, Y. Chai, H. Niu, Y. Cao, H. Liu, L. Bai, Y. Yuan, *Anal. Chim. Acta* **2012**, *745*, 137; b) J. Huang, J. Tian, Y. Zhao, S. Zhao, *Sens. Actuat. B: Chemical* **2015**, *206*, 570.
[153] B. Jin, P. Wang, H. Mao, B. Hu, H. Zhang, Z. Cheng, Z. Wu, X. Bian, C. Jia, F. Jing, *Biosens. Bioelectron.* **2014**, *55*, 464.
[154] a) Y. Cao, R. Yuan, Y. Chai, H. Liu, Y. Liao, Y. Zhuo, *Talanta* **2013**, *113*, 106; b) Y. Zhang, M. Su, L. Ge, S. Ge, J. Yu, X. Song, *Carbon* **2013**, *57*, 22; c) X. Jiang, Y. Chai, H. Wang, R. Yuan, *Biosens. Bioelectron.* **2014**, *54*, 20; d) J. Yan, M. Yan, L. Ge, S. Ge, J. Yu, *Sens. Actuat. B: Chemical* **2014**, *193*, 247.
[155] H. D. Jang, S. K. Kim, H. Chang, J.-W. Choi, *Biosens. Bioelectron.* **2015**, *63*, 546.
[156] L. Cao, L. Cheng, Z. Zhang, Y. Wang, X. Zhang, H. Chen, B. Liu, S. Zhang, J. Kong, *Lab Chip* **2012**, *12*, 4864.
[157] A. Gulzar, P. Yang, F. He, J. Xu, D. Yang, L. Xu, M. O. Jan, *Chem. Biol. Interact.* **2017**, *262*, 69.
[158] L. Fan, H. Ge, S. Zou, Y. Xiao, H. Wen, Y. Li, H. Feng, M. Nie, *Int. J. Biol. Macromol.* **2016**, *93*, 582.
[159] Q. Zhang, H. Chi, M. Tang, J. Chen, G. Li, Y. Liu, B. Liu, *RSC Adv.* **2016**, *6*, 87258.
[160] X. T. Zheng, X. Q. Ma, C. M. Li, *J. Colloid Interface Sci.* **2016**, *467*, 35.
[161] Y. H. Park, S. Y. Park, I. In, *J. Indust. Eng. Chem.* **2015**, *30*, 190.
[162] a) Q. Pan, Y. Lv, G. R. Williams, L. Tao, H. Yang, H. Li, L. Zhu, *Carbohydr. Polym.* **2016**, *151*, 812; b) Y. Lv, L. Tao, S. A. Bligh, H. Yang, Q. Pan, L. Zhu, *Mater. Sci. Eng.: C* **2016**, *59*, 652.
[163] W. Chen, X. Wen, G. Zhen, X. Zheng, *RSC Adv.* **2015**, *5*, 69307.
[164] L. Guo, H. Shi, H. Wu, Y. Zhang, X. Wang, D. Wu, L. An, S. Yang, *Carbon* **2016**, *107*, 87.
[165] A. Pourjavadi, Z. M. Tehrani, S. Jokar, *Polymer* **2015**, *76*, 52.
[166] S. Dinda, M. Kakran, J. Zeng, T. Sudhaharan, S. Ahmed, D. Das, S. T. Selvan, *ChemPlusChem* **2016**, *81*, 100.
[167] M. Wojtoniszak, K. Urbas, M. Perużyńska, M. Kurzawski, M. Droździk, E. Mijowska, *Chem. Phys. Lett.* **2013**, *568*, 151.
[168] L. Du, S. Suo, D. Luo, H. Jia, Y. Sha, Y. Liu, *J. Nanopart. Res.* **2013**, *15*, 1708.
[169] Z. Xu, S. Wang, Y. Li, M. Wang, P. Shi, X. Huang, *ACS Appl. Mater. Interfaces* **2014**, *6*, 17268.
[170] H. Kim, R. Namgung, K. Singha, I.-K. Oh, W. J. Kim, *Bioconjugate Chem.* **2011**, *22*, 2558.
[171] H. Kim, J. Kim, M. Lee, H. C. Choi, W. J. Kim, *Adv. Healthcare Mater.* **2016**, *5*, 1918.
[172] J. T. Robinson, S. M. Tabakman, Y. Liang, H. Wang, H. Sanchez Casalongue, D. Vinh, H. Dai, *J. Am. Chem. Soc.* **2011**, *133*, 6825.
[173] O. Akhavan, E. Ghaderi, *Small* **2013**, *9*, 3593.

[174] J. Yu, Y. H. Lin, L. Yang, C. C. Huang, L. Chen, W. C. Wang, G. W. Chen, J. Yan, S. Sawettanun, C. H. Lin, *Adv. Healthcare Mater.* **2016**, *6*, 1600804.
[175] D.-K. Lim, A. Barhoumi, R. G. Wylie, G. Reznor, R. S. Langer, D. S. Kohane, *Nano Lett.* **2013**, *13*, 4075.
[176] C. Hou, H. Quan, Y. Duan, Q. Zhang, H. Wang, Y. Li, *Nanoscale* **2013**, *5*, 1227.
[177] F. Wang, Q. Sun, B. Feng, Z. Xu, J. Zhang, J. Xu, L. Lu, H. Yu, M. Wang, Y. Li, *Adv. Healthcare Mater.* **2016**, *5*, 2227.
[178] D. Hu, J. Zhang, G. Gao, Z. Sheng, H. Cui, L. Cai, *Theranostics* **2016**, *6*, 1043.
[179] S. Gao, L. Zhang, G. Wang, K. Yang, M. Chen, R. Tian, Q. Ma, L. Zhu, *Biomaterials* **2016**, *79*, 36.
[180] L.-S. Lin, X. Yang, G. Niu, J. Song, H.-H. Yang, X. Chen, *Nanoscale* **2016**, *8*, 2116.
[181] a) S. Goenka, V. Sant, S. Sant, *J. Controlled Release* **2014**, *173*, 75; b) N. Dubey, R. Bentini, I. Islam, T. Cao, A. H. Castro Neto, V. Rosa, *Stem Cells Int.* **2015**, 2015.
[182] W. C. Lee, C. H. Y. Lim, H. Shi, L. A. Tang, Y. Wang, C. T. Lim, K. P. Loh, *ACS Nano* **2011**, *5*, 7334.
[183] J. Lu, Y. S. He, C. Cheng, Y. Wang, L. Qiu, D. Li, D. Zou, *Adv. Funct. Mater.* **2013**, *23*, 3494.
[184] O. Akhavan, E. Ghaderi, M. Shahsavar, *Carbon* **2013**, *59*, 200.
[185] a) H. Liu, J. Cheng, F. Chen, D. Bai, C. Shao, J. Wang, P. Xi, Z. Zeng, *Nanoscale* **2014**, *6*, 5315; b) H. Liu, J. Cheng, F. Chen, F. Hou, D. Bai, P. Xi, Z. Zeng, *ACS Appl. Mater. Interfaces* **2014**, *6*, 3132; c) X. Xie, K. Hu, D. Fang, L. Shang, S. D. Tran, M. Cerruti, *Nanoscale* **2015**, *7*, 7992.
[186] S. Shah, P. T. Yin, T. M. Uehara, S. T. D. Chueng, L. Yang, K. B. Lee, *Adv. Mater.* **2014**, *26*, 3673.
[187] a) M. Tang, Q. Song, N. Li, Z. Jiang, R. Huang, G. Cheng, *Biomaterials* **2013**, *34*, 6402; b) F. Veliev, A. Briançon-Marjollet, V. Bouchiat, C. Delacour, *Biomaterials* **2016**, *86*, 33.
[188] a) Y. Dong, J. Cai, X. You, Y. Chi, *Analyst* **2015**, *140*, 7468; b) Y. Wang, A. Hu, *J. Mater. Chem. C* **2014**, *2*, 6921.
[189] a) J. Shen, Y. Zhu, X. Yang, C. Li, *Chem. Commun.* **2012**, *48*, 3686; b) J.-L. Li, B. Tang, B. Yuan, L. Sun, X.-G. Wang, *Biomaterials* **2013**, *34*, 9519; c) Z. Fan, S. Li, F. Yuan, L. Fan, *RSC Adv.* **2015**, *5*, 19773.
[190] L. Zhang, Z.-Y. Zhang, R.-P. Liang, Y.-H. Li, J.-D. Qiu, *Anal. Chem.* **2014**, *86*, 4423.
[191] Z.-b. Qu, X. Zhou, L. Gu, R. Lan, D. Sun, D. Yu, G. Shi, *Chem. Commun.* **2013**, *49*, 9830.
[192] S. Kiran, R. Misra, *J. Biomedical Mater. Res. A* **2015**, *103*, 2888.
[193] A. S. Krishna, P. A. Nair, C. Radhakumary, K. Sreenivasan, *Mater. Res. Express* **2016**, *3*, 055001.
[194] P. Shen, Y. Xia, *Anal. Chem.* **2014**, *86*, 5323.
[195] Y. He, X. Wang, J. Sun, S. Jiao, H. Chen, F. Gao, L. Wang, *Anal. Chim. Acta* **2014**, *810*, 71.
[196] L. Zhang, D. Peng, R. P. Liang, J. D. Qiu, *Chem. Eur. J.* **2015**, *21*, 9343.
[197] H. Wang, J. Yi, D. Velado, Y. Yu, S. Zhou, *ACS Appl. Mater. Interfaces* **2015**, *7*, 15735.
[198] J. Zhang, M. Yang, C. Li, N. Dorh, F. Xie, F.-T. Luo, A. Tiwari, H. Liu, *Biosensors* **2015**, *24*, 31.
[199] H. Miao, L. Wang, Y. Zhuo, Z. Zhou, X. Yang, *Biosens. Bioelectron.* **2016**, *86*, 83.
[200] H. Chen, Y. Xie, A. M. Kirillov, L. Liu, M. Yu, W. Liu, Y. Tang, *Chem. Commun.* **2015**, *51*, 5036.
[201] J. Ryu, E. Lee, K. Lee, J. Jang, *J. Mater. Chem. B* **2015**, *3*, 4865.
[202] I. Al-Ogaidi, H. Gou, Z. P. Aguilar, S. Guo, A. K. Melconian, A. K. A. Al-Kazaz, F. Meng, N. Wu, *Chem. Commun.* **2014**, *50*, 1344.
[203] S. Li, J. Luo, X. Yang, Y. Wan, C. Liu, *Sens. Actuat. B: Chemical* **2014**, *197*, 43.
[204] H. Yang, W. Liu, C. Ma, Y. Zhang, X. Wang, J. Yu, X. Song, *Electrochim. Acta* **2014**, *123*, 470.
[205] A. Salinas-Castillo, M. Ariza-Avidad, C. Pritz, M. Camprubí-Robles, B. Fernández, M. J. Ruedas-Rama, A. Megia-Fernández, A. Lapresta-Fernández, F. Santoyo-Gonzalez, A. Schrott-Fischer, *Chem. Commun.* **2013**, *49*, 1103.
[206] Y. Lin, C. Wang, L. Li, H. Wang, K. Liu, K. Wang, B. Li, *ACS Appl. Mater. Interfaces* **2015**, *7*, 27262.
[207] a) Y. Hou, Q. Lu, J. Deng, H. Li, Y. Zhang, *Anal. Chim. Acta* **2015**, *866*, 69; b) Q. Xu, J. Zhao, Y. Liu, P. Pu, X. Wang, Y. Chen, C. Gao, J. Chen, H. Zhou, *J. Mater. Science* **2015**, *50*, 2571; c) Q. Xu, P. Pu, J. Zhao, C. Dong, C. Gao, Y. Chen, J. Chen, Y. Liu, H. Zhou, *J. Mater. Chem. A* **2015**, *3*, 542; d) L. Li, B. Yu, T. You, *Biosens. Bioelectron.* **2015**, *74*, 263; e) Y. Dong, G. Li, N. Zhou, R. Wang, Y. Chi, G. Chen, *Anal. Chem.* **2012**, *84*, 8378; f) L. Zhou, Y. Lin, Z. Huang, J. Ren, X. Qu, *Chem. Commun.* **2012**, *48*, 1147; g) K. Qu, J. Wang, J. Ren, X. Qu, *Chem. Eur. J.* **2013**, *19*, 7243; h) W. Lu, X. Qin, S. Liu, G. Chang, Y. Zhang, Y. Luo, A. M. Asiri, A. O. Al-Youbi, X. Sun, *Anal. Chem.* **2012**, *84*, 5351; i) A. Zhao, C. Zhao, M. Li, J. Ren, X. Qu, *Anal. Chim. Acta* **2014**, *809*, 128; j) W. Wei, C. Xu, J. Ren, B. Xu, X. Qu, *Chem. Commun.* **2012**, *48*, 1284; k) A. Gupta, A. Chaudhary, P. Mehta, C. Dwivedi, S. Khan, N. C. Verma, C. K. Nandi, *Chem. Commun.* **2015**, *51*, 10750; l) C. Wang, C. Wang, P. Xu, A. Li, Y. Chen, K. Zhuo, *J. Mater. Sci.* **2016**, *51*, 861.
[208] B. Kong, A. Zhu, C. Ding, X. Zhao, B. Li, Y. Tian, *Adv. Mater.* **2012**, *24*, 5844.
[209] C. H. Park, H. Yang, J. Lee, H.-H. Cho, D. Kim, D. C. Lee, B. J. Kim, *Chem. Mater.* **2015**, *27*, 5288.
[210] J. Wang, S. Su, J. Wei, R. Bahgi, L. Hope-Weeks, J. Qiu, S. Wang, *Physica E: Low-dimensional Syst. Nanostructures* **2015**, *72*, 17.
[211] a) J. Jana, M. Ganguly, T. Pal, *PCCP* **2015**, *17*, 2394; b) J. Deng, Q. Lu, Y. Hou, M. Liu, H. Li, Y. Zhang, S. Yao, *Anal. Chem.* **2015**, *87*, 2195.
[212] L. Zhu, G. Xu, Q. Song, T. Tang, X. Wang, F. Wei, Q. Hu, *Sens. Actuat. B: Chemical* **2016**, *231*, 506.
[213] W. Kong, D. Wu, G. Li, X. Chen, P. Gong, Z. Sun, G. Chen, L. Xia, J. You, Y. Wu, *Talanta* **2017**, *165*, 677.
[214] G. Liu, Z. Chen, X. Jiang, D.-Q. Feng, J. Zhao, D. Fan, W. Wang, *Sens. Actuat. B: Chemical* **2016**, *228*, 302.
[215] Y. Xu, X. Chen, R. Chai, C. Xing, H. Li, X.-B. Yin, *Nanoscale* **2016**, *8*, 13414.
[216] S. Pang, Y. Zhang, C. Wu, S. Feng, *Sens. Actuat. B: Chemical* **2016**, *222*, 857.
[217] P. Ni, H. Dai, Z. Li, Y. Sun, J. Hu, S. Jiang, Y. Wang, Z. Li, *Talanta* **2015**, *144*, 258.
[218] T. T. Bui, S.-Y. Park, *Green Chem.* **2016**, *18*, 4245.
[219] S. H. Qaddare, A. Salimi, *Biosens. Bioelectron.* **2017**, *89*, 773.
[220] Q. Huang, X. Lin, J.-J. Zhu, Q.-X. Tong, *Biosens. Bioelectron.* **2017**, *94*, 507.
[221] S. Nandi, M. Ritenberg, R. Jelinek, *Analyst* **2015**, *140*, 4232.
[222] S. Bhattacharya, S. Nandi, R. Jelinek, *RSC Adv.* **2017**, *7*, 588.
[223] M. L. Bhaisare, G. Gedda, M. S. Khan, H.-F. Wu, *Anal. Chim. Acta* **2016**, *920*, 63.
[224] Q. Wang, X. Huang, Y. Long, X. Wang, H. Zhang, R. Zhu, L. Liang, P. Teng, H. Zheng, *Carbon* **2013**, *59*, 192.
[225] C. Liu, P. Zhang, X. Zhai, F. Tian, W. Li, J. Yang, Y. Liu, H. Wang, W. Wang, W. Liu, *Biomaterials* **2012**, *33*, 3604.
[226] Q. Wang, C. Zhang, G. Shen, H. Liu, H. Fu, D. Cui, *J. Nanobiotechnology* **2014**, *12*, 58.
[227] H. Ding, F. Du, P. Liu, Z. Chen, J. Shen, *ACS Appl. Mater. Interfaces* **2015**, *7*, 6889.

[228] J. Xu, F. Zeng, H. Wu, C. Hu, C. Yu, S. Wu, *Small* **2014**, *10*, 3750.
[229] S. Nandi, R. Malishev, K. P. Kootery, Y. Mirsky, S. Kolusheva, R. Jelinek, *Chem. Commun.* **2014**, *50*, 10299.
[230] K. Jiang, S. Sun, L. Zhang, Y. Lu, A. Wu, C. Cai, H. Lin, *Angew. Chem. Int. Ed.* **2015**, *54*, 5360.
[231] J. Tang, B. Kong, H. Wu, M. Xu, Y. Wang, Y. Wang, D. Zhao, G. Zheng, *Adv. Mater.* **2013**, *25*, 6569.
[232] S. K. Bhunia, A. Saha, A. R. Maity, S. C. Ray, N. R. Jana, *Sci. Rep.* **2013**, *3*, 1473.
[233] S. K. Bhunia, A. R. Maity, S. Nandi, D. Stepensky, R. Jelinek, *ChemBioChem* **2016**, *17*, 614.
[234] M. Zheng, S. Ruan, S. Liu, T. Sun, D. Qu, H. Zhao, Z. Xie, H. Gao, X. Jing, Z. Sun, *ACS Nano* **2015**, *9*, 11455.
[235] A. B. Bourlinos, A. Bakandritsos, A. Kouloumpis, D. Gournis, M. Krysmann, E. P. Giannelis, K. Polakova, K. Safarova, K. Hola, R. Zboril, *J. Mater. Chem.* **2012**, *22*, 23327.
[236] J. Wang, Z. Zhang, S. Zha, Y. Zhu, P. Wu, B. Ehrenberg, J.-Y. Chen, *Biomaterials* **2014**, *35*, 9372.
[237] J. Ge, M. Lan, B. Zhou, W. Liu, L. Guo, H. Wang, Q. Jia, G. Niu, X. Huang, H. Zhou, *Nat. Commun.* **2014**, *5*, 4596.
[238] NIH, USA, Comparison of Stationary Breast Tomosynthesis and 2-D Digital Mammography in Patients With Known Breast Lesions, http://clinicaltrials.gov/ct2/show/record/NCT01773850.
[239] NIH, USA, Diagnosis of Gastric Lesions With Na-nose, http://clinicaltrials.gov/ct2/show/study/NCT01420588.
[240] a) A. A. Shvedova, A. Pietroiusti, B. Fadeel, V. E. Kagan, *Toxicol. Appl. Pharmacol.* **2012**, *261*, 121; b) H. Y. Mao, S. Laurent, W. Chen, O. Akhavan, M. Imani, A. A. Ashkarran, M. Mahmoudi, *Chem. Rev.* **2013**, *113*, 3407.
[241] a) O. Salihoglu, S. Balci, C. Kocabas, *Appl. Phys. Lett.* **2012**, *100*, 213110; b) L. Wang, K. Y. Pu, J. Li, X. Qi, H. Li, H. Zhang, C. Fan, B. Liu, *Adv. Mater.* **2011**, *23*, 4386.
[242] L. Feng, Z. Liu, *Nanomedicine* **2011**, *6*, 317.
[243] W. Zhang, Z. Guo, D. Huang, Z. Liu, X. Guo, H. Zhong, *Biomaterials* **2011**, *32*, 8555.
[244] Z. Liu, J. T. Robinson, S. M. Tabakman, K. Yang, H. Dai, *Mater. Today* **2011**, *14*, 316.
[245] A. Battigelli, C. Ménard-Moyon, T. Da Ros, M. Prato, A. Bianco, *Adv. Drug Delivery Revs.* **2013**, *65*, 1899.
[246] a) F. T. Andón, A. A. Kapralov, N. Yanamala, W. Feng, A. Baygan, B. J. Chambers, K. Hultenby, F. Ye, M. S. Toprak, B. D. Brandner, *Small* **2013**, *9*, 2721; b) J. Russier, C. Ménard-Moyon, E. Venturelli, E. Gravel, G. Marcolongo, M. Meneghetti, E. Doris, A. Bianco, *Nanoscale* **2011**, *3*, 893.
[247] G. P. Kotchey, B. L. Allen, H. Vedala, N. Yanamala, A. A. Kapralov, Y. Y. Tyurina, J. Klein-Seetharaman, V. E. Kagan, A. Star, *ACS Nano* **2011**, *5*, 2098.
[248] a) Y. Sato, A. Yokoyama, Y. Nodasaka, T. Kohgo, K. Motomiya, H. Matsumoto, E. Nakazawa, T. Numata, M. Zhang, M. Yudasaka, *Sci. Rep.* **2013**, *3*, 2516; b) C. M. Girish, A. Sasidharan, G. S. Gowd, S. Nair, M. Koyakutty, *Adv. Healthcare Mater.* **2013**, *2*, 1489; c) A. Nunes, C. Bussy, L. Gherardini, M. Meneghetti, M. A. Herrero, A. Bianco, M. Prato, T. Pizzorusso, K. T. Al-Jamal, K. Kostarelos, *Nanomedicine* **2012**, *7*, 1485.
[249] L. Liu, C. Zhu, M. Fan, C. Chen, Y. Huang, Q. Hao, J. Yang, H. Wang, D. Sun, *Nanoscale* **2015**, *7*, 13619.
[250] V. E. Kagan, N. V. Konduru, W. Feng, B. L. Allen, J. Conroy, Y. Volkov, I. I. Vlasova, N. A. Belikova, N. Yanamala, A. Kapralov, *Nat. Nanotechnol.* **2010**, *5*, 354.
[251] N. Lu, J. Li, R. Tian, Y.-Y. Peng, *Chem. Res. Toxicol.* **2014**, *27*, 1070.